



TREBALL FI DE CARRERA

Títol

**MODELACIÓN DE TRANSPORTE REACTIVO: AVANCE DE
UNA SOLUCIÓN HIPERALCALINA A LO LARGO DE UNA
FRACTURA Y SU EFECTO EN LA MINERALOGÍA**

Autor/a

Jana J. Montori Laforga

Tutor/a

Maarten W. Saaltink i Josep M. Soler

Departament

Departament d'Enginyeria del Terreny, Cartogràfica i Geofísica

Intensificació

Hidrologia Subterrània

Data

21 d'octubre de 2009



Escola Tècnica Superior d'Enginyers
de Camins, Canals i Ports de Barcelona

UNIVERSITAT POLITÈCNICA DE CATALUNYA

Títol

**MODELACIÓN DE TRANSPORTE REACTIVO: AVANCE DE
UNA SOLUCIÓN HIPERALCALINA A LO LARGO DE UNA
FRACTURA Y SU EFECTO EN LA MINERALOGÍA**

Autor/a

Jana J. Montori Laforga

Tutor/a

Maarten W. Saaltink i Josep M. Soler

Especialitat

Hidrología Subterránea

Data

21 de octubre de 2009

Resum

El objetivo de este estudio es llevar a cabo una serie de cálculos, modelizando un transporte reactivo unidimensional, para simular la alteración de una fractura y el alcance de un penacho de pH elevado derivado de la circulación de soluciones hiperalcalinas a lo largo de dicha fractura. La modelización representa la fracturación localizada en la isla de Olkiluoto (Finlandia), donde se sitúan las instalaciones de ONKALO (posible futuro Almacenamiento Geológico Profundo de residuos radiactivos de alta actividad). Para impedir el paso del agua al repositorio está previsto sellar las fracturas con cemento. Sin embargo, el continuo contacto del cemento con el agua subterránea puede degradarlo, permitiendo el paso de un agua mucho más reactiva (penacho hiperalcalino).

La longitud del dominio unidimensional (fractura) es de 200 m y los cálculos se realizan para tiempos de hasta 10000 años. Se ha asumido una temperatura constante igual a 25°C, excepto en unos pocos casos donde se ha incorporado un pulso de calor de 200 años.

En este trabajo se presentan los resultados que se extraen de los cálculos realizados a partir del código de transporte reactivo Retraso (REactive TRAnsport of SOlutes). En estos cálculos se han tenido en cuenta varias soluciones de pH elevado, varias velocidades de flujo y varias superficies de los minerales primarios.

Una conclusión que es común en todos los casos es que la roca no tiene la capacidad de amortiguamiento suficiente para reducir considerablemente el pH de las soluciones que circulan en el dominio de cálculo. Sin embargo, hay una cierta reducción del pH para (i) las condiciones de flujo más lento, (ii) los casos de pH más bajo, (iii) cuando se incluyen en los cálculos minerales secundarios que contienen Mg, y (iv) cuando las superficies de reacción de los minerales primarios son más grandes (debido por ejemplo a la presencia de una harina de falla)..

Otra observación importante es que los resultados son muy diferentes dependiendo de la inclusión o no de minerales secundarios que contengan Mg en los cálculos (brucita, saponita). En la mayoría de los casos, si se incluyen los minerales secundarios con Mg, la precipitación de brucita y saponita causa el sellado de la porosidad en la entrada de la fractura. Por otra parte, si la modelización se realiza sin minerales secundarios que contengan Mg, hay un aumento de la entrada de la fractura para los casos con soluciones iniciales con un pH menor a 12. Este aumento de la porosidad está causado por la disolución de calcita. Para los casos en que la solución inicial tiene un pH más alto, hay un sellado en el inicio de la fractura por precipitación de C-S-H, independientemente de la inclusión en el estudio de minerales secundarios que contengan Mg o no.

Los resultados de los cálculos incorporando una variación de temperatura a lo largo del tiempo muestran que la anomalía (pulso de calor) es demasiado breve para causar efectos significativos y duraderos.

A la vista de todos los resultados, el posible sellado de la fractura por las soluciones de pH elevado parece ser una posibilidad muy factible. Este sellado sería coherente con los resultados de los experimentos de laboratorio y de campo (Grimsel Test Site) realizados en el proyecto GTS-HPF y con los estudios previos de los efectos de penachos de pH elevado en diferentes tipos de rocas. El sellado de la porosidad de la fractura significaría que el flujo de la solución a través de la fractura se podría ralentizar o detener rápidamente. Sin embargo, para llevar a cabo los cálculos no se ha considerado ningún cambio a lo largo del tiempo en la porosidad y permeabilidad. Los resultados pueden considerarse como una estimación de la posible evolución química del sistema en caso de que el flujo de la solución continuara a pesar del sellado en la entrada de la fractura (desacoplamiento de propiedades químicas y físicas).

A mi padre

RESUMEN

El objetivo de este estudio es llevar a cabo una serie de cálculos, modelizando un transporte reactivo unidimensional, para simular la alteración de una fractura y el alcance de un penacho de pH elevado derivado de la circulación de soluciones hiperalcalinas a lo largo de dicha fractura. La modelización representa la fracturación localizada en la isla de Olkiluoto (Finlandia), donde se sitúan las instalaciones de ONKALO (posible futuro Almacenamiento Geológico Profundo de residuos radiactivos de alta actividad). Para impedir el paso del agua al repositorio está previsto sellar las fracturas con cemento. Sin embargo, el continuo contacto del cemento con el agua subterránea puede degradarlo, permitiendo el paso de un agua mucho más reactiva (penacho hiperalcalino).

La longitud del dominio unidimensional (fractura) es de 200 m y los cálculos se realizan para tiempos de hasta 10000 años. Se ha asumido una temperatura constante igual a 25°C, excepto en unos pocos casos donde se ha incorporado un pulso de calor de 200 años.

En este trabajo se presentan los resultados que se extraen de los cálculos realizados a partir del código de transporte reactivo *Retraso (REactive TRAnsport of SOlutes)*. En estos cálculos se han tenido en cuenta varias soluciones de pH elevado, varias velocidades de flujo y varias superficies de los minerales primarios.

Una conclusión que es común en todos los casos es que la roca no tiene la capacidad de amortiguamiento suficiente para reducir considerablemente el pH de las soluciones que circulan en el dominio de cálculo. Sin embargo, hay una cierta reducción del pH para (i) las condiciones de flujo más lento, (ii) los casos de pH más bajo, (iii) cuando se incluyen en los cálculos minerales secundarios que contienen Mg, y (iv) cuando las superficies de reacción de los minerales primarios son más grandes (debido por ejemplo a la presencia de una harina de falla).

Otra observación importante es que los resultados son muy diferentes dependiendo de la inclusión o no de minerales secundarios que contengan Mg en los cálculos (brucita, saponita). En la mayoría de los casos, si se incluyen los minerales secundarios con Mg, la precipitación de brucita y saponita causa el sellado de la porosidad en la entrada de la fractura. Por otra parte, si la modelización se realiza sin minerales secundarios que contengan Mg, hay un agrandamiento de la entrada de la fractura para los casos con soluciones iniciales con un pH menor a 12. Este aumento de la porosidad está causado por la disolución de calcita. Para los casos en que la solución inicial tiene un pH más alto, hay un sellado en el inicio de la fractura por precipitación de C-S-H, independientemente de la inclusión en el estudio de minerales secundarios que contengan Mg o no.

Los resultados de los cálculos incorporando una variación de temperatura a lo largo del tiempo muestran que la anomalía (pulso de calor) es demasiado breve para causar efectos significativos y duraderos.

A la vista de todos los resultados, el posible sellado de la fractura por las soluciones de pH elevado parece ser una posibilidad muy factible. Este sellado sería coherente con los resultados de los experimentos de laboratorio y de campo (Grimsel Test Site) realizados en el proyecto GTS-HPF y con los estudios previos de los efectos de penachos de pH elevado en diferentes tipos de rocas. El sellado de la porosidad de la fractura significaría que el flujo de la solución a través de la fractura se podría ralentizar o detener rápidamente. Sin embargo, para llevar a cabo los cálculos no se ha considerado ningún cambio a lo largo del tiempo en la porosidad y permeabilidad. Los resultados pueden considerarse como una estimación de la posible evolución química del sistema en caso de que el flujo de la solución continuara a pesar del sellado en la entrada de la fractura (desacoplamiento de propiedades químicas y físicas).

Palabras clave: modelización, pH, fractura, porosidad, C-S-H, brucita, saponita, portlandita, cemento

RESUM

L'objectiu d'aquest estudi és dur a terme una sèrie de càlculs, modelitzant un transport reactiu unidimensional, per simular l'alteració d'una fractura i l'abast d'una ploma de pH elevat derivat de la circulació de solucions hiperalcalines al llarg d'aquesta fractura. La modelització representa les fractures localitzades a l'illa de Olkiluoto (Finlàndia), on se situen les instal·lacions de ONKALO (possible futur Emmagatzematge Geològic Profund de residus radioactius d'alta activitat). Per impedir el pas de l'aigua al dipòsit està previst segellar les fractures amb ciment. No obstant, el continu contacte del ciment amb l'aigua subterrània pot degradar-lo, permetent el pas d'una aigua molt més reactiva (ploma hiperalcalina).

La longitud del domini unidimensional (fractura) és de 200 m i els càlculs es realitzen per a temps de fins a 10.000 anys. S'ha assumit una temperatura constant igual a 25 ° C, excepte en uns pocs casos on s'ha incorporat un pols de calor de 200 anys.

En aquest treball es presenten els resultats que s'estreuen dels càlculs realitzats a partir del codi de transport reactiu *Retraso (REactive TRAnsport of SOlutes)*. En aquests càlculs s'han tingut en compte diverses solucions de pH elevat, diverses velocitats de flux i diverses superfícies dels minerals primaris.

Una conclusió que és comú en tots els casos és que la roca no té la capacitat d'amortiment suficient per reduir considerablement el pH de les solucions que circulen en el domini de càlcul. No obstant això, hi ha una certa reducció del pH per a (i) les condicions de flux més lent, (ii) els casos de pH més baix, (iii) quan s'inclouen en els càlculs minerals secundaris que contenen Mg, i (iv) quan les superfícies de reacció dels minerals primaris són més grans (degut per exemple a la presència d'una farina de falla) .

Una altra observació important és que els resultats són molt diferents depenen de la inclusió o no de minerals secundaris que continguin Mg en els càlculs (brucita, saponita). En la majoria dels casos, si s'hi inclouen els minerals secundaris amb Mg, la precipitació de brucita i saponita causa el segellat de la porositat a l'entrada de la fractura. D'altra banda, si la modelització es realitza sense minerals secundaris que continguin Mg, l'entrada de la fractura es fa més gran per als casos amb solucions inicials amb un pH menor a 12. Aquest augment de la porositat està causat per la dissolució de calcita. Per als casos en què la solució inicial té un pH més alt, hi ha un segellat en l'inici de la fractura per precipitació de C-S-H, independentment de la inclusió en l'estudi de minerals secundaris que continguin Mg o no.

Els resultats dels càlculs incorporant una variació de temperatura al llarg del temps mostren que l'anomalia (pols de calor) és massa breu per causar efectes significatius i duradors.

A la vista de tots els resultats, el possible segellat de la fractura per les solucions de pH elevat sembla ser una possibilitat molt factible. Aquest segellat seria coherent amb els resultats dels experiments de laboratori i de camp (Grimsel Test Site) realitzats en el projecte GTS-HPF i amb els estudis previs dels efectes de plomes de pH elevat en diferents tipus de roques. El segellat de la porositat de la fractura significaria que el flux de la solució a través de la fractura es podria alentir o aturar ràpidament. No obstant, per dur a terme els càlculs no s'ha considerat cap canvi al llarg del temps en la porositat i permeabilitat. Els resultats poden considerar-se com una estimació de la possible evolució química del sistema en cas que el flux de la solució continués malgrat el segellat a l'entrada de la fractura (desacoblament de propietats químiques i físiques).

Paraules clau: modelització, pH, fractura, porositat, C-S-H, brucita, saponita, portlandita, ciment

ABSTRACT

The objective of this study is to perform a series of scoping calculations (one-dimensional reactive transport modeling) simulating the alteration of a fracture and the extension of the high-pH plume arising from the circulation of hyperalkaline solutions along the fracture. The modeling represents a fracture located on the island of Olkiluoto (Finland), where ONKALO facilities are located (possible future Deep Geological Repository of high level waste). Injecting of cement is expected to seal the fractures and prevent the flow of water to the galleries of the repository. However, the continuous contact with ground water can degrade the cement, allowing the flow of a much more reactive solution (hyperalkaline plume).

The length of the one-dimensional domain is 200 m and calculations were performed for times up to 10000 years. A constant temperature equal to 25°C was assumed in the calculations, except in a few cases where a short-lived (200 a) heat pulse was incorporated into the calculations.

A series of scoping calculations covering a range of different high-pH solutions, flow velocities and primary mineral surface areas were performed. The calculations were performed with the Retraso (REactive TRAnsport of SOlutes) reactive transport code.

A conclusion that is common to all the cases is that the rock does not have sufficient buffering capacity to significantly reduce the pH of the circulating solutions within the calculation domain. However, there is some reduction of pH for (i) the slowest flow conditions, (ii) the lowest pH cases, (iii) when Mg-containing secondary minerals are included in the calculations, and (iv) when reactive surface areas of the primary minerals are larger (due, for instance, to the presence of fault gouge).

Another important observation is that there is a significantly different result depending on the inclusion or not of Mg-containing secondary minerals (brucite, saponite) in the calculations. In most cases, if Mg secondary minerals are included, the precipitation of brucite and saponite causes the sealing of porosity at the fracture inlet. On the other hand, if the modeling is performed without Mg secondary minerals, there is an increase in porosity at the fracture inlet for the cases with incoming solutions with pH less than 12. This increase in porosity is caused by the dissolution of calcite. For the highest pH cases, there is sealing of the fracture inlet by C-S-H, regardless of the inclusion of Mg-containing secondary minerals.

The results from the calculations incorporating a variable temperature history show that the temperature anomaly (heat pulse) is too short-lived to cause any significant and lasting effects.

In view of all the results, sealing of the fracture by the high-pH solutions seems to be a very definite possibility. This sealing would be consistent with the results of the laboratory and field (Grisel Test Site) experiments conducted within the GTS-HPF project and with previous studies of the effects of high-pH plumes on different types of rocks. The sealing of fracture porosity would mean that flow of solution through the fracture would slow down or stop rather quickly. However, no feedback between porosity and permeability changes was implemented in the calculations. The results can be considered as an estimate of the possible chemical evolution of the system in the case that fluid flow would continue despite the sealing of porosity at the fracture inlet (uncoupling of chemical and physical properties).

Keywords: modeling, pH, fracture, porosity, C-S-H, brucite, saponite, portlandite, cement

TABLE OF CONTENTS

1. INTRODUCTION.....	2
2. BACKGROUND	3
2.1. RADIOACTIVE WASTE	3
2.2. DEEP GEOLOGICAL REPOSITORY – HOW IT WORKS	3
2.2.1. Definition and characteristics	3
2.2.2. Engineering barriers (artificial).....	4
2.2.3. Natural barriers.....	7
2.3. INTERNATIONAL SITUATION.....	9
2.4. SITUATION IN FINLAND.....	11
2.5. ONKALO	12
2.5.2. Current status of work in Onkalo	12
2.5.3. Geological context.....	13
2.5.4. Olkiluoto lithology.....	14
2.5.5. Olkiluoto brittle deformation (fractures).....	15
2.6. GROUTING AND POSSIBLE HYPERALKALINE PLUME	16
3. OBJECTIVE.....	18
4. METHODOLOGY	19
4.1. MODELCODE AND GOVERNING EQUATIONS	19
4.2. CONCEPTUAL MODEL AND PARAMETERS.....	23
5. RESULTS.....	34
5.1. REFERENCE CASES	34
5.1.1. $Q = 631 \text{ l/a}$, pH 10.5, no Mg-containing secondary minerals.....	35
5.1.2. $Q = 631 \text{ l/a}$, pH 10.5, with Mg-containing secondary minerals.....	35
5.1.3. $Q = 631 \text{ l/a}$, pH 12, no Mg-containing secondary minerals.....	36
5.1.4. Conclusions.....	36
5.2. INITIAL CASES. COMPARISON OF $Q = 3154, 631, 158, 32 \text{ l/a}$.	52
5.2.1. $Q = 3154, 631, 158, 32 \text{ l/a}$, pH 10.5, no Mg-containing secondary minerals	52
5.2.2. $Q = 3154, 631, 158, 32 \text{ l/a}$, pH 10.5, with Mg-containing secondary minerals	52
5.2.3. $Q = 3154, 631, 158, 32 \text{ l/a}$, pH 11, no Mg-containing secondary minerals	53
5.2.4. $Q = 3154, 631, 158, 32 \text{ l/a}$, pH 11, with Mg-containing secondary minerals	53
5.2.5. $Q = 3154, 631, 158, 32 \text{ l/a}$, pH 12, no Mg-containing secondary minerals.....	53
5.2.6. $Q = 3154, 631, 158, 32 \text{ l/a}$, pH 12, with Mg-containing secondary minerals	54
5.2.7. Conclusions	54
5.3. $Q=631 \text{ l/a}$. COMPARISON OF (A) HIGH-PH SOLUTION 1 ($T = 25^\circ\text{C}$), (B) HIGH-PH SOLUTION 1 (VARIABLE T), (C) HIGH-PH SOLUTION 2 (EXPERIMENTAL, $T = 25^\circ\text{C}$) AND (D) HIGH-PH SOLUTION 3 (EXPERIMENTAL, $T = 25^\circ\text{C}$)	75
5.3.1. $Q=631 \text{ l/a}$, lower pH cases, no Mg-containing secondary minerals	75
5.3.2. $Q=631 \text{ l/a}$, lower pH cases, with Mg-containing secondary minerals	76
5.3.3. $Q=631 \text{ l/a}$, intermediate pH cases, no Mg-containing secondary minerals	76
5.3.4. $Q=631 \text{ l/a}$, intermediate pH cases, with Mg-containing secondary minerals	77
5.3.5. $Q=631 \text{ l/a}$, higher pH cases, no Mg-containing secondary minerals.....	77
5.3.6. $Q=631 \text{ l/a}$, higher pH cases, with Mg-containing secondary minerals	77
5.4. $Q = 631 \text{ l/a}$, PH = 10.5. COMPARISON OF REFERENCE CASE WITH A CASE WITH LARGE SURFACE AREAS (X100) FOR PRIMARY MINERALS.....	100
6. DISCUSSION AND CONCLUSIONS	106
ACKNOWLEDGEMENTS.....	114
REFERENCES.....	115

1. INTRODUCTION

Currently, **radioactive materials** are used in several areas of human activity such as medicine, industry, research, education and energy production. One of the problems of nuclear energy is the generation of **radioactive waste**. These wastes must be properly isolated until the virtual disappearance of its activity. **Deep geological repository** seems the most suitable option for final disposal of this waste. Deep geological repository is based on isolating the waste in a confining rock many meters deep. For this, we have to find a rock with hydraulic, mechanical, geochemical, structural and stability characteristics suitable for optimal isolation. One of these rocks may be crystalline rocks such as granites and gneisses. Their main problem is the existence of fractures, through which radionuclides may be transported. To improve on isolation, fractures of the confining rock may be sealed by injecting cement to inhibit the flow of water to store the waste storage. However, the interaction of groundwater with cement can induce the formation and liberation of hyperalkaline solutions along fractures.

Thus, the objective of this study is the realization of **numerical modeling** to investigate the effect on the mineralogy of the host-rock, caused by the hyperalkaline solution. At the same time, it studies the capacity of the host-rock to neutralize the solution.

The model aims to represent the Deep Geological Repository, currently being developed in **Olkiluoto**, Finland. This repository is built in a large rock massif formed by gneiss, which include some fractures. Injecting of cement is used to seal the fractures and prevent the passage of water to the galleries of the repository. However, the cement could deteriorate over time by the contact with water. This would cause more water to pass the cement and, consequently, increase the alkalinity by reacting with it. When this hyperalkaline water flows through the fracture, it reacts with the rock through dissolution-precipitation reactions.

The reactive transport modeling will try to find out which minerals are dissolved and which precipitated along the fracture over time, and evaluate possible changes in the fracture porosity.

The results presented in this work are published by POSIVA in a report (Montori et al., 2008).

2. BACKGROUND

Before starting with the subject of the project it is necessary to understand what a deep geological repository is, besides knowing the context of the study area. Also, it is important to describe the grouting and possible hyperalkaline plume.

The information presented in the following chapters (2.1, 2.2 and 2.3) is based largely on the compilation published by Astudillo (2001) and Badillo-Almaraz and Vargas (2007).

2.1. Radioactive Waste

The radioactive wastes are materials that contain radioactive isotopes above a legally established level. They are often byproducts of a nuclear process, such as nuclear fission, but they can also be generated during the processing of fuel for reactors or nuclear weapons or in medical applications such as radiotherapy or nuclear medicine. Residues are classified into Low and Intermediate Level West (LILW), with half-lives of radioactive isotopes at or below 30 years, and High Level Waste (HLW), with radioactive isotopes with half-lives exceeding 30 years.

These wastes must be properly isolated and confined until their activity has almost disappeared. It is believed that this occurs 10 times after their half-life. For the LILW is sufficient to isolate them in surface storage. But for the HLW, we need other final management systems to ensure their isolation and confinement for tens or hundreds of thousands of years.

Deep geological repository seems the most appropriate, safe and viable option for the final management of this waste. The design of this type of storage has developed a breakthrough in recent years. The following section summarizes its performance and characteristics.

2.2. Deep geological repository – how it works

2.2.1. Definition and characteristics

Deep geological repository (DGR) is the isolation of waste, whether fuel elements or high level waste, by designing a series of natural and artificial barriers to a depth of between 300 and 800 meters (see Figure 1).

This type of storage is based on the confining potential that certain geological formations have, provided they are stable, have a great thickness and a holding capacity without preferential migration pathways. This fact is reflected in many deposits (oil, gas, metals, etc.) that have been confined for millions of years without contact with the atmosphere in places that have met a number of geological, geochemical, structural and hydrogeological requirements.

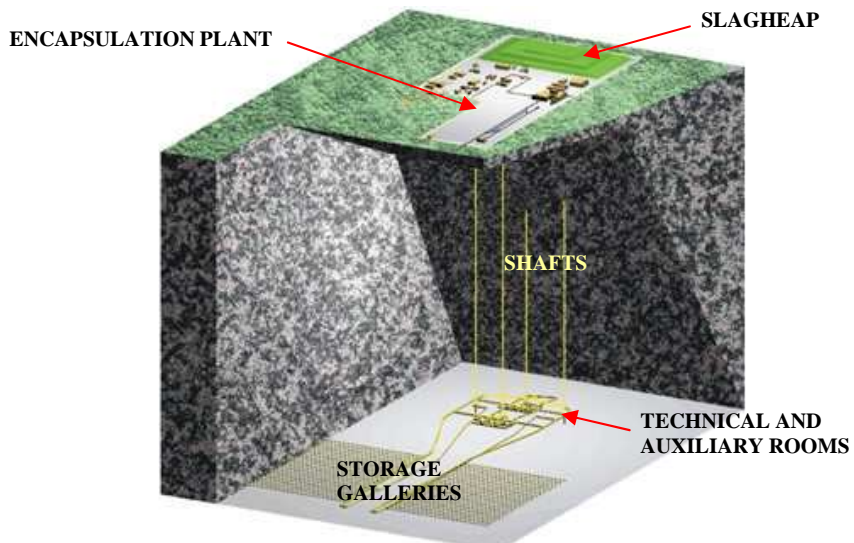


Figure 1 - Schematic of a repository from Astudillo (2001).

The operation of the DGR is based on the so-called multi-barrier principle, which involves combining a series of artificial and natural barriers to isolate waste from the biosphere (Figure 2). Each of the barriers will impose conditions of isolation and specific delay, with a redundant system as a whole.

With the imposition of such barriers, the aim is to maximize the transit time of any stored radionuclides that could be released, so that if they were to reach the biosphere, their activity had declined sufficiently to achieve an absence of undesirable impact to humans and the environment.

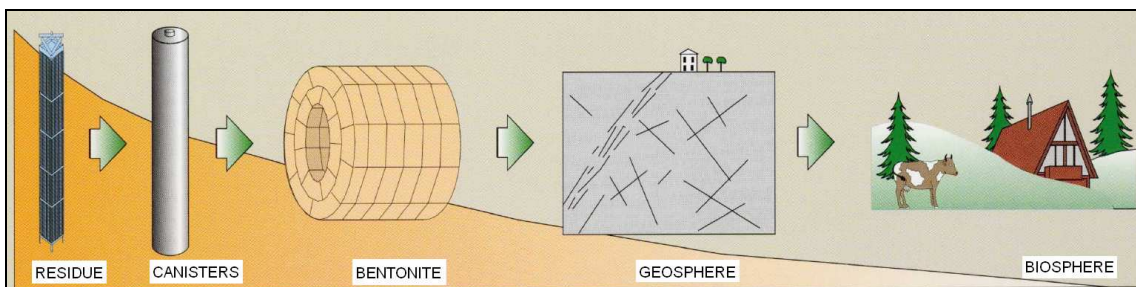


Figure 2 - Artificial and natural barriers. Image from Salamanca's University website (<http://ocw.usal.es/ciencias-experimentales/gestion-de-residuos-radiactivos/contenidos>).

2.2.2. Engineering barriers (artificial)

The engineered barriers are designed considering the characteristics of the host rock and the conditions of pressure, temperature and radiation to which will be subject in the different phases of long-term operation of the facility. On the other hand, they must be connected with the natural barrier system.

The components of these barriers must meet certain basic requirements:

- Isolate the repository from water from the geological barrier.
- Provide mechanical protection against possible seismic or disruptive events.
- Maximum retardation of radionuclide release
- Dissipation of heat from the waste and gas from corrosion of the containers

The components of the artificial or engineering barriers are:

- A. The chemical form of the waste itself.
- B. The storage metal canisters.
- C. The filling and sealing materials (engineered barrier of compacted clay).

A. Chemical form of the residue

The solubility of materials containing radionuclides is low and offers a high resistance to corrosion. Therefore, if the site is appropriate and barriers are well designed and built, it would take millions of years to complete dissolution because of the small volume of water which could be in contact with the waste.

B. Metal storage canisters

The canisters are used to contain the high-level waste, being in direct contact with it. They are a basic component within the multi-barrier concept of a repository, both during their operational phase and the long term. During the operational phase should be able to tightly confine waste and protect it structurally against any tension that might occur in the handling process, in addition to dissipate heat. Furthermore, it is important to provide biological shielding to allow handling.

Once the phase of handling and repository construction is finished, the canisters should confer structural strength against ground movement, slowing the arrival of water to waste and dissipating heat properly. It also has the function of retarding the release of the radionuclides, due to the interaction between radionuclides and canister degradation products.

The capsules must be of materials that dissipate heat well, corrosion resistant (to slow the arrival of water to waste), high durability (to protect mechanically to waste) and stable forehead to radiation.

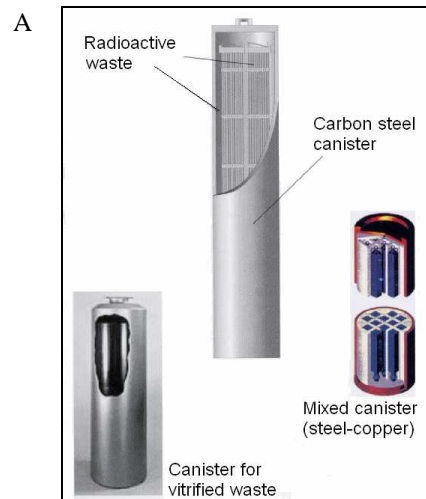


Figure 3 – Examples of metal storage canisters. (A) image from Astudillo (2001); (B) image from Wikipedia website (<http://en.wikipedia.org/wiki/KBS-3>).

The most common materials for making capsules are copper, titanium and carbon steel (see Figure 3). Copper is thermodynamically stable and has high resistance to corrosion; however, its mechanical strength is lower than other materials like steel. On the other hand, titanium materials can not guarantee certain durability because, although they have a high mechanical and corrosion strength, they are sensitive to localized corrosion and become brittle in presence of H₂. Finally, carbon steel capsules are mechanically very resistant and corrosion behavior is good. However, they can generate accumulations of gas and have a shorter service life.

C. Engineering barrier of compacted clay

Between the canisters and the geological formation, a type of compacted clay that allows the sealing of the repository is emplaced. The chosen clay material is bentonite (Figure 4), commonly originated from the alteration of volcanic rocks (volcanic glass). Bentonite mostly contains clay minerals of the smectite group. These clay minerals are phyllosilicates, with structural features that confer their spectacular properties of hydration, sealing and retention.

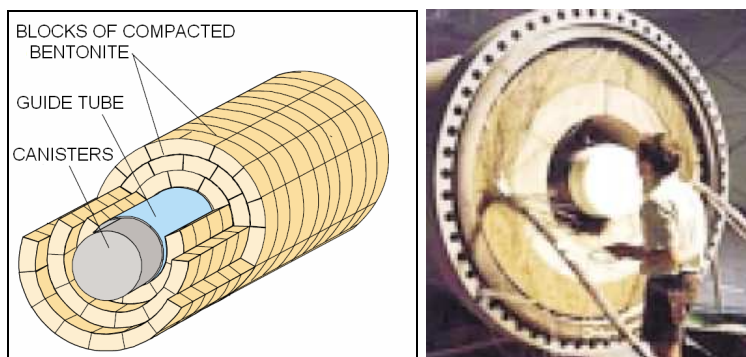


Figure 4 – Engineering barrier of compacted clay (bentonite).
Images retrieved from Astudillo (2001)

The properties of bentonite are:

i) Hydro-mechanical properties.

The bentonite has the ability to absorb water, varying in volume and increasing its plasticity thereby causing the sealing of the fractures and fissures of the repository environment and protecting it mechanically from ground deformations. Its low permeability slows the arrival of water. Also bentonite has adequate capacity to dissipate heat and gas (when saturated).

ii) Geochemical properties.

- High cation exchange capacity to maintain relatively constant water chemistry, being able to retain radionuclides.
- High specific surface area that contributes to a significant retention of radionuclides and to conservation of water chemistry.

- Long-term stability against chemical and physical changes because it is a very stable natural material.

Thanks to these properties, the bentonite barrier has the ability to:

- Minimize the volume and flow of water: The minimization of the access of water to the metal canister and the residue. Hydrated bentonite seals the fractures and fissures generated on the excavation.
- Constant water chemistry: It has the ability to stabilize and homogenize the chemical composition of water.
- Mechanical protection: It holds the mechanical stresses from the geological barrier, thus protecting the container from mechanical deformation of the ground motion.
- Retardation: It delays the transport to the geosphere of radionuclides that can be liberated.
- Heat dissipation: It dissipates the heat in the waste and the gas generated in the corrosion of containers.

2.2.3. Natural barriers

Natural barriers play a key role in the storage of waste, since they will influence the operation of other barriers and, in turn, are responsible for longer-term safety of the system, even considering the degradation of engineered barriers and the occurrence of undesirable events.

They are divided into two systems: biosphere, which represents the whole of ecosystems (soil, water, living things, etc.) that receive the impact of the repository, and geosphere, which is the geological formation where the repository is located and the waters and gases contained in it. The latter has to prevent radionuclides, which come from the repository and that are carried by groundwater, from reaching the biosphere in short periods of time.

The geological barrier is defined by the principle that nature has a great capacity for retention and preservation, as demonstrated by the large deposits preserved for millions of years. For this reason, it is essential a good selection process and characterization for the identification of geological formations with the hydraulic, mechanical, geochemical, structural and stability characteristics appropriate to meet the basic requirements that are required for a geological barrier.

The functional requirements of the geological formation for working as a barrier are:

- Protect the set of engineered barriers, ensuring stable conditions for physical-chemistry, hydraulics, mechanics and geochemistry.
- Ensuring a low water flow, slow and steady in the repository.
- Preventing migration of radionuclides from the repository and to biosphere.
- Allow constructive and operational viability of the repository.
- Isolate the repository from human activity.

Furthermore, to meet these requirements, geological repository must have:

- Lithological uniformity and structural simplicity.
- Thickness, depth and size large enough to isolate the repository from natural processes or human activities.
- Tectonics and seismic stability.
- Low permeability and hydraulic gradient.
- Conditions for retention of radionuclides (reducing and retardation capacities, immobilization).
- Ability to perform or simulate its operation using numerical modeling.

The lithologies of geological formations that meet these characteristics may be very different. However, at present, the main lithologies that are considered at international level are: crystalline rocks (granites, gneisses), clay rocks (plastic and compacted) and evaporite rocks (stratiform and diapirs). This does not exclude other lithologies that may meet the conditions above (volcanic tuff, schists, etc.).

Below are the most important features of the main lithologies:

A. Crystalline rocks (granites, gneisses)

They originate from the solidification of magma within the lithosphere. They can rise to shallow levels in orogenic processes. Also, they can be subject to the subsequent stages of geological deformation that may produce fracturing at all levels, erosion, etc. This group also includes the metamorphic derivatives of these igneous rocks.

The crystalline rocks are characterized by:

- Low permeability.
- Low solubility of the minerals they contain.
- Variable chemical retention capacity and high redox capacity.
- High resistance to mechanical and chemical alteration.
- Tectonic stability
- Moderate thermal conductivity.
- Stable during excavation
- High compressive strength.
- Diffusive transport of solutes in the matrix and advective/dispersive transport in fractures and fissures.

B. Clay rocks

Clay rock is any type of rock containing a high proportion of clay fraction or clay minerals. This group includes a wide spectrum of lithologies, ranging from non-consolidated clays and muds to low-grade metamorphic rocks. They are formed in sedimentary environment and, over time, may have undergone consolidation processes, with expulsion of water and precipitation of minerals (diagenesis) giving rise to rocks

composed of clay minerals, with a variable degree of compaction, together with other minerals that may have precipitated (carbonates, sulfates, silica, etc.).

According to its origin, hydraulic, mechanical and geochemical properties can be very variable, but they are always characterized by:

- Very low permeability.
- Diffusive transport of solutes.
- High retention capacity.
- Variable plasticity and self-sealing capacity
- Low thermal conductivity.
- Low solubility of their minerals.
- Lower resistance to erosion.
- Need for support systems during excavation.
- Mineralogical / chemical homogeneity
- High salinity of pore waters.

C. Evaporitic rocks

These are sedimentary rocks originating from the precipitation of salts by evaporation of water or from high-salinity brines. The rocks are made mainly of chlorides, sulfates and carbonates.

These salts may have been covered by later materials, producing recrystallization and adaptation to new conditions of pressure and temperature (formation of rock salt). The salts have a much lower density than the rest of sedimentary rocks, high thermal conductivity and plastic behavior. This allows the salt to be mobilized, ascending to lower pressure or loading areas (salt diapirs). Among the salts, halite (NaCl), either as a stratiform deposit or a diapir, is considered a favorable lithology for a repository.

The main features are:

- Very low permeability and porosity.
- High thermal conductivity.
- Little or no fracturing, due to its plasticity
- Self-sealing properties.
- Easy excavation.
- Low retention capacity.
- High erosion and dissolution.
- Very low water content.

2.3. International situation

Internationally, it is considered that the Deep Geological Repository (DGR) is the safest and most viable solution for the end management of high-level radioactive waste. Many countries are developing specific technology for making it operational.

The most advanced country in this type of storage is the **United States**, since it already has a plant in operation called Waste Isolation Pilot Plant (WIPP), located in Carlsbad (New Mexico). The DGR is built in stratiform salt formations at a depth of 600 m. and is designed to house high-level radioactive waste from the American military program. Preparations are also under way for another repository for civilian source HLW in Yucca Mountain (Nevada). This facility will be located in a volcanic tuff formation of the Nevada desert.

In the Americas there are two countries that are making progress in this area, Canada and Argentina.

Canada has developed the technology and the concept of DGR, focusing it on the storage in granites. The project is technically feasible but it needs a program to gain public support. Studies have been carried out by firms Atomic Energy of Canada Limited (AECL) and Ontario Power Generation. This country has an Underground Laboratory in granites in Pinawa (Winnipeg). It is also considering building a waste storage for low and intermediate activity in clayey limestones (King, 2006).

In the case of **Argentina**, since the 80's they are trying to implement this type of storage, but it is being hampered by social rejection. For this reason, it has developed a Strategic Plan for Radioactive Waste Management where communication to the public must be a key factor.

In Western Europe, many countries are developing this storage system. For example, **Germany** already decided in the 60's that all radioactive waste would be stored in deep geological formations and began research for the emplacement of waste in salt deposits. The Gorleben salt dome was selected, based on economic criteria and geoscience. However, in recent years its development has slowed down. A more complete analysis on gas generation, human intrusion, recoverability, etc is being performed, together with the search for other potential sites.

The management of high level waste in **France** is based on three programs, one on partitioning and transmutation, one on long-term temporary storage and a third on deep geological repository. Since 1999 there is an underground laboratory at Bure (Meuse/Haute-Marne) in a compacted clay of Callavo-Oxfordian age. Research to characterize these clays and analyze its viability as a repository is under way.

The program of geological storage in **Sweden** is developing from underground laboratories (Stripa and Aspo) to make the necessary scientific studies and to develop technologies. Simultaneously, a site selection plan has been used to choose three possible areas: Oskarshamm, Tierp and Osthamar.

In addition, **Switzerland** has the Grimsel underground laboratory in granite and Mt Terri underground laboratory in clay for the technological and scientific development of the DGR. . In turn, Switzerland has a temporary storage for all types of radioactive waste in Würenlingen (Zwilag).

In the case of **Belgium**, studies have focused on storage in plastic clays. An underground laboratory called HADES-URL has been created in Mol.

The Netherlands is also interested in developing this type of storage, but it will only be allowed if it is shown that the isolated waste may be recoverable for a long period of time.

Among the countries of Eastern Europe, **Russia** has been doing injections of liquid radioactive waste in deep geological formations since the 60's. A plan for the identification of low-permeability deep geological formations is also under way.

Ukraine, the third largest producer of radioactive waste, plans to build a DGR in 2030 that would be located in crystalline rocks near Chernobyl.

Asian countries such as **China** and **Japan** have developed studies to search for possible sites of DGR. China has selected a granitic area of the Gobi desert for that purpose. Japan is developing two underground rock laboratories to investigate the feasibility of the disposal of high level waste. One of them is in crystalline rock (Mizunami) and the other one in sedimentary rock (Honorobe).

Concerning the situation in **Spain**, since 1987 studies have been conducted for the acquisition of knowledge for the disposal of waste in DGR, having developed generic designs storage systems for three types of geological formations: clay, granite and salt. However, the Sixth Plan for Radioactive Waste Management approved by the government in July 2006 gave priority to the availability of temporary storage for the waste for the next 60 years. Thus, decisions about the final disposal solution have been postponed for about 15 years.

2.4. Situation in Finland

According to Astudillo (2001), together with Sweden, Finland currently holds the EU's most advanced program in the field of final disposal of spent nuclear fuel. It has been preparing for storage for over 25 years.

In 1999, after conducting a program of detailed site selection and environmental impact assessment, the island of Olkiluoto, located in the municipality of Eurajoki, was chosen as the most suitable site for the realization of a DGR. Subsequently, in December 2000, the project was approved by the Government.

Construction work of underground facilities for the rock characterization site, known as ONKALO, began in June 2004. Alongside, several investigations are being performed to characterize in detail the possible future repository. It is planned to be completed by 2012, with an operational DGR possible for 2020.

2.5. Onkalo

The information presented in the following chapters (2.5.1 and 2.5.2) is based on the data of the Posiva website (<http://www.posiva.fi/en>).

2.5.1. Geographical Location

Onkalo is the name given to the underground research facility built for the characterization of rock for the disposal of spent nuclear fuel in Finland. It is situated on the island of Olkiluoto in the municipality of Eurajoki, in southwestern Finland, as shown in Figure 5.

The main information presented in this chapter is based on the article published by Soler and Mäder (2006).

2.5.2. Current status of work in Onkalo

The Posiva company began building Onkalo in June 2004 and from the beginning of its construction in situ investigations have been done. Onkalo design (shown in Figure 6) consists of an access tunnel of 5.5 m wide and 6.3 m high and a slope of 10%. The project was completed with three vertical shafts, one for staff and two for ventilation, a characterization level and an area designated for technical and support galleries.



Figure 5 – Location of the island of Olkiluoto in the Gulf of Bothnia in western Finland

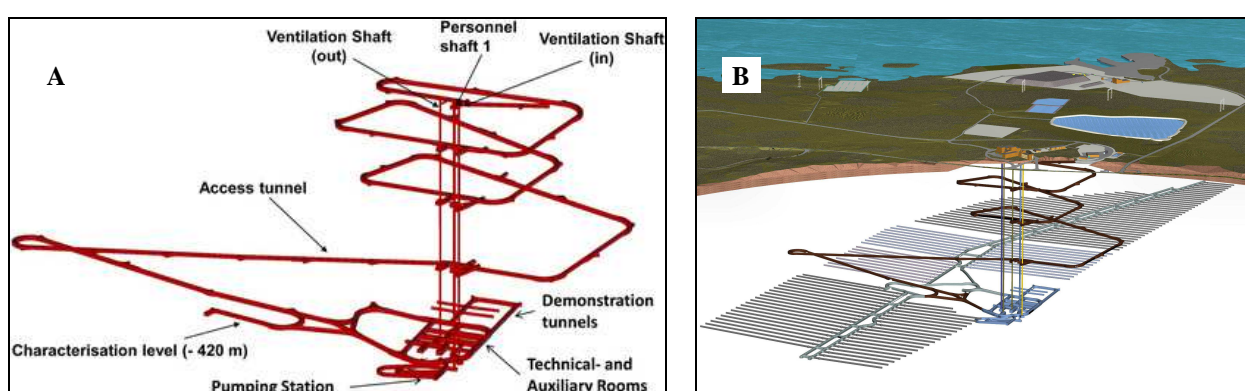


Figure 6 - Design Onkalo facilities.(A) Schematic structure of the facilities; (B) 3D view of the facilities. Diagrams taken from Posiva website (<http://www.posiva.fi/en>)

The underground tunnels, which will constitute the final reservoir of radioactive waste, are being excavated in Onkalo. These facilities currently serve as research base for the characterization of the area. In figure 7 areas already excavated can be seen.

During excavation, the data is being collected and geological, hydrological and geochemical researches are being carried out to characterize the reservoir rock. The excavation of the tunnel, besides facilitate the characterization of the rock, it also provides an opportunity to develop new techniques of excavation and final disposal techniques in realistic conditions. In future, these facilities may be used as an example of construction and of repository.

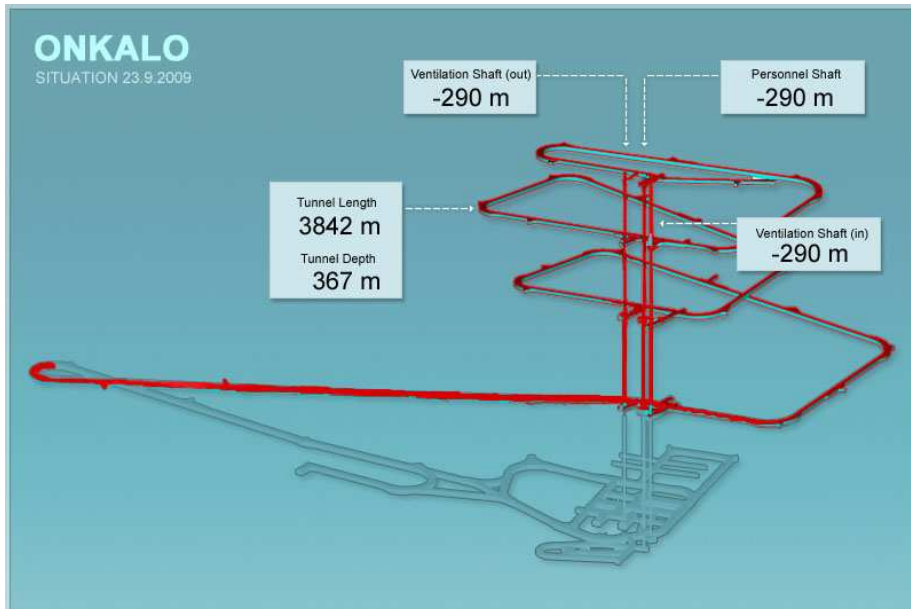


Figure 7 - Current status (September 2009) of underground excavations Onkalo.
Diagram taken from Posiva website (<http://www.posiva.fi/en>)

2.5.3. Geological context

To understand the origin of the lithology of the area it is necessary to understand the regional geology of Olkiluoto (summarized below from Kärki and Paulamäki, 2006).

Olkiluoto is located in the southern part of the Satakunta region, an area in southwestern Finland where the bedrock is composed of metasedimentary and metavolcanic rocks deformed and metamorphosed during the Paleoproterozoic Svecofennica orogeny, ca. 1910 - 1800 million years ago. This bedrock rock is composed of migmatites and high-grade mica gneisses that may contain cordierite, sillimanite or garnet porphyroblasts. Occasionally, mafic and intermediate volcanic amphibolites, uralite porphyrites and hornblende gneisses occur as interlayers in supracrustal sequences.

In the region there are also materials from the Mesoproterozoic (between 1.600-1.000 million years ago) originated in the cratonic states of Svecofennides. The oldest materials found in this Era are batholiths of granitic composition produced 1580 million years ago. Subsequently, approximately 1.400-1.300 million years ago, typical fluvial and deltaic sediments were deposited. These sediments, which were intruded at later stages by olivine diabase dikes, have been preserved by a graben structure.

The sequence of geological events that occurred in the study area is summarized according to the study of Mattila et al (2008):

- 1) 1.830-1.650 Ma: Compressive deformation related with the Svecofénnica orogeny (formation of thrust faults)
- 2) 1.650-1.550 Ma: Extensional tectonics related to the emplacement of granites (intrusion of diabase dikes and formation of Satakunta graben)
- 3) 1.560-1.270 Ma: Formation of strike-slip faults with reactivation of old structures
- 4) 1.270-1.100 Ma: Extensional period related to the onset of Sveconorwegian orogeny
- 5) 900-600 Ma: Neoproterozoic exhumation stage
- 6) 600-420 Ma: Platform sedimentation stage
- 7) 420-350 Ma: Foreland during the Caledonian orogeny stage
- 8) Opening of the North Atlantic and western elevation of Scandinavia
- 9) Neotectonic movements (postglacial and recent crustal movements)

2.5.4. Olkiluoto lithology

Olkiluoto rocks can be divided into four groups (Kärki and Paulamäki 2006, Andersson et al. 2007) that are gneisses, migmatites gneisses, TGG-gneisses (TGG = tonalite-granodiorite-granite) and pegmatitic granites. There are also diabase dikes that cut the previous groups. The following map (Figure 5) shows the disposition of these materials.

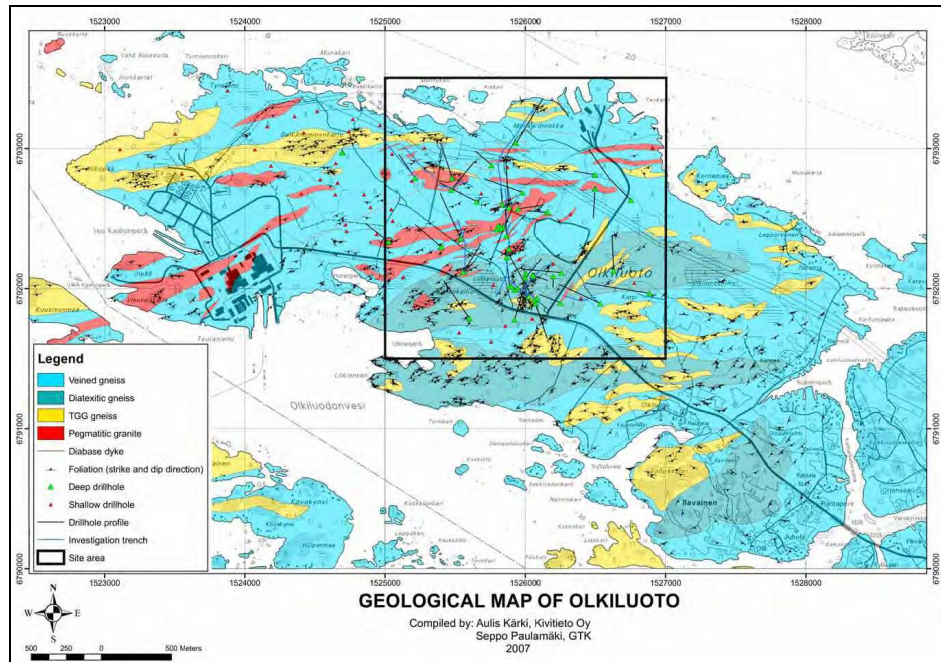


**Figure 8 - Olkiluoto lithologic map extracted from Mattila et al (2008).
The Olkiluoto area is boxed in black.**

The group of **gneisses** includes homogeneous quartz mica-bearing gneisses, banded mica gneisses and hornblende or pyroxene-bearing mafic gneisses. The **migmatitic gneisses** have about 20 - 40% of leucosoma. They can be divided into three subgroups

according to their migmatite structure: veined gneisses, stromatic gneisses, and diatexitic gneisses. The **TGG gneisses** are medium-grained, relatively homogeneous rocks that may have blastomylonitic foliation, but resemble plutonic, unfoliated rocks. **Pegmatitic granites** are leucocratic rocks that contain garnet, tourmaline and cordierite phenocrysts.

2.5.5. Olkiluoto brittle deformation (fractures)

From the previous explanation in the section: 2.5.3. *Geological context* and according to Mattila et al (2008), we can conclude that in the study area there are four main deformational phases (Figure 6) which are:

- A) Compressive deformation (1.830-1.650 Ma in age) in direction NW / SE to NWW/SEE related to Svecofénnica orogeny which causes the formation of faults.
- B) Extensional tectonics (1.650-1.550 Ma ago) related to the emplacement of granites, the intrusion of diabase dikes and the formation of graben Satakunta. The intrusion of diabase dikes occur in NEE-SWW direction. In this period old thrusts are reactivated with dip-slip component.
- C) Between 1560 and 1270 million years ago, compressive deformation with a very important strike-slip component very important forms strike-slip faults and reactivates ancient structures (the old faults are reactivated with strike-slip component).
- D) After the previous compressive period, there is evidence of several reactivation of faults in extensional regime (dip-slip component) in the Mesoproterozoic (related to the onset of Sveconorwegian orogeny), Neoproterozoic (states of exhumation) and Lower Cambrian (foreland sedimentation).

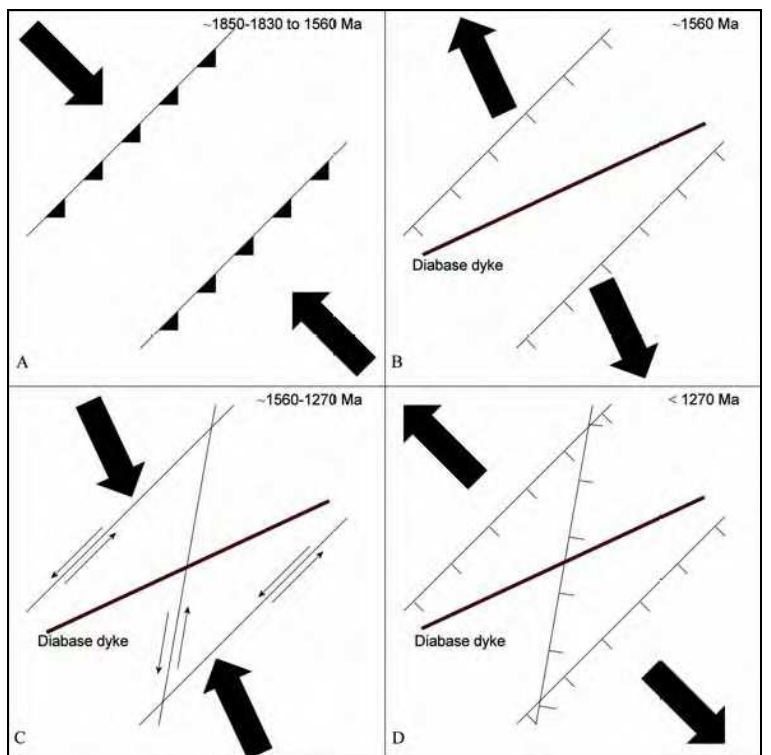


Figure 9 - Schematic representation (Mattila et al,2008) of brittle deformation at the island of Olkiluoto from 1850 Ma onwards. (A) Thrust with crustal shortening at about 1850-1830 Ma to 1560 Ma ago; (B) Extension with intrusion of diabase dykes (1560 Ma ago); (C) Formation of strike-slip faults with reactivation of older structures at approximately 1560-1270 Ma; (D) Extension and reactivation of existing structures after previous situations. Thick arrows indicate the direction of maximum crustal contraction or extension and thin arrows the sense of movement.

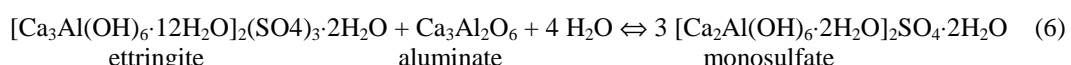
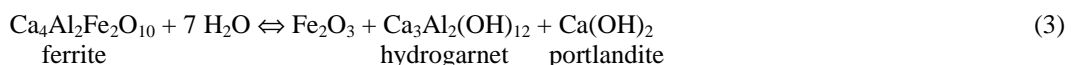
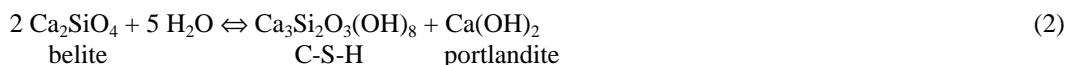
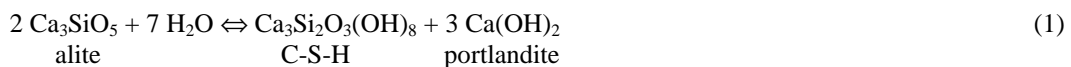
The faults generated during these deformational periods can act as water flow channels to the repository depth. These fractures can cause problems in the isolation of radioactive waste. The most conductive ones will be sealed with cement (grouting) to minimize water flow.

2.6. Grouting and possible hyperalkaline plume

The main information presented in this chapter is based on the article published by Soler and Mäder (2006).

Posiva is planning to inject cement (grouting) in the most conductive fractures near the repository, in order to reduce the flow of water.

According to Soler (2007), the hydration of Portland cement clinker is a complex process which consists of a series of successive chemical reactions. The main reactions of the mixture of water and gypsum with Portland cement clinker are:



As seen in these chemical reactions, the hydration of cement clinker (alite, belite, tricalcium aluminate, ferrite) and added gypsum causes the formation of portlandite, C-S-H gel, hydrogarnet, ettringite, monosulfate and iron oxide.

The interaction between groundwater and this cement causes the formation of high pH solutions (pH 12.5–13.5), mainly due to the dissolution of the portlandite (Ca(OH)_2) of the hydrated cement. These solutions may react with the rocks hosting the repositories and change their physical and chemical properties.

The evolution of the chemical composition of the solutions resulting from the degradation of cement in contact with groundwater is divided into different phases:

- **First stage:** the solution composition is dominated by the dissolution of the alkali hydroxides in the cement, giving an initial pH of about 13.5.

- **Second stage:** is dominated by the dissolution of $\text{Ca}(\text{OH})_2$ giving a pH of around 12.5.
- **Third stage:** is characterized by the dissolution of the CSH phases.
- Finally, phases other than CSH are dissolved (katoite, ettringite and secondary gibbsite). pH drops to normal groundwater values.

The hyperalkaline solutions associated with the first two stages are chemically very aggressive. That is to say, they are very far from equilibrium with respect to the minerals in the hosting rock formations. For this reason, they may induce the dissolution and precipitation of different mineral phases. The duration of the different stages depends on the amount of the cement and on the flux of groundwater circulating through the system. In principle, the duration of the first stage is short (exchange of a very few pore volumes in the cement). The main concern regards the second stage.

For grouting, Posiva is also planning to use special low alkali cement. This is why in our calculations, besides Ordinary Portland Cement (initially planned), we also use solution compositions corresponding to the leaching of low alkali cement, which has a smaller portlandite content.

3. OBJECTIVE

It is currently planned to use cement grout to seal conductive fractures at the ONKALO site in Finland (potential site for a deep geological repository for high-level radioactive waste). The interaction between groundwater and the grout may cause the formation and release of hyperalkaline solutions along these fractures (Fig. 10). The objective of this study was to perform a series of scoping calculations (one-dimensional reactive transport modeling) simulating the extension of the high-pH plume and its associated mineralogical alteration. The work was based on preliminary calculations by Lehikoinen et al. (2007).

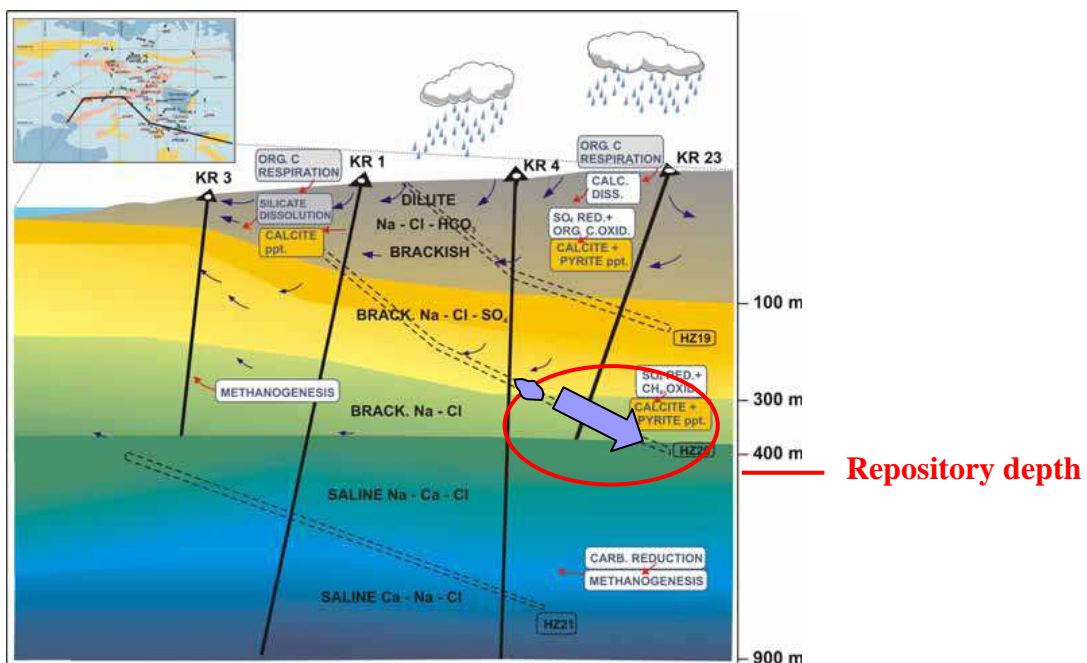


Figure 10 - Schematic cross section showing the concept behind the calculations. The grout used to seal the fracture could interact with groundwater, causing the release of hyperalkaline solutions. Cross section is from Andersson et al. (2007).

The goal was to perform a sensitivity analysis by changing the values of flow velocity, fracture aperture, solution composition (including the effects of using different types of cement) and temperature. The calculations were performed in a one-dimensional system in this first modeling effort. However, calculations would have to be performed in two or three dimensions to capture the possible evolution of the fluid flow field in a system subject to changes in porosity and permeability. Also, since a feedback between porosity and permeability changes was not implemented in the calculations, the results can be considered as an estimate of the possible chemical evolution of the system in the case that fluid flow would continue despite the sealing of porosity at the fracture inlet shown by the results (uncoupling of chemical and physical properties). Even under a spatially and temporally variable flow field, sealing of the fracture inlet would most probably impose an overall decrease in flow rates along the fracture or fracture system and a decrease in the extension of the high-pH plume in the direction of flow.

4. METHODOLOGY

4.1. Modelcode and Governing Equations

The calculations were performed with the Retraso reactive transport code (Saaltink et al., 2004), which numerically solves the equations of conservation of solute mass for each component in the system. For the calculations performed in this study, these equations were of the form

$$\frac{\partial(\phi U_j)}{\partial t} = \nabla \cdot (D \nabla U_j) - \nabla \cdot (q U_j) + R_j \quad j = 1, \dots, N_c \quad (1)$$

where U_j is the total concentration in solution of component or primary species j , ϕ is porosity, t is time, D is the effective diffusion coefficient plus the mechanical dispersion coefficient, q is the Darcy flux, R_m is the mineral dissolution (-) or precipitation (+) rate, v_{jm} is the stoichiometric coefficient of j in mineral m , and N_c is the number of primary species in the system.

The combined diffusion-dispersion coefficient D is given by

$$D = \alpha q + D_e \quad (2)$$

where α is the longitudinal dispersivity and D_e is the effective diffusion coefficient.

The reaction term R_j results from the sum of all the individual mineral-water reactions which affect the concentration of the j^{th} species

$$R_j = -\sum_{m=1}^{N_m} v_{jm} r_m \quad (3)$$

where r_m is the net rate of precipitation ($r_m > 0$) or dissolution ($r_m < 0$) of mineral per unit volume of rock, v_{im} is the number of moles of j per mole of mineral m , and N_m is the number of minerals present in the rock.

In order to describe how the reaction rate term R_j is treated in Retraso, it is useful at this moment to introduce the concepts of primary and secondary species. The total number of species in solution (N_{tot}), can be distributed between N_c primary species (also called components) and N_x secondary species. The number of primary species (N_c), which is the number of independent chemical components in the system, will be given by the total number of species (N_{tot}) minus the number of independent chemical equilibria relating them. The different equilibrium relationships can be written as the production or destruction of one mole of secondary species, and take the form

$$A_i \Leftrightarrow \sum_{j=1}^{N_c} v_{ij} A_j \quad (i = 1, 2, \dots, N_x) \quad (4)$$

where A_j and A_i are the chemical formulas of the primary and secondary species, respectively, and v_{ij} is the number of moles of primary species j in one mole of secondary species i . The chemical equilibria provide an algebraic link between the primary and secondary species via the law of mass action for each reaction. The concentration of a secondary species i is given by

$$X_i = K_i^{-1} \gamma_i^{-1} \prod_{j=1}^{N_c} (\gamma_j C_j)^{v_{ij}} \quad (i = 1, 2, \dots, N_x) \quad (5)$$

where the K_i are the equilibrium constants of reaction (8), and γ_j and γ_i are the activity coefficients of the primary and secondary species, respectively. The activity coefficients are calculated according to the extended Debye-Hückel formulation, given by

$$\log \gamma_i = -\frac{AZ_i^2 I^{1/2}}{1 + B\dot{a}_i I^{1/2}} + \dot{b}I \quad (6)$$

where Z is the ionic charge and I is the ionic strength. The parameter \dot{a}_i is an ion size parameter and is included in the thermodynamic database (Eq3nr database, Wolery et al., 1990). The parameters A , B and \dot{b} are dependent on temperature and are tabulated in Helgeson and Kirkham (1974).

The expression

$$U_j = C_j + \sum_{i=1}^{N_x} v_{ij} X_i \quad (7)$$

defines the total concentration of primary species j , U_j (Reed, 1982; Lichtner, 1985; Kirkner and Reeves, 1988). Also, in this formulation of the transport-reaction equation, it is assumed that the diffusion coefficients are the same for all the aqueous species (both primary and secondary).

The mineral reaction rate laws implemented in the code are of the form

$$r_m = \text{sgn}(\log[Q_m/K_m]) A_m \sum_r \left(k_{m,r} \prod_{i=1}^{N_c+N_x} a_i^p \right) f(\Delta G) \quad (8)$$

where sgn means sign, Q_m is the ion activity product, K_m is the equilibrium constant of the mineral dissolution reaction (ionic activity product at equilibrium), A_m is the mineral surface area per unit volume of rock, k_m is the growth or dissolution rate constant (in units of moles of mineral per unit surface area per time), a_i is the activity

of an inhibiting or catalyzing species, raised to an empirically determined power p , and $f(\Delta G)$ is a function describing the dependence of the rate on solution saturation state (this function guarantees that the rate is zero at equilibrium). The summation term refers to different parallel reactions for a given mineral. For instance, two or three parallel reactions are commonly used to be able to describe the rate under different pH conditions.

The rate constant at a given temperature ($k_{m,T}$) is calculated according to

$$k_{m,T} = k_{m,25} \exp\left(\frac{E_a}{R}\left(\frac{1}{T_{25}} - \frac{1}{T}\right)\right) \quad (9)$$

where $k_{m,25}$ is the rate constant at 25°C, E_a is the apparent activation energy of the reaction, R is the gas constant and T is temperature (K).

The ion activity product is defined as

$$Q_m = \prod_{j=1}^{N_c} a_j^{\nu_{mj}} \quad (10)$$

where a_j are the activities of the species making up the mineral m , and ν_{mj} are the stoichiometric coefficients. The effect of solution saturation state is given by the last term of Eq. (7), which can be expressed in terms of the Gibbs Free Energy of the reaction (ΔG)

$$f(\Delta G) = \left| \exp\left(M \frac{\Delta G}{RT}\right) - 1 \right|^n = \left| \left(\frac{Q_m}{K_m} \right)^M - 1 \right|^n \quad (11)$$

M and n are two positive numbers which are normally determined experimentally. If no experimental information is available, it is common practice to make both M and n equal to unity, which reflects the dependence of the net rate of an elementary reaction on solution saturation state, as derived from Transition State Theory (Lasaga, 1998).

Mineral grains are assumed to be spherical, with their whole surface area in contact with fluid (“floating” grains). Mineral volume fractions and surface areas are calculated according to

$$\phi_m = \frac{4}{3} \pi r_m^3 N_m \quad (12)$$

$$A_m = 4 \pi r_m^2 N_m \quad (13)$$

where r_m is the grain radius, and N_m is the number of grains per volume of rock (constant for each mineral).

Mineral volume fractions are updated by making use of the calculated reaction rates and the duration of the time increment for each time step along the simulation (amounts of mineral dissolved or precipitated at each time step). Grain radii and mineral surface areas are updated according to Eqs. 12 and 13.

The spatial discretization of the reaction-transport differential equations (Eq. 1) is done following the finite element method. The resulting algebraic non-linear equations are solved using Newton's method.

4.2. Conceptual Model and Parameters

The goal of the one-dimensional reactive transport calculations was to perform a sensitivity analysis of the possible effects of the high-pH plume by changing the values of flow velocity, fracture aperture, solution composition and temperature.

The length of the one-dimensional domain was 200 m and calculations were performed for times up to 10000 years. A constant temperature equal to 25°C was assumed in the calculations, except when otherwise indicated. Figure 2 shows the spatial discretization used in the 1D domain. Smaller elements (smaller Δx) were used near the fracture inlet. Initial porosity was 0.5 in all cases. Flow velocity was constant for each case, i.e. no coupling between changes in porosity and flow was taken into account. Constant values of the dispersivity ($\alpha=2\text{m}$) and effective diffusion coefficient ($D_e=5.0\text{E}-10 \text{ m}^2/\text{s}$) were also used. This point has to be taken into account when interpreting the results of the simulations. The boundary condition for the transport equation (Eq. 1) at the inlet was set to a mass flux equal to the water flow times the total aqueous concentration (U) for each component.



Figure 11 - Schematic diagram showing the dimensions and spatial discretization in the one-dimensional domain.

The initial set of cases (flow velocities, fracture apertures, solution compositions) that was taken into account is summarized in Table 1. Notice that the flow velocities are larger than the value of $1.6\times 10^{-4} \text{ kg/m}^2/\text{s}$ used by Lehikoinen et al. (2007). Table 2 shows the chemical composition of the solutions used for the transport boundary condition at the inlet. The different solutions are intended to simulate the leaching of a conventional cement (pH 12) or low-pH cements. The solution composition for the pH 12 case (Table 2) corresponds to the one reported by Lehikoinen et al. (2007). Solution compositions for the pH 10.5 and pH 11 cases were calculated by dilution of the pH 12 solution. For simplicity, iron (pyrite and Fe species in solution) was not included in the simulations, given the small amount of pyrite in the rock (2.5 vol%).

Based on experimental data supplied by Posiva (results from leaching experiments using hydrated cements with different compositions), additional compositions of the high-pH solutions were formulated (Tables 3a, 3b). Experiments had been performed at 12°C and 50°C, using two types of leaching solutions with different salinities. The experimental results at 12°C using the more saline leaching solution (OL-SR; conditions more similar to the simulated case; Table 3a) were used to formulate these compositions. An additional set of solution compositions, corresponding to the results of the leaching experiments at 12°C and using the fresh leaching solution (ALL-MR)

are included in the calculations (Table 3b). Notice that, unlike in the initial cases, the lower-pH compositions do not correspond to a dilution of the solution with the highest pH.

The composition of the initial solution (Olkiluoto groundwater) in the fracture was estimated from the data in Andersson et al. (2007) for a depth between 300 and 400 m. Equilibrium with respect to calcite, kaolinite, K-feldspar and quartz was also imposed. This composition is given in Table 4. Given the high flow velocities (Table 1) and small residence times of water along the fracture (0.32 to 3.2 a), the composition of the initial groundwater is not a determinant factor in the calculations.

Table 1 - Parameter values for the different modeling runs.

Q [l/a]	Q(kg/m ² /s)	pH	width [m]	volume aperture [m]
3154	10 ⁻²	10.5	1.0	0.010
3154	10 ⁻²	11		0.010
<u>3154</u>	<u>10⁻²</u>	<u>12</u>		<u>0.010</u>
631	5x10 ⁻³	10.5		0.004
631	5x10 ⁻³	11		0.004
<u>631</u>	<u>5x10⁻³</u>	<u>12</u>		<u>0.004</u>
158	2.5x10 ⁻³	10.5		0.002
158	2.5x10 ⁻³	11		0.002
<u>158</u>	<u>2.5x10⁻³</u>	<u>12</u>		<u>0.002</u>
32	10 ⁻³	10.5		0.001
32	10 ⁻³	11		0.001
<u>32</u>	<u>10⁻³</u>	<u>12</u>		<u>0.001</u>

Table 2 - Composition (pH and total concentrations in mol/kg_H₂O) of the high-pH solutions flowing into the fracture in the model. Initial cases. All three solutions are supersaturated with respect to brucite, sepiolite and saponites. The pH 12 solution is also supersaturated with respect to C-S-H (Ca/Si = 1.2, 1.667).

pH	Al	Carbonate	Ca	Cl	K	Mg	Na	SO4	SiO2
12	3.70E-07	7.50E-06	2.20E-02	7.98E-02	3.10E-04	2.50E-03	4.90E-02	6.50E-04	2.70E-04
11	2.59E-08	5.25E-07	1.54E-03	5.61E-03	2.17E-05	1.75E-04	3.43E-03	4.55E-05	1.89E-05
10.5	7.77E-09	1.58E-07	4.62E-04	1.69E-03	6.51E-06	5.25E-05	1.03E-03	1.37E-05	5.67E-06

The mineralogical composition of the rock (fracture) and the values of the mineral surface areas and porosity (Table 5) were based on those reported by Lehikoinen et al. (2007). Flat mineral surfaces originally measured on the fracture walls were converted into spherical grains filling the fracture. As a result, the smaller fracture apertures contain larger mineral surface areas (m²/m³fracture). To simulate initially small precipitation rates for the secondary minerals, small values of the initial surface areas (0.001 m²/m³) were used for the secondary precipitates.

Table 3a - Composition (pH and total concentrations in mol/kg_H₂O) of the high-pH solutions derived from experimental results using the saline leaching solution (OL-SR). Concentrations equal to 10⁻⁶ mol/kg_H₂O (shaded) correspond to measurements below detection limit. The 1st solution (pH 12.17) is supersaturated with respect to brucite and portlandite. The 2nd solution (pH 11.60) is supersaturated with respect to brucite and saponites. The 3rd one (pH 9.7) is supersaturated with respect to mesolite, scolecite, sepiolite, stilbite and saponites.

pH	Al	Carbonate	Ca	Cl	K	Mg	Na	SO4	SiO2
12.17	1.00E-06	1.00E-06	1.20E-01	4.20E-01	6.00E-04	1.00E-06	2.10E-01	2.30E-05	5.00E-06
11.60	1.00E-06	1.00E-06	1.10E-01	4.20E-01	6.00E-04	4.00E-06	2.10E-01	4.00E-05	2.00E-05
9.70	1.00E-06	1.00E-06	1.00E-01	4.10E-01	8.00E-04	2.00E-03	2.05E-01	8.00E-05	7.00E-05

Table 3b - Composition (pH and total concentrations in mol/kg_H₂O) of the high-pH solutions derived from experimental results using the fresh leaching solution (ALL-MR). Concentrations equal to 10⁻⁶ mol/kg_H₂O (shaded) correspond to measurements below detection limit. The 1st solution (pH 12.45) is supersaturated with respect to brucite and portlandite. The 2nd solution (pH 11.90) is supersaturated with respect to brucite and saponites. The 3rd one (pH 10.60) is supersaturated with respect to albite, illite, K-feldspar, quartz, laumontite, mesolite, scolecite, sepiolite, stilbite and saponites.

pH	Al	Carbonate	Ca	Cl	K	Mg	Na	SO4	SiO2
12.45	1.00E-06	1.00E-06	1.90E-02	1.60E-03	1.00E-04	1.00E-06	2.50E-03	3.00E-05	5.00E-06
11.90	1.00E-06	1.00E-06	4.00E-03	1.01E-03	1.50E-04	1.00E-06	2.50E-03	4.00E-05	1.00E-04
10.60	1.00E-06	1.00E-06	5.00E-04	1.79E-03	2.00E-04	3.00E-06	2.40E-03	2.50E-04	1.00E-03

Table 4 - Composition (pH and total concentrations in mol/kg_H₂O) of the initial solution in the fracture.

pH	Al	Carbonate	Ca	Cl	K	Mg	Na	SO4	SiO2
8	3.57E-08	9.42E-05	4.99E-02	2.38E-01	3.07E-04	4.00E-03	1.30E-01	2.63E-04	1.04E-04

The potential secondary minerals that were taken into account are C-S-H gel (5 different phases with different Ca/Si ratios, ranging from 0 –amorphous silica– to 1.67), brucite, portlandite, zeolites (analcime, laumontite, mesolite, natrolite, scolecite, stilbite, phillipsite, mordenite), sepiolite and saponites (Ca, H, K, Mg and Na saponites). The solubilities of the different minerals are from the Eq3nr database included with the code, except for the C-S-H gel. The solubilities of the phases corresponding to the C-S-H gel were calculated from the model given by Kulik and Kersten (2001).

All the reactions (speciation in solution and mineral reactions) and their associated equilibrium constants are given in Tables 6 and 7. Some calculations were run under variable temperature. Tables 8 and 9 show the parameters needed to calculate the equilibrium constants at temperatures different from 25°C. These parameters were derived from the original thermodynamic parameters in the Eq3nr database and Kulik and Kersten (2001).

Table 5 - Initial mineralogical composition (volume fractions and surface areas). Surface areas are reported for the 4 different values of fracture aperture (0.01, 0.004, 0.002 and 0.001 m).

MINERAL	V (m ³ /m ³)	A _{0.01} (m ² /m ³)	A _{0.004} (m ² /m ³)	A _{0.002} (m ² /m ³)	A _{0.001} (m ² /m ³)
Calcite	0.199	5.62E+01	1.41E+02	2.81E+01	5.62E+02
Kaolinite	0.067	2.52E+01	6.30E+01	1.26E+02	2.52E+02
Illite	0.075	2.84E+01	7.10E+01	1.42E+02	2.84E+02
Quartz	0.044	2.50E+01	6.25E+01	1.25E+02	2.50E+02
Cordierite	0.019	1.06E+01	2.65E+01	5.31E+01	1.06E+02
Albite	0.037	2.12E+01	5.31E+01	1.06E+02	2.12E+02
K-feldspar	0.033	1.90E+01	4.74E+01	9.48E+01	1.90E+02
Pyrite (V=0.025) not included					

Reaction rate laws for the primary minerals were based on those reported by Lehikoinen et al. (2007; illite, quartz, cordierite) and also from the scientific literature (albite, calcite, K-feldspar, kaolinite). Fast reaction rate constants were used for all the secondary minerals, simulating conditions close to local equilibrium for those phases. Precipitation of albite and K-feldspar was inhibited by imposing a large supersaturation threshold for precipitation.

Table 6 - Equilibrium constants ($\log K$, $25^\circ C$) and stoichiometric coefficients for equilibria in solution (speciation). Reactions are written as the destruction of 1 mole of the species in the first column.

Reaction	$\log K$	Primary species									
		al+3	ca+2	cl-	hco3-	sio2(aq)k+	mg+2	na+	h+	so4-2	
al(oh)2+	10.0991	1.000	0.000	0.000	0.000	0.000	0.000	0.000	-2.000	0.000	
al(oh)3(aq)	16.1577	1.000	0.000	0.000	0.000	0.000	0.000	0.000	-3.000	0.000	
al(so4)2-	-4.9000	1.000	0.000	0.000	0.000	0.000	0.000	0.000	0.000	2.000	
al(oh)4-	22.1477	1.000	0.000	0.000	0.000	0.000	0.000	0.000	-4.000	0.000	
aloh+2	5.0114	1.000	0.000	0.000	0.000	0.000	0.000	0.000	-1.000	0.000	
also4+	-3.0100	1.000	0.000	0.000	0.000	0.000	0.000	0.000	0.000	1.000	
ca(h3sio4)2(aq)	15.0532	0.000	1.000	0.000	0.000	2.000	0.000	0.000	-2.000	0.000	
cac1+	0.6956	0.000	1.000	1.000	0.000	0.000	0.000	0.000	0.000	0.000	
cac12(aq)	0.6436	0.000	1.000	2.000	0.000	0.000	0.000	0.000	0.000	0.000	
caco3(aq)	7.0017	0.000	1.000	0.000	1.000	0.000	0.000	0.000	-1.000	0.000	
cah2sio4(aq)	18.5616	0.000	1.000	0.000	0.000	1.000	0.000	0.000	-2.000	0.000	
cah3sio4+	8.7916	0.000	1.000	0.000	0.000	1.000	0.000	0.000	-1.000	0.000	
cahco3+	-1.0467	0.000	1.000	0.000	1.000	0.000	0.000	0.000	0.000	0.000	
caoh+	12.8500	0.000	1.000	0.000	0.000	0.000	0.000	0.000	-1.000	0.000	
caso4(aq)	-2.1111	0.000	1.000	0.000	0.000	0.000	0.000	0.000	0.000	1.000	
co2(aq)	-6.3447	0.000	0.000	0.000	1.000	0.000	0.000	0.000	1.000	0.000	
oh-	13.9951	0.000	0.000	0.000	0.000	0.000	0.000	0.000	-1.000	0.000	
h2sio4-2	22.9116	0.000	0.000	0.000	0.000	1.000	0.000	0.000	0.000	-2.000	0.000
co3-2	10.3288	0.000	0.000	0.000	1.000	0.000	0.000	0.000	0.000	-1.000	0.000
hsio4-	-1.9791	0.000	0.000	0.000	0.000	0.000	0.000	0.000	0.000	1.000	1.000
kcl(aq)	1.4946	0.000	0.000	1.000	0.000	0.000	1.000	0.000	0.000	0.000	0.000
khso4(aq)	-0.8136	0.000	0.000	0.000	0.000	0.000	1.000	0.000	0.000	1.000	1.000
koh(aq)	14.4600	0.000	0.000	0.000	0.000	0.000	1.000	0.000	0.000	-1.000	0.000
kso4-	-0.8796	0.000	0.000	0.000	0.000	0.000	1.000	0.000	0.000	0.000	1.000
mg(h3sio4)2(aq)	13.7232	0.000	0.000	0.000	0.000	2.000	0.000	1.000	0.000	-2.000	0.000
mg4(oh)4+4	39.7500	0.000	0.000	0.000	0.000	0.000	0.000	4.000	0.000	-4.000	0.000
mgcl+	0.1349	0.000	0.000	1.000	0.000	0.000	0.000	1.000	0.000	0.000	0.000
mgco3(aq)	7.3499	0.000	0.000	0.000	1.000	0.000	0.000	1.000	0.000	-1.000	0.000
mgh2sio4(aq)	17.4816	0.000	0.000	0.000	0.000	1.000	0.000	1.000	0.000	-2.000	0.000
mgh3sio4+	8.5416	0.000	0.000	0.000	0.000	1.000	0.000	1.000	0.000	-1.000	0.000
mghco3+	-1.0357	0.000	0.000	0.000	1.000	0.000	0.000	1.000	0.000	0.000	0.000
mgoh+	11.7851	0.000	0.000	0.000	0.000	0.000	0.000	1.000	0.000	-1.000	0.000

Table 6 - (continued)

Reaction	log K	Primary species									
		al+3	ca+2	cl-	hco3-	sio2(aq)k+	mg+2	na+	h+	so4-2	
mgso4(aq)	-2.4117	0.000	0.000	0.000	0.000	0.000	0.000	1.000	0.000	0.000	1.000
nacl(aq)	0.7770	0.000	0.000	1.000	0.000	0.000	0.000	0.000	1.000	0.000	0.000
naco3-	9.8144	0.000	0.000	0.000	1.000	0.000	0.000	0.000	1.000	-1.000	0.000
nahco3(aq)	-0.1541	0.000	0.000	0.000	1.000	0.000	0.000	0.000	1.000	0.000	0.000
nahsio3(aq)	8.3040	0.000	0.000	0.000	0.000	1.000	0.000	0.000	1.000	-1.000	0.000
naoh(aq)	14.1800	0.000	0.000	0.000	0.000	0.000	0.000	0.000	1.000	-1.000	0.000
naso4-	-0.8200	0.000	0.000	0.000	0.000	0.000	0.000	0.000	1.000	0.000	1.000
hsio3-	9.9525	0.000	0.000	0.000	0.000	1.000	0.000	0.000	0.000	-1.000	0.000

Table 7 - Equilibrium constants ($\log K$, 25°C) and stoichiometric coefficients for the different mineral reactions. Reactions are written as the dissolution of 1 mole of mineral.

Reaction	log K	Primary species									
		al+3	ca+2	cl-	hco3-	sio2(aq)k+	mg+2	na+	h+	so4-2	
albite	1.9098	1.000	0.000	0.000	0.000	3.000	0.000	0.000	1.000	-4.000	0.000
calcite	1.8487	0.000	1.000	0.000	1.000	0.000	0.000	0.000	0.000	-1.000	0.000
cordierite~hydr	46.4048	4.000	0.000	0.000	0.000	5.000	0.000	2.000	0.000	-16.000	0.000
illite	7.0602	2.300	0.000	0.000	0.000	3.500	0.600	0.250	0.000	-8.000	0.000
k-feldspar	-1.1300	1.000	0.000	0.000	0.000	3.000	1.000	0.000	0.000	-4.000	0.000
kaolinite	5.1007	2.000	0.000	0.000	0.000	2.000	0.000	0.000	0.000	-6.000	0.000
quartz	-3.9993	0.000	0.000	0.000	0.000	1.000	0.000	0.000	0.000	0.000	0.000
csh-00	-1.2000	0.000	0.000	0.000	0.000	1.000	0.000	0.000	0.000	0.000	0.000
csh-04	6.4767	0.000	0.560	0.000	0.000	1.390	0.000	0.000	0.000	-1.120	0.000
csh-08	24.6311	0.000	1.820	0.000	0.000	2.270	0.000	0.000	0.000	-3.640	0.000
csh-12	18.8013	0.000	1.200	0.000	0.000	1.000	0.000	0.000	0.000	-2.400	0.000
csh-1667	29.1328	0.000	1.670	0.000	0.000	1.000	0.000	0.000	0.000	-3.340	0.000
analcime	5.3191	0.960	0.000	0.000	0.000	2.040	0.000	0.000	0.960	-3.840	0.000
brucite	16.2980	0.000	0.000	0.000	0.000	0.000	0.000	1.000	0.000	-2.000	0.000
laumontite	11.9573	2.000	1.000	0.000	0.000	4.000	0.000	0.000	0.000	-8.000	0.000
mesolite	11.9183	1.990	0.660	0.000	0.000	3.010	0.000	0.000	0.680	-7.960	0.000
mordenite	-6.0300	0.940	0.290	0.000	0.000	5.060	0.000	0.000	0.360	-3.760	0.000
natrolite	16.8110	2.000	0.000	0.000	0.000	3.000	0.000	0.000	2.000	-8.000	0.000
phillipsite	87.3700	3.000	0.000	0.000	0.000	5.000	3.000	0.000	0.000	-12.000	0.000
portlandite	22.5552	0.000	1.000	0.000	0.000	0.000	0.000	0.000	0.000	-2.000	0.000
scolecite	14.1674	2.000	1.000	0.000	0.000	3.000	0.000	0.000	0.000	-8.000	0.000
sepiolite	30.4439	0.000	0.000	0.000	0.000	6.000	0.000	4.000	0.000	-8.000	0.000
stilbite	-0.8087	2.180	1.020	0.000	0.000	6.820	0.010	0.000	0.140	-8.720	0.000
saponite-ca	26.0080	0.330	0.170	0.000	0.000	3.670	0.000	3.000	0.000	-7.320	0.000
saponite-h	25.0501	0.330	0.000	0.000	0.000	3.670	0.000	3.000	0.000	-6.990	0.000
saponite-k	25.7254	0.330	0.000	0.000	0.000	3.670	0.330	3.000	0.000	-7.320	0.000
saponite-mg	25.9702	0.330	0.000	0.000	0.000	3.670	0.000	3.160	0.000	-7.320	0.000
saponite-na	26.0639	0.330	0.000	0.000	0.000	3.670	0.000	3.000	0.330	-7.320	0.000

Table 8 - Coefficients for the calculation of the equilibrium constants for equilibria in solution (speciation) as a function of temperature.
 $\ln K = f_1 \ln T + f_2 + f_3 T + f_4/T + f_5/T^2$

Reaction	f_1	f_2	f_3	f_4	f_5
al(oh)2+	-3.1641E+01	2.0018E+02	-5.0184E-05	1.0079E+03	-1.2296E+03
al(oh)3(aq)	2.2779E+01	-1.8548E+02	1.0545E-04	2.7677E+04	2.7081E+03
al(oh)4-	1.2802E+03	-8.1663E+03	-1.2389E+00	4.6037E+05	-2.7876E+07
al(so4)2-	1.5352E+01	-1.2424E+02	-1.8177E-04	2.6203E+04	-5.9511E+03
aloh+2	5.2714E+01	-3.3778E+02	-5.4911E-02	2.1860E+04	-7.0863E+05
also4+	6.6574E+02	-4.2081E+03	-7.0552E-01	2.3154E+05	-1.4058E+07
co2(aq)	-1.2376E-06	3.4661E+01	1.0266E-09	-4.8556E-04	3.1010E-02
co3-2	3.0068E+02	-1.9050E+03	-3.0720E-01	1.0740E+05	-6.6801E+06
ca(h3sio4)2(aq)	6.0672E+02	-3.8438E+03	-6.1349E-01	2.1505E+05	-1.3323E+07
caco3(aq)	3.3235E+02	-2.0958E+03	-3.2687E-01	1.1458E+05	-6.0879E+06
cacl+	-7.7775E-07	4.2740E+01	6.4548E-10	-3.0499E-04	1.9468E-02
cacl2(aq)	-4.4687E-09	2.0243E+01	4.0159E-12	-1.6053E-06	9.3257E-05
cah2sio4(aq)	3.2655E+02	-2.0797E+03	-3.2830E-01	1.1925E+05	-7.5881E+06
cah3sio4+	1.1200E+02	-6.9758E+02	-1.1931E-01	4.3797E+04	-1.9792E+06
cahco3+	6.1709E+02	-3.9196E+03	-6.0905E-01	2.1560E+05	-1.2683E+07
caoh+	2.4101E+02	-1.5445E+03	-2.4994E-01	8.9405E+04	-6.1020E+06
caso4(aq)	-2.6862E+02	1.7165E+03	2.6939E-01	-9.0164E+04	6.0723E+06
h2sio4-2	2.2957E+02	-1.5145E+03	-1.1881E-01	1.1038E+05	-6.7123E+06
hsio4-	-2.9350E+02	1.8821E+03	2.9647E-01	-1.0429E+05	6.6943E+06
hsio3-	3.5492E+02	-2.2777E+03	-3.4618E-01	1.3365E+05	-8.3658E+06
kcl(aq)	2.6361E+02	-1.6715E+03	-2.6135E-01	9.2507E+04	-5.2790E+06
khso4(aq)	5.6348E+02	-3.6025E+03	-5.5401E-01	2.0876E+05	-1.2882E+07
koh(aq)	-3.1114E-06	3.3295E+01	2.5817E-09	-1.2203E-03	7.7909E-02
kso4-	3.5078E+02	-2.2360E+03	-3.4289E-01	1.2684E+05	-7.8100E+06
mg(h3sio4)2(aq)	-1.1129E-06	3.1599E+01	9.2454E-10	-4.3601E-04	2.7805E-02
mg4(oh)4+4	6.7674E+02	-4.4158E+03	-5.3437E-01	2.8754E+05	-1.3656E+07
mgco3(aq)	3.3044E+02	-2.1029E+03	-3.3087E-01	1.2130E+05	-7.7916E+06
mgcl+	3.5643E+02	-2.2487E+03	-3.4554E-01	1.2302E+05	-6.6449E+06
mgh2sio4(aq)	4.5059E-07	4.0253E+01	-3.7423E-10	1.7657E-04	-1.1263E-02
mgh3sio4+	3.8278E-07	1.9668E+01	-3.1752E-10	1.5018E-04	-9.5913E-03
mghco3+	3.3586E+02	-2.1451E+03	-3.3127E-01	1.2459E+05	-7.9994E+06
mgso4(aq)	-2.6862E+02	1.7114E+03	2.6939E-01	-9.0164E+04	6.0723E+06

Table 8 - (continued)

Reaction	f_1	f_2	f_3	f_4	f_5
naco3-	1.2474E+03	-7.9285E+03	-1.2138E+00	4.3593E+05	-2.5258E+07
nacl(aq)	2.9504E+02	-1.8745E+03	-2.8917E-01	1.0494E+05	-6.2703E+06
nahco3(aq)	1.2713E+02	-8.1208E+02	-5.5008E-02	4.3289E+04	-1.6410E+06
nahsio3(aq)	-4.4503E+02	2.8235E+03	4.3870E-01	-1.5447E+05	8.8050E+06
naoh(aq)	2.9779E+02	-1.9469E+03	-2.1694E-01	1.2835E+05	-8.5795E+06
naso4-	-9.1335E+02	5.8007E+03	8.9383E-01	-3.0910E+05	1.8308E+07
oh-	5.2654E+02	-3.3614E+03	-4.8986E-01	1.8746E+05	-1.0950E+07
mgoh+	-1.3200E+01	3.1649E+01	8.1467E-02	1.8818E+04	-1.8624E+06

Table 9 - Coefficients for the calculation of the equilibrium constants for the different mineral reactions as a function of temperature.
 $\ln K = f_1 \ln T + f_2 + f_3 T + f_4/T + f_5/T^2$

Reaction	f_1	f_2	f_3	f_4	f_5
albite	9.2733E+02	-6.0831E+03	-7.4320E-01	3.9652E+05	-2.7064E+07
calcite	3.2804E+02	-2.0809E+03	-3.3256E-01	1.1664E+05	-6.7526E+06
cordierite~hydr	2.1179E+03	-1.3841E+04	-1.8284E+00	9.1046E+05	-5.5804E+07
illite	1.3083E+03	-8.5454E+03	-1.1073E+00	5.4845E+05	-3.5726E+07
k-feldspar	8.9170E+02	-5.8444E+03	-7.1904E-01	3.7862E+05	-2.6162E+07
kaolinite	8.1713E+02	-5.3315E+03	-7.0764E-01	3.3980E+05	-2.1434E+07
quartz	2.3189E+02	-1.5311E+03	-1.7198E-01	1.0045E+05	-7.5533E+06
csh-00	-1.4814E+01	9.5578E+01	1.2713E-02	-6.4701E+03	3.5273E+05
csh-04	1.8244E+00	-1.1599E+01	-6.6655E-05	4.8182E+03	-2.1059E+03
csh-08	5.7470E+00	-3.4874E+01	-3.3052E-05	1.7550E+04	-7.5826E+02
csh-12	4.0692E+00	-2.7419E+01	-3.0931E-04	1.4229E+04	-9.4128E+03
csh-1667	4.8947E+00	-3.4103E+01	1.5461E-04	2.1827E+04	3.5744E+03
analcime	7.3072E+02	-4.7770E+03	-6.0057E-01	3.0787E+05	-2.0242E+07
brucite	1.3208E+02	-8.4520E+02	-1.2303E-01	5.7698E+04	-2.3667E+06
laumontite	1.3884E+03	-9.0865E+03	-1.1471E+00	5.9046E+05	-3.8674E+07
mesolite	1.2254E+03	-7.9803E+03	-1.0473E+00	5.0715E+05	-3.2244E+07
mordenite	1.3552E+03	-8.9033E+03	-1.0633E+00	5.7984E+05	-4.0856E+07
natrolite	1.2076E+03	-7.8689E+03	-1.0161E+00	5.0414E+05	-3.2048E+07
phillipsite	-1.1323E-06	2.0118E+02	9.3847E-10	-4.4459E-04	2.8414E-02
portlandite	1.1676E+02	-7.3747E+02	-1.1354E-01	5.4022E+04	-2.0603E+06
scolecite	1.2347E+03	-8.0383E+03	-1.0641E+00	5.1182E+05	-3.2299E+07
sepiolite	1.9381E+03	-1.2684E+04	-1.5221E+00	8.3057E+05	-5.5122E+07
stilbite	2.1448E+03	-1.4040E+04	-1.7398E+00	9.0236E+05	-6.1298E+07
saponite-ca	1.3650E+03	-8.9155E+03	-1.1207E+00	5.8235E+05	-3.7393E+07
saponite-h	1.3476E+03	-8.8050E+03	-1.1030E+00	5.7555E+05	-3.7053E+07
saponite-k	1.3583E+03	-8.8706E+03	-1.1132E+00	5.7897E+05	-3.7289E+07
saponite-mg	1.3686E+03	-8.9407E+03	-1.1235E+00	5.8406E+05	-3.7468E+07
saponite-na	1.3649E+03	-8.9145E+03	-1.1177E+00	5.8186E+05	-3.7398E+07

Table 10 - Rate parameters for the different minerals. Multiple entries for a given mineral refer to different parallel reactions (summation term in the rate law).

Mineral	E_a (kcal/mol)	k_{25} (mol/m ² /s)	M	n	p
albite	14.3	1.00E-10	0.4	14	0.49
albite	14.3	1.77E-15	0.4	14	-0.30
calcite	8.0	1.00E-02	1	1	0.66
calcite	8.0	1.00E-06	1	1	0
illite	13.0	1.00E-11	1	1	0.34
illite	13.0	1.70E-13	1	1	0
illite	13.0	3.00E-17	1	1	-0.40
K-feldspar	12.9	1.00E-10	1	1	0.50
K-feldspar	12.9	2.50E-17	1	1	-0.45
kaolinite	15.0	1.70E-11	1	1	0.50
kaolinite	15.0	2.50E-17	1	1	-0.30
quartz	17.0	4.60E-14	1	1	0
quartz	17.0	5.10E-17	1	1	-0.50
cordierite	15.0	1.60E-04	1	1	1.00
cordierite	15.0	6.30E-12	1	1	0
cordierite	15.0	1.30E-18	1	1	-0.80
Second. mins.	15.0	1.00E-08	1	1	0

References.

Albite: Chou and Wollast, 1985; Burch et al., 1993; Soler and Lasaga, 1998.

Calcite: Morse and Arvidson, 2002.

Illite: Lehtinen et al., 2007; Brantley, 2005.

K-feldspar: Schweda, 1989,1990; Blum and Stillings, 1995.

Kaolinite: Nagy et al.,1991; Ganor et al., 1995.

Quartz: Lehtinen et al., 2007; Brantley, 2005.

Cordierite: Lehtinen et al., 2007.

5. RESULTS.

The presentation of the results has been organized as follows:

- (a) Comparison of results within a first group of three reference cases ($Q = 631 \text{ l/a}$, pH 10.5, with and without Mg secondary minerals; $Q = 631 \text{ l/a}$, pH 10.5, only without Mg secondary minerals). These cases had been presented previously in a progress report. This first comparison has been kept as a separate chapter to facilitate the presentation of the main processes.
- (b) Comparison between all the cases (Table 1), corresponding to the initial set of high-pH solution compositions (Table 2).
- (c) Comparison of results for the case with $Q = 631 \text{ l/a}$ and making use of (i) the initial set of high-pH solution compositions (Table 2), (ii) high-pH solution compositions derived from cement leaching experiments using the saline leaching solution (Table 3a), (iii) high-pH solution compositions derived from cement leaching experiments using the fresh leaching solution (Table 3b), and (iv) the initial set of high-pH solution compositions (Table 2) and a variable temperature history caused by the heat generation of the waste.
- (d) Comparison of results between the reference case at $Q = 631 \text{ l/a}$ and the same case but using larger ($\times 100$) reactive surface areas for the primary minerals. This case is intended to investigate the potential effect of larger surface areas caused, for instance, by the presence of a fault gouge.

5.1. Reference Cases

Two different modeling runs were performed for each case shown in Table 1; one including Mg-containing secondary minerals (brucite, sepiolite, saponites) and another one without those minerals. The reason is that precipitation of these Mg-containing minerals leads to a quick sealing of the fracture inlet. A feedback between porosity, permeability and fluid flow has not been implemented in these calculations. Therefore, modeling runs with and without Mg-containing secondary minerals serve as a means to bracket the possible chemical evolution of the system.

Only three sets of results will be shown in this section (Table 11). The case with a pH 11 input solution is similar to the case with pH 10.5 and will not be shown here. Only the run without Mg-containing secondary minerals will be shown for the case with pH 12, because precipitation of C-S-H leads to the sealing of the fracture inlet, even without allowing the precipitation of Mg-containing minerals.

Table 11 - Parameter values for the different modeling runs. Shaded values correspond to the cases shown in this section.

Q [l/a]	Q(kg/m ² /s)	pH	volume aperture [m]
3154	10 ⁻²	10.5	0.010
3154	10 ⁻²	11	0.010
3154	10 ⁻²	12	0.010
631	5x10 ⁻³	10.5	0.004 with and without Mg-secondary minerals
631	5x10 ⁻³	11	0.004
631	5x10 ⁻³	12	0.004 only without Mg-secondary minerals
158	2.5x10 ⁻³	10.5	0.002
158	2.5x10 ⁻³	11	0.002
158	2.5x10 ⁻³	12	0.002
32	10 ⁻³	10.5	0.001
32	10 ⁻³	11	0.001
32	10 ⁻³	12	0.001

5.1.1. Q = 631 l/a, pH 10.5, no Mg-containing secondary minerals

Results (mineral contents and pH; Figs. 12, 13) are shown for times equal to 1000, 5000, and 10000 a. The most striking feature is the increase in porosity at the fracture inlet, caused by the dissolution of calcite. The dissolution of calcite at the fracture inlet causes the advance of a reaction front, marked by the sharp boundary in calcite content and porosity. Another feature is the precipitation of mesolite (Na-Ca zeolite) further down the fracture. Notice also that cordierite dissolved very quickly along the whole domain (it is already completely dissolved at t = 1000 a). The magnitude of the dissolution of the other primary minerals is very small (their contents are practically unaltered after 10000 a).

Regarding solution composition (Figs. 13, 14), notice that the rock is not reactive enough to change in any substantial measure the pH of the incoming solution. The concentrations of the major components (Na, Ca, Cl) and Mg do not change along the fracture, because reaction rates are too small to alter the large concentrations in the incoming solution (flow rates are large). Cl and SO₄ are not involved in any mineral reaction. Carbonate concentration increases sharply near the fracture inlet due to the dissolution of calcite. Silica increases slightly along the fracture due to minor dissolution of aluminosilicates and quartz. K concentration remains practically unaltered (only minor dissolution of illite and K-feldspar). Al concentrations show larger changes (they are affected by several mineral reactions, including mesolite), but they are always less than 10⁻⁵ mol/kg H₂O. The kink in the Si and Al concentration curves corresponds to the point where mesolite precipitation starts.

5.1.2. Q = 631 l/a, pH 10.5, with Mg-containing secondary minerals

Mineralogical evolution for this case (Fig. 15) is similar to the previous one, but with a very significant difference. The intense precipitation of brucite (Mg(OH)₂) right at the

fracture inlet causes the quick sealing of the fracture. Ca-saponite also precipitates at the fracture inlet and further down the domain. The sealing of fracture porosity would mean that flow of solution through the fracture would stop. However, no feedback between porosity and permeability changes has been implemented in the calculations. The results can be considered as an estimate of the possible chemical evolution of the system in the case that fluid flow would continue despite the sealing of porosity at the fracture inlet (uncoupling of chemical and physical properties).

Regarding solution composition (Figs. 16, 17), notice that the rock is not reactive enough to change in any substantial measure the pH of the incoming solution (except for a slight decrease in pH in early stages). The concentrations of the major components (Na, Ca, Cl) do not change along the fracture, because reaction rates are too small to alter the large concentrations in the incoming solution (flow rates are large). However, marked changes in Mg concentration can be observed, due to the precipitation of brucite (only at the fracture inlet) and saponite. Al and Si concentrations are also affected by these reactions (the sharp gradients at about 100 m in Fig. 8 correspond to the advancing mesolite-saponite reaction front). Carbonate concentration increases sharply near the fracture inlet due to the dissolution of calcite. K concentration remains practically unaltered (only minor dissolution of illite and K-feldspar).

5.1.3. $Q = 631 \text{ l/a}$, pH 12, no Mg-containing secondary minerals

The mineralogical evolution for this case (Fig. 18) shows that the precipitation of C-S-H ($\text{Ca/Si} = 1.2$) at the fracture inlet causes the sealing of the fracture. The precipitation of this phase only happens with the pH 12 input solution. Notice also that the magnitude of calcite dissolution is much smaller than in the previous cases, due to the fact that the incoming pH 12 solution is already close to equilibrium with respect to calcite. As in the previous cases, the rock is not reactive enough to change in any substantial measure the pH of the incoming solution (Fig. 13). Solution composition remains also rather constant (Fig. 19). Only Al concentration increases significantly along the fracture, due to aluminosilicate dissolution (Al is not captured by the precipitating C-S-H gel in the calculations).

5.1.4. Conclusions

One-dimensional reactive transport calculations have been performed to simulate the alteration of a fracture and the extension of the high-pH plume arising from the circulation of hyperalkaline solutions through the fracture. The calculations have been performed with the Retraso reactive transport code.

The results from three different cases have been shown in this section (reference cases, Table 11). The results show that the rock is not reactive enough to neutralize the high pH of the incoming solutions in any of the cases. For the case with a pH 10.5 (and also pH 11) incoming solution, an increase in porosity at the fracture inlet caused by the dissolution of calcite is observed if no Mg-containing secondary minerals are included in the calculations. However, if those minerals are included, the precipitation of brucite leads to a quick sealing of the fracture inlet. The sealing of the fracture is also observed for the case with a pH 12 incoming solution. In this case, the sealing is caused by the

precipitation of C-S-H gel ($\text{Ca/Si} = 1.2$), even without including Mg-containing secondary minerals in the calculations.

The sealing of fracture porosity would mean that flow of solution through the fracture would slow down or stop rather quickly. However, no feedback between porosity and permeability changes has been implemented in the calculations. The results can be considered as an estimate of the possible chemical evolution of the system in the case that fluid flow would continue despite the sealing of porosity at the fracture inlet (uncoupling of chemical and physical properties).

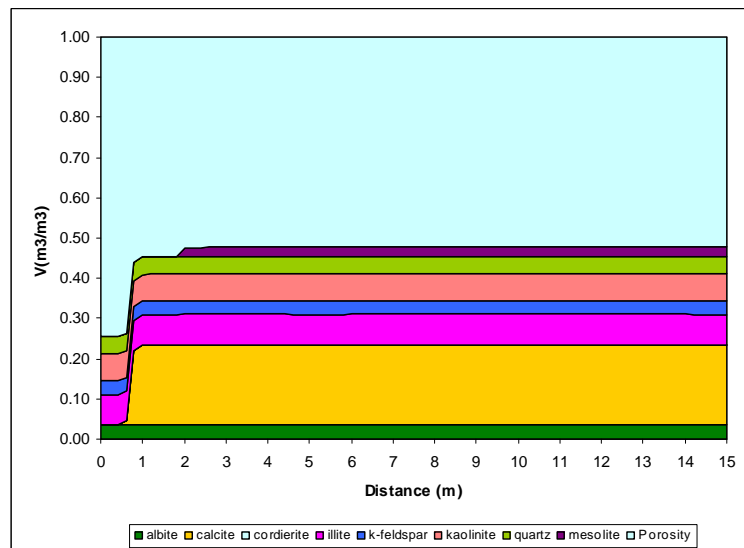
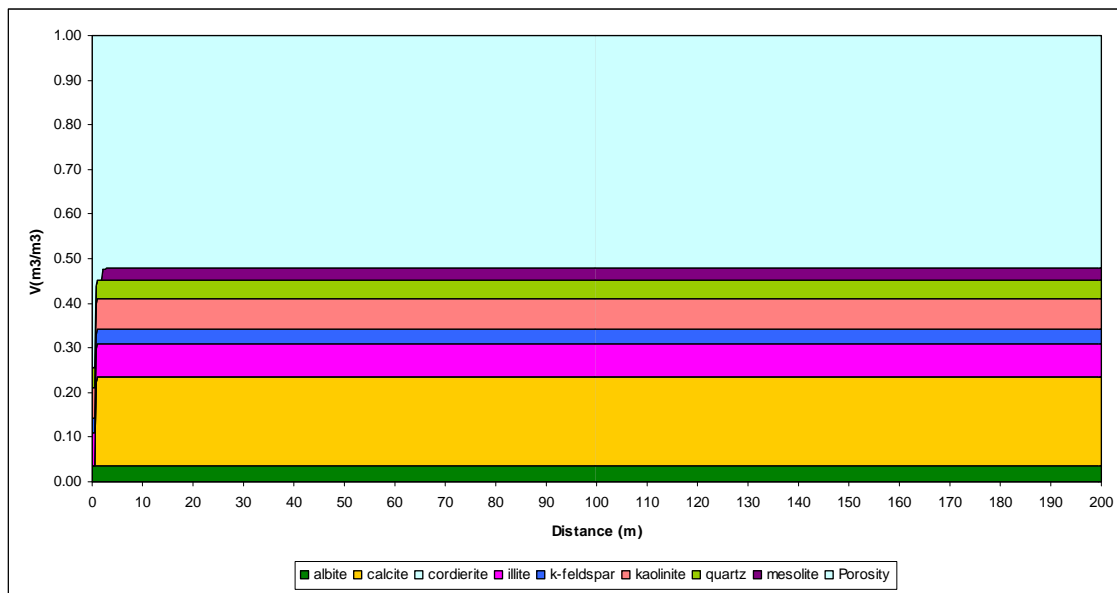


Figure 12a - Volumetric mineral content and porosity for the case with input pH equal to 10.5 and without including Mg-containing secondary minerals. $t = 1000 \text{ a}$. The second plot is a close up of the region near the fracture inlet.

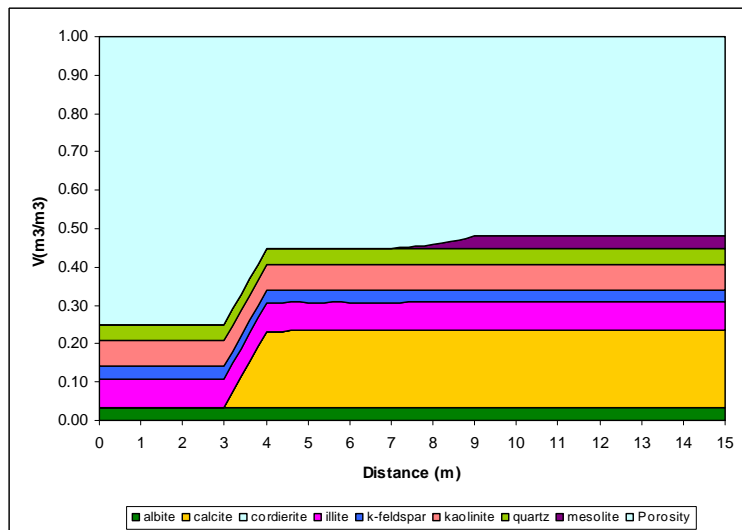
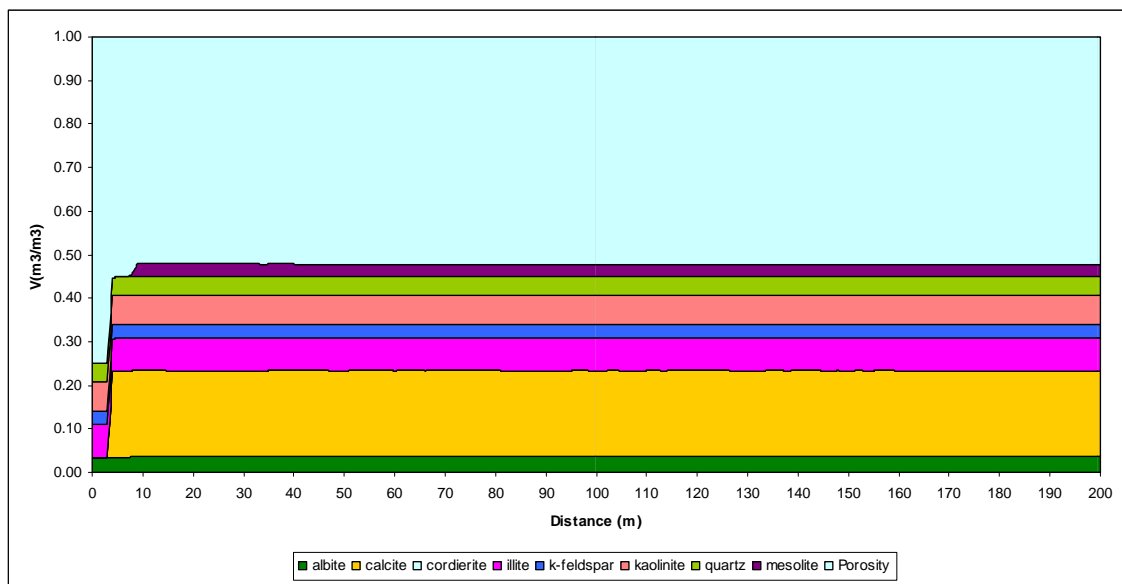


Figure 12b - Volumetric mineral content and porosity for the case with input pH equal to 10.5 and without including Mg-containing secondary minerals. $t = 5000 \text{ a}$. The second plot is a close up of the region near the fracture inlet.

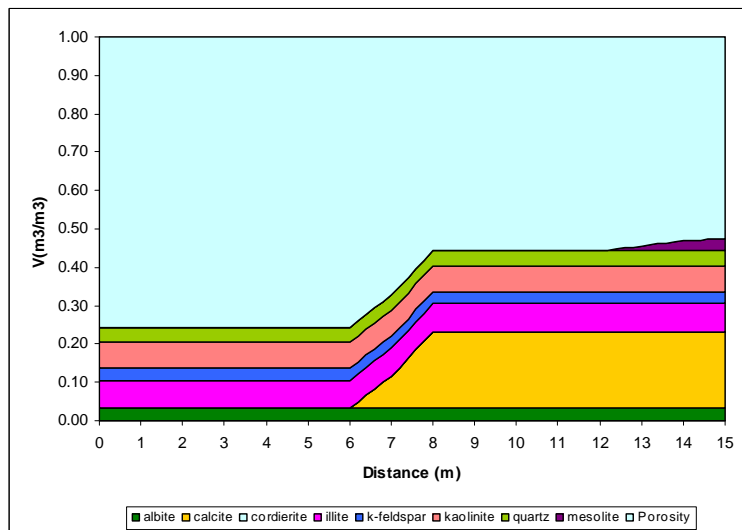
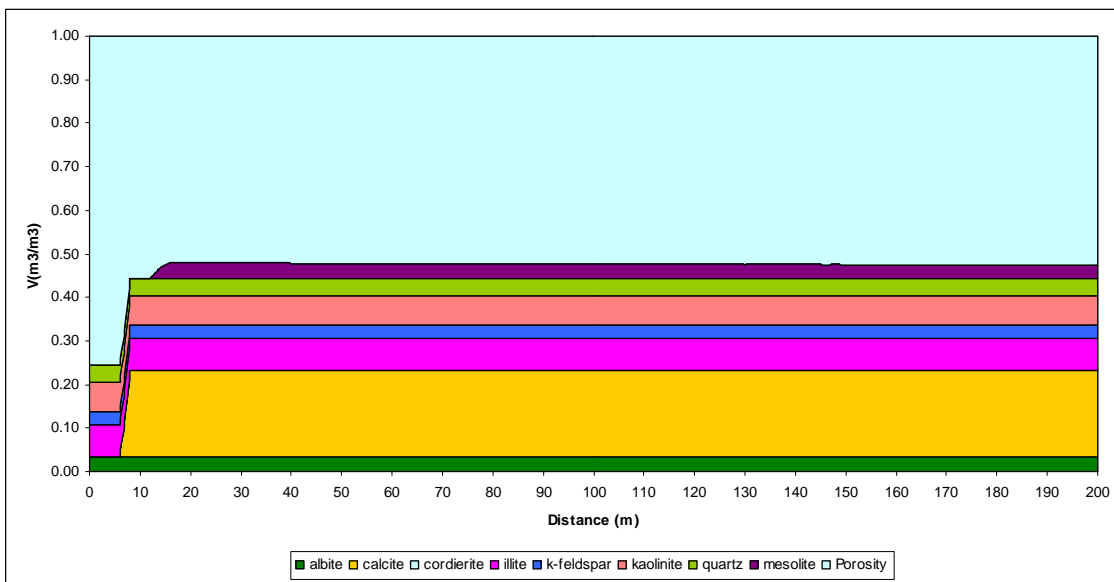


Figure 12c - Volumetric mineral content and porosity for the case with input pH equal to 10.5 and without including Mg-containing secondary minerals. $t = 10000 \text{ a}$. The second plot is a close up of the region near the fracture inlet.

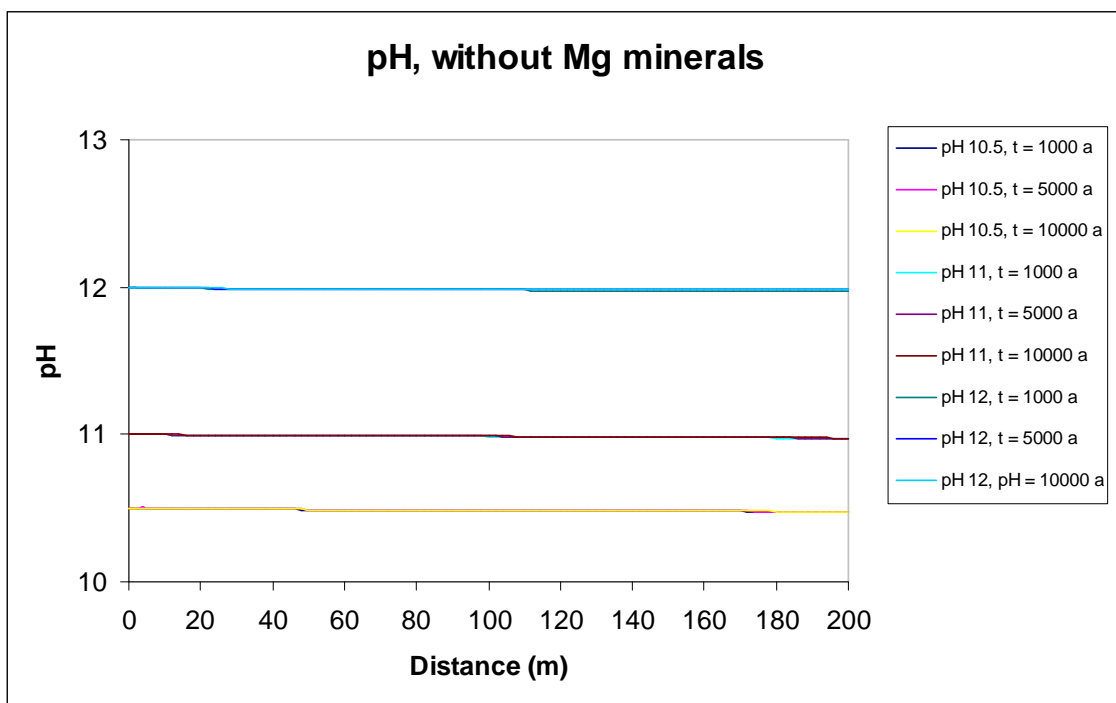


Figure 13 - Solution pH vs. distance for all the cases (no Mg-containing secondary minerals allowed). Notice that curves for each pH fall one on top of another.

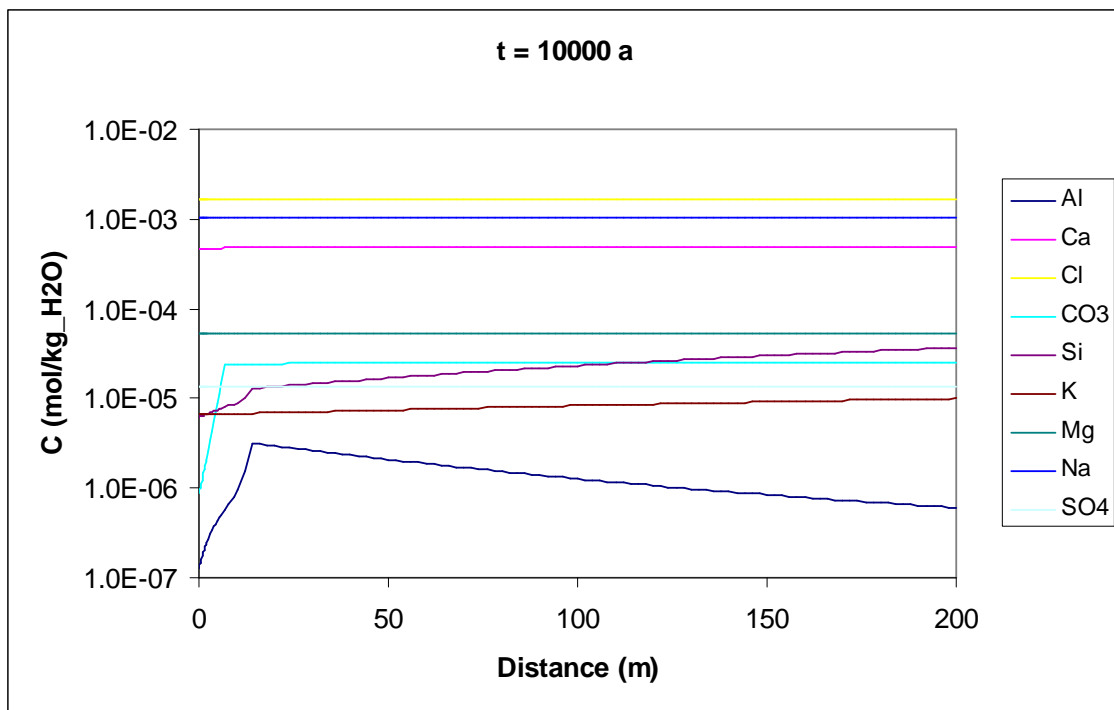


Figure 14 - Total concentrations vs. distance for the case with input pH equal to 10.5 and without including Mg-containing secondary minerals. $t = 10000 \text{ a}$.

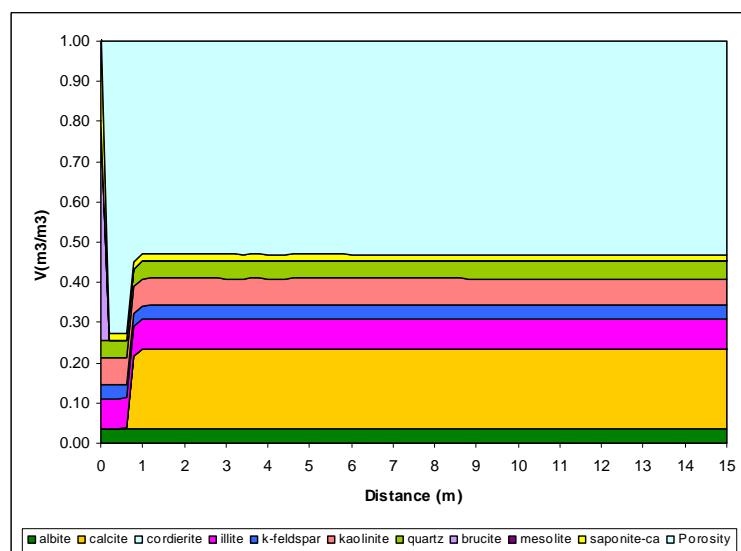
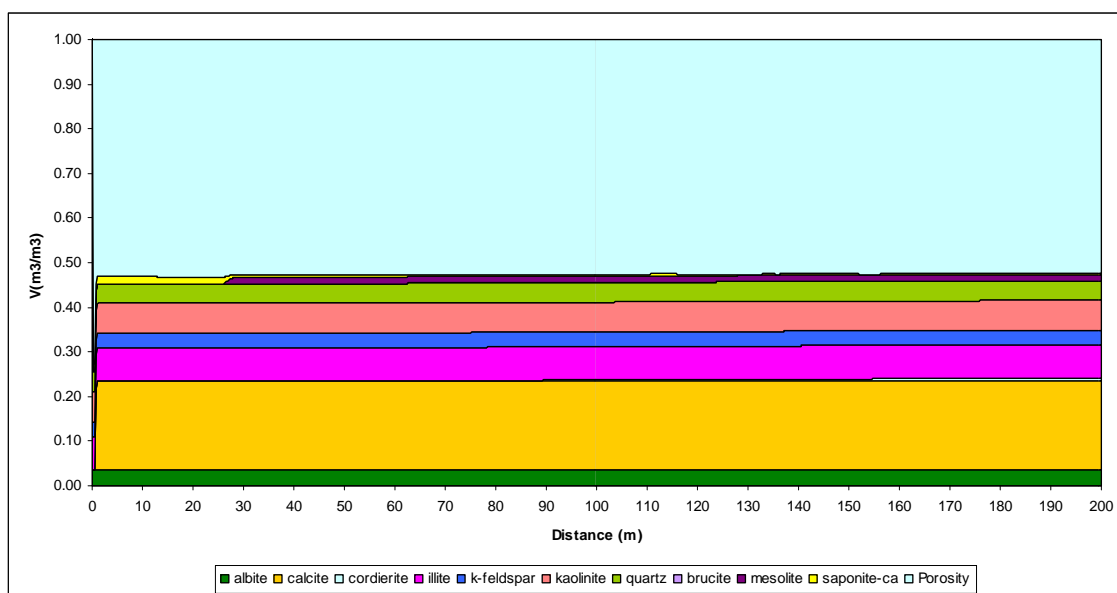


Figure 15a - Volumetric mineral content and porosity for the case with input pH equal to 10.5 and including Mg-containing secondary minerals. $t = 1000 \text{ a}$. The second plot is a close up of the region near the fracture inlet.

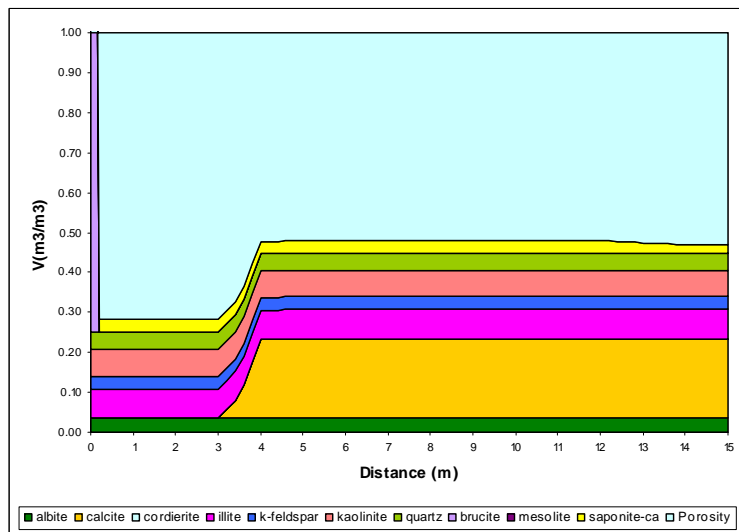
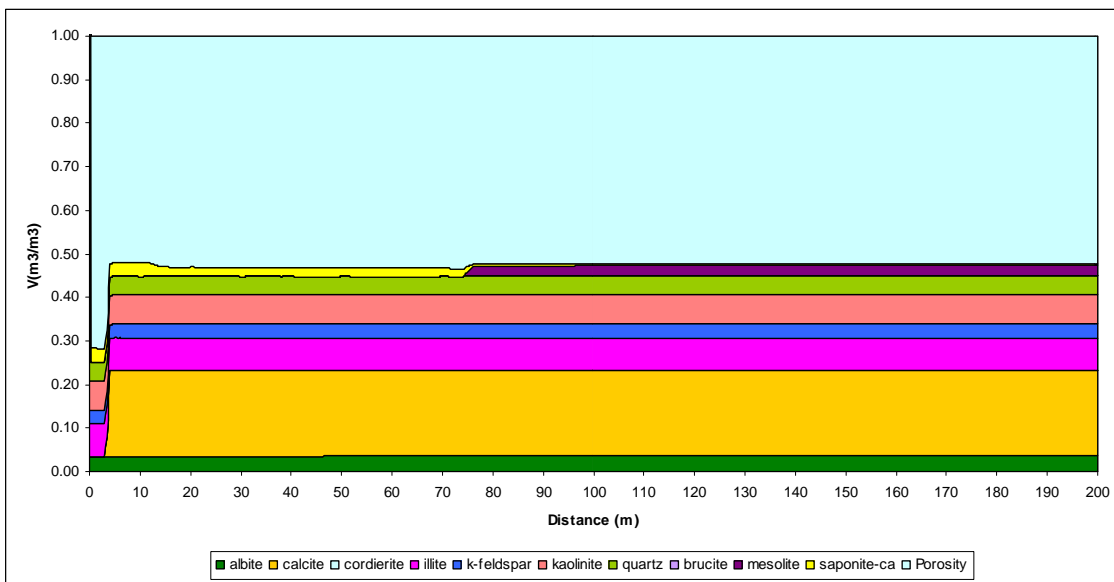


Figure 15b - Volumetric mineral content and porosity for the case with input pH equal to 10.5 and including Mg-containing secondary minerals. $t = 5000$ a. The second plot is a close up of the region near the fracture inlet.

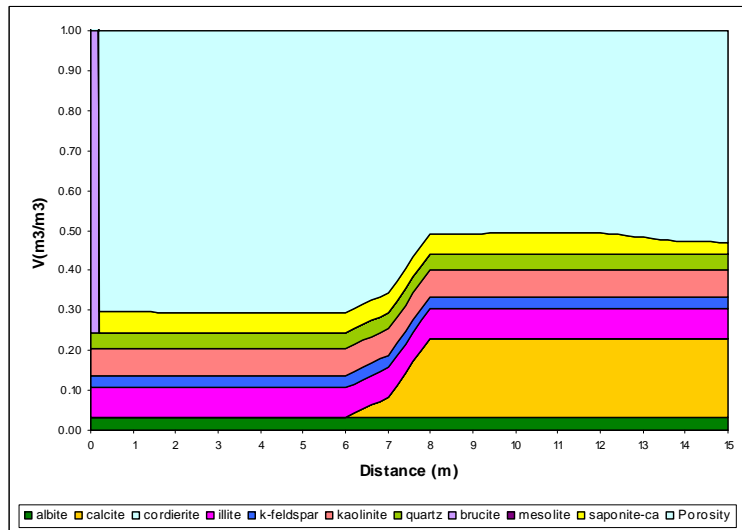
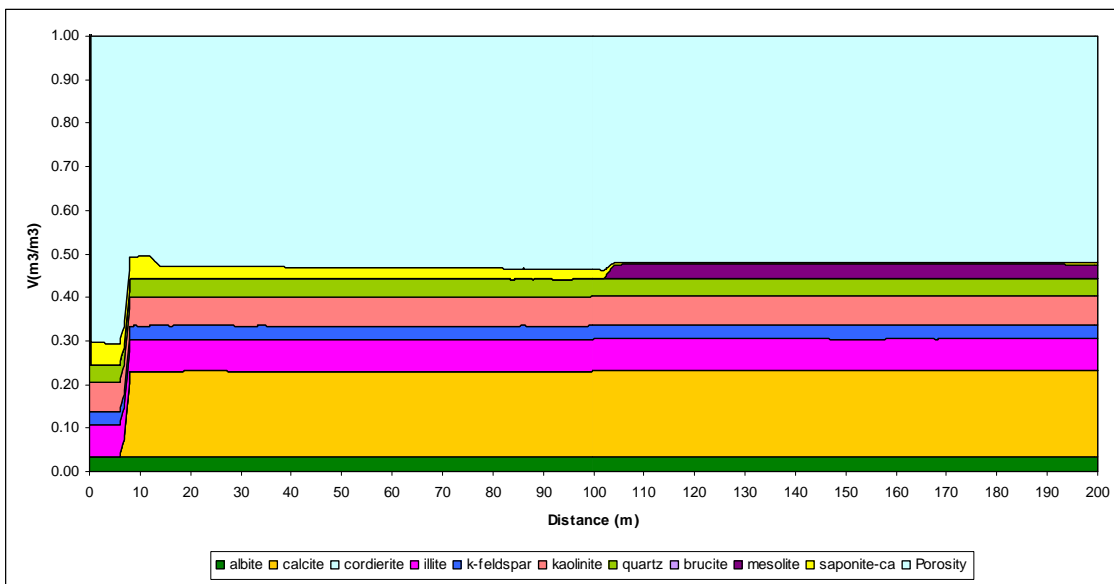


Figure 15c - Volumetric mineral content and porosity for the case with input pH equal to 10.5 and including Mg-containing secondary minerals. $t = 10000 \text{ a}$. The second plot is a close up of the region near the fracture inlet.

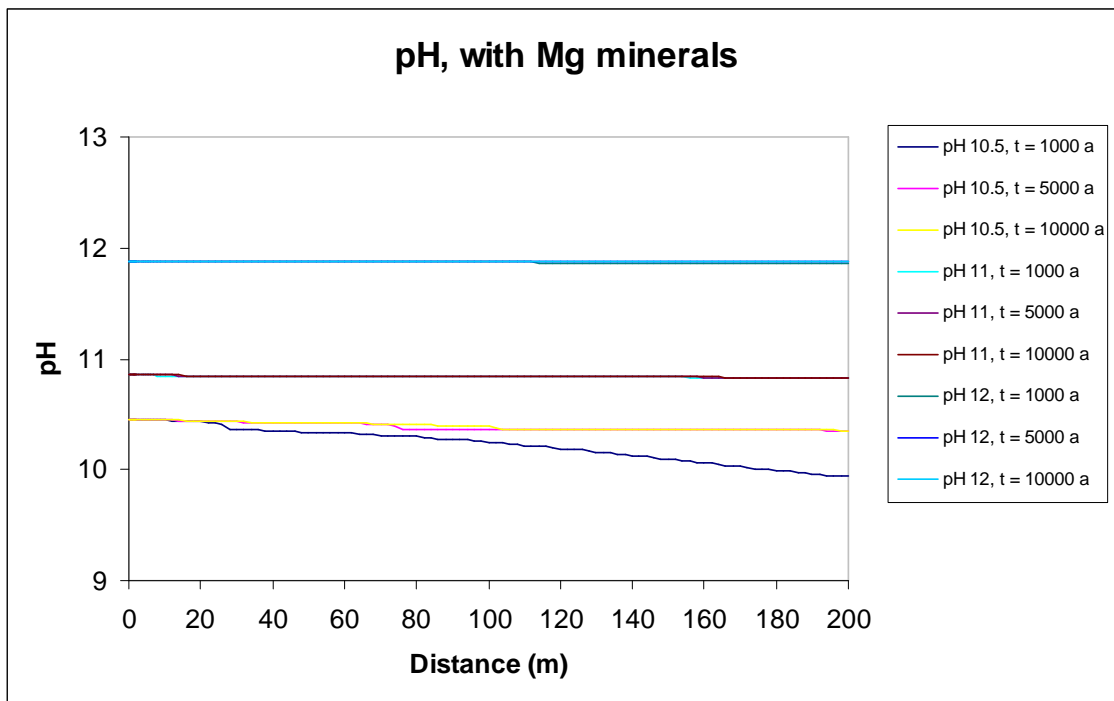


Figure 16 - Solution pH vs. distance for all the cases (including Mg-containing secondary minerals).

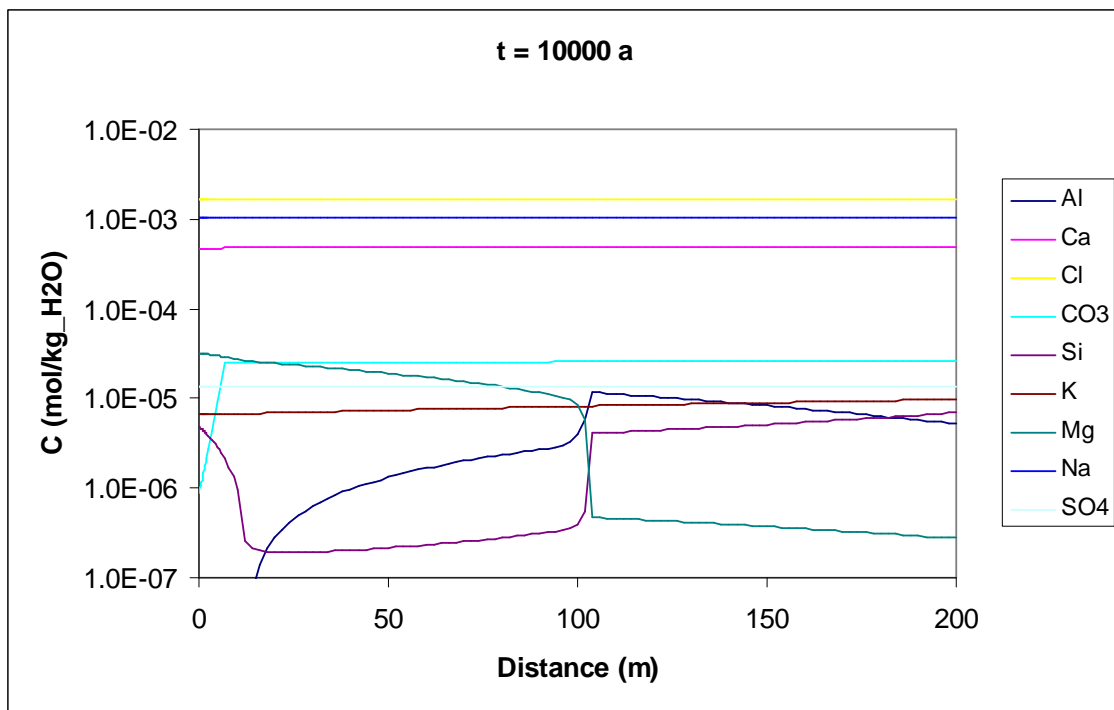


Figure 17 - Total concentrations vs. distance for the case with input pH equal to 10.5 and including Mg-containing secondary minerals. $t = 10000 \text{ a}$.

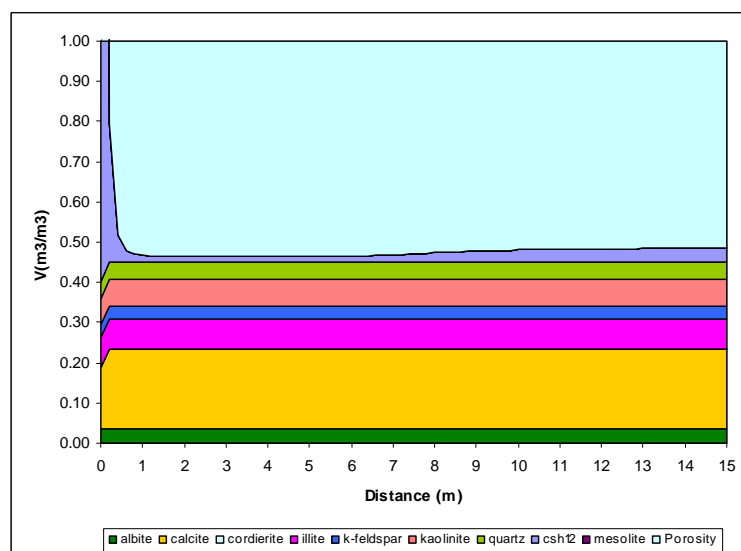
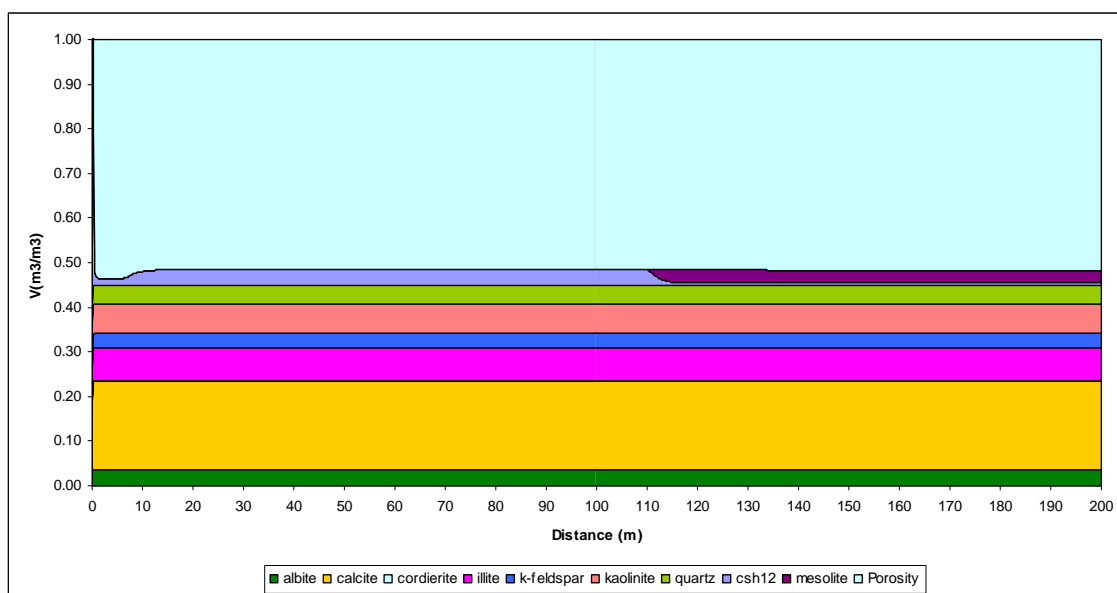


Figure 18a - Volumetric mineral content and porosity for the case with input pH equal to 12 and without including Mg-containing secondary minerals. $t = 1000 \text{ a}$. The second plot is a close up of the region near the fracture inlet.

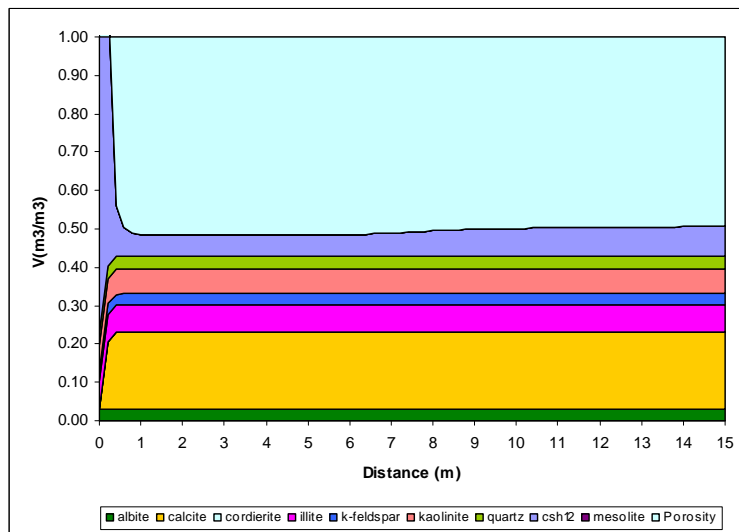
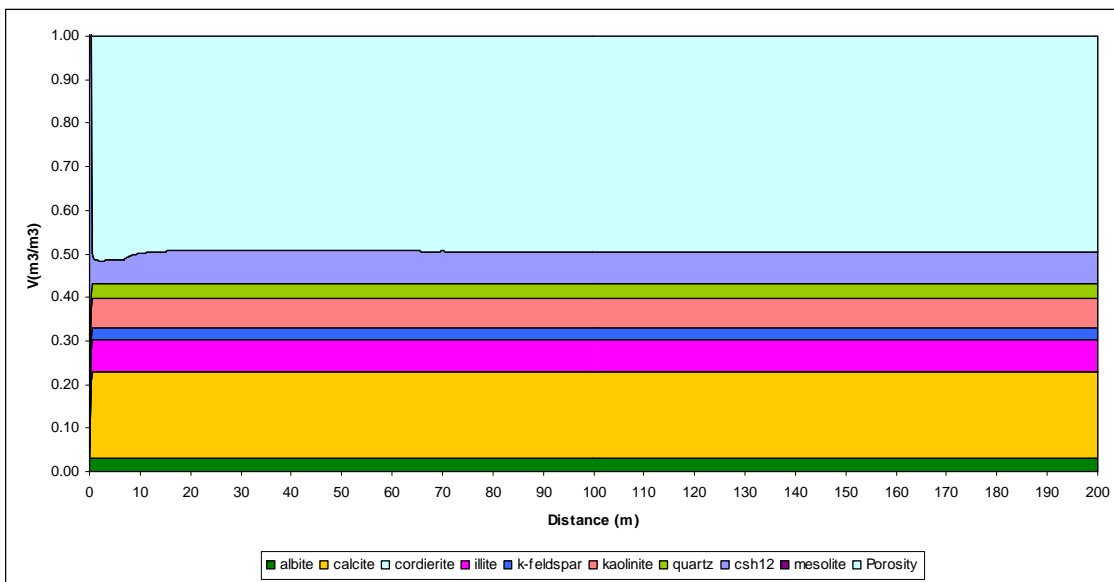


Figure 18b - Volumetric mineral content and porosity for the case with input pH equal to 12 and without including Mg-containing secondary minerals. $t = 5000 \text{ a}$. The second plot is a close up of the region near the fracture inlet.

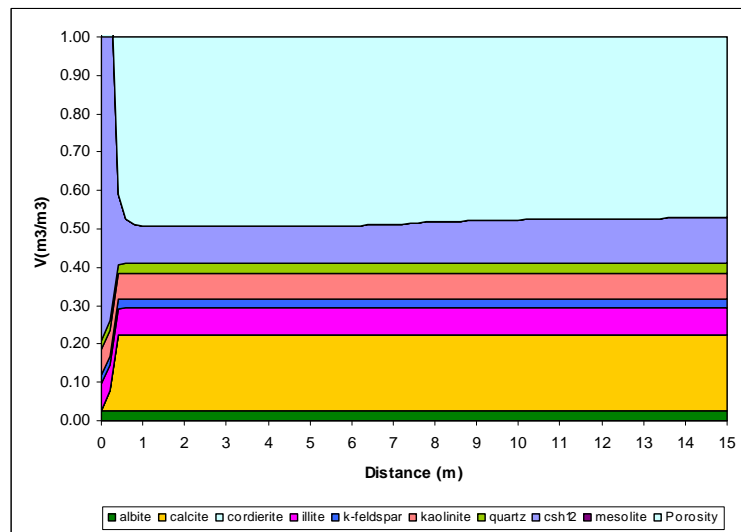
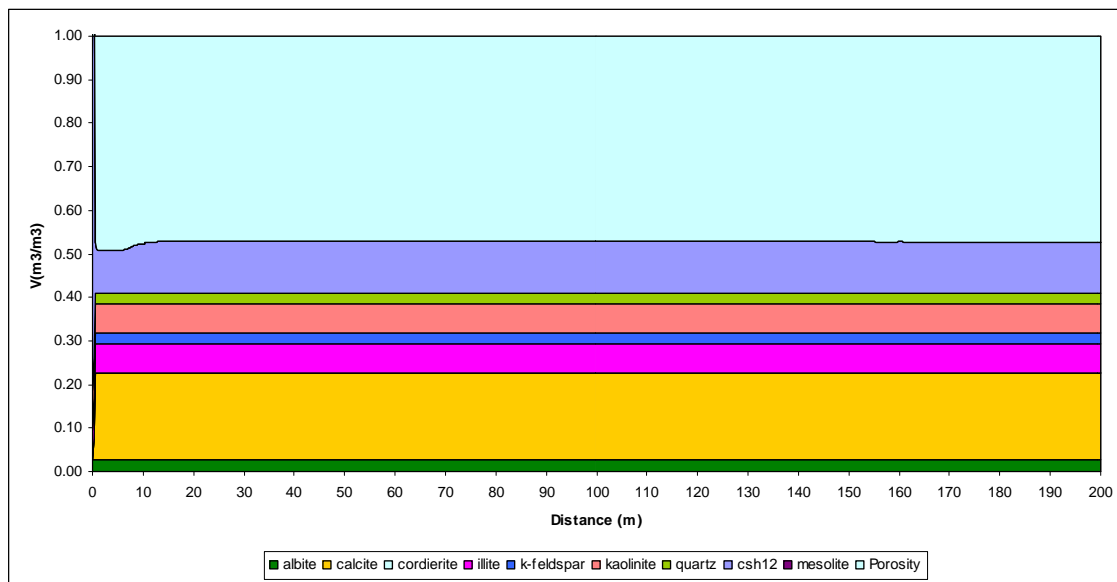


Figure 18c - Volumetric mineral content and porosity for the case with input pH equal to 12 and without including Mg-containing secondary minerals. $t = 10000 \text{ a}$. The second plot is a close up of the region near the fracture inlet.

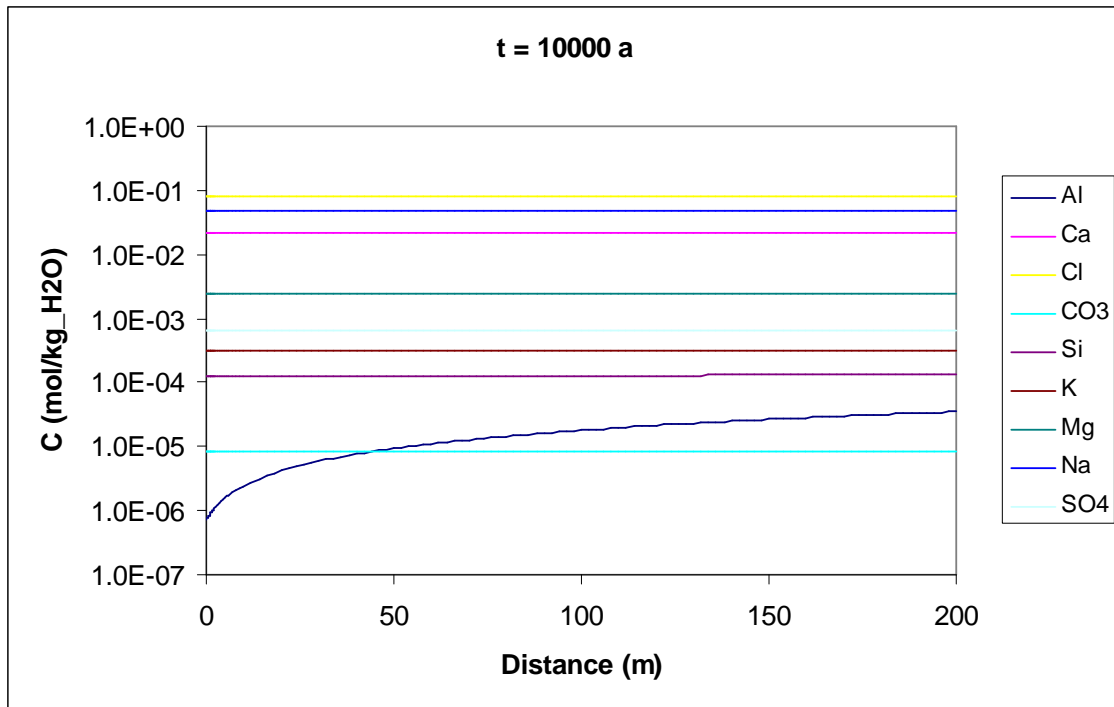


Figure 19 - Total concentrations vs. distance for the case with input pH equal to 12 and without including Mg-containing secondary minerals. $t = 10000 \text{ a}$.

5.2. Initial Cases. Comparison of Q = 3154, 631, 158, 32 l/a.

In this chapter the results for the different flow and pH values shown in Table 1 will be compared. Two simulations are associated with each case; one including Mg-containing secondary minerals (brucite, sepiolite, saponites) and another one without including them.

As mentioned previously, a feedback between porosity, permeability and fluid flow has not been implemented in the calculations. Modeling runs with and without Mg-containing secondary minerals serve as a means to bracket the possible chemical evolution of the system.

5.2.1. Q = 3154, 631, 158, 32 l/a, pH 10.5, no Mg-containing secondary minerals

(Mineral contents and pH; Figs. 20, 26)

In all cases, the following observations can be made:

- an increase in porosity at the fracture inlet, caused by the dissolution of calcite
- precipitation of mesolite (Na-Ca zeolite) further down the fracture
- quick dissolution of cordierite (it is already completely dissolved at t = 1000 a)
- minor dissolution of other primary minerals

The main difference between the different cases is that reaction fronts (calcite dissolution, mesolite precipitation) advance faster when flow is also faster (shorter residence time of the solution). Stilbite (Ca-Na zeolite) precipitation can also be observed in the case with the slowest flow (longest residence time of solution).

Notice that the rock is not reactive enough to change in any substantial measure the pH of the incoming solution. At most, a minor reduction in pH can be observed when flow is slowest.

5.2.2. Q = 3154, 631, 158, 32 l/a, pH 10.5, with Mg-containing secondary minerals

(Mineral contents and pH; Figs. 21, 27)

Mineralogical evolution for these cases is similar to the previous ones, but with a very significant difference. There is an intense precipitation of brucite and Ca-saponite at the fracture inlet that causes the quick sealing of fracture porosity. The precipitation of brucite stops in the first centimeters, but the precipitation of Ca-saponite continues along the domain. The anomalous Ca-saponite peak at t = 10000 a may be related to the calcite dissolution front, but it could also reflect a numerical artifact.

The sealing of the fracture (Mg-minerals) is faster when flow is faster. For instance, for Q = 32 l/a there is no precipitation of brucite and no sealing at t = 1000 a and only partial sealing at t = 10000 a. Moreover, Ca-saponite and stilbite precipitate towards the

end of the domain. In the case of $Q = 158 \text{ l/a}$, the sealing of the fracture inlet is complete at 10000 a, but not at 1000 a.

As in the case without Mg minerals, the rock is not reactive enough to change the pH of the incoming solution. Only with the slowest flow values is there a minor decrease in pH. The somewhat larger decrease at $t = 1000 \text{ a}$ for the smallest pH and flow values is caused by the dissolution of a small amount of remaining cordierite (not yet completely dissolved).

5.2.3. $Q = 3154, 631, 158, 32 \text{ l/a, pH 11, no Mg-containing secondary minerals}$

(Mineral contents and pH; Figs. 22, 26)

Results of this case are very similar at the case with pH 10.5 and no Mg-containing secondary minerals. For all cases there is an increase in porosity at the fracture inlet, precipitation of mesolite further down the fracture, fast dissolution of cordierite and minor dissolution of the other primary minerals.

The differences between the different flow cases are the same as before. Reaction fronts (calcite dissolution, mesolite precipitation) advance faster when flow is also faster (shorter residence time of the solution). Additionally, the amount of primary mineral dissolution and secondary mineral precipitation at a given position is larger when flow is slower. This is especially evident in the case of mesolite (larger amounts of mesolite at a given location when flow is slower). This effect is caused by the larger reactive surface areas of primary minerals when flow is slower (smaller fracture aperture; Table 5). This effect was too small to be noticeable in the case with a pH 10.5 input solution.

5.2.4. $Q = 3154, 631, 158, 32 \text{ l/a, pH 11, with Mg-containing secondary minerals}$

(Mineral contents and pH; Figs. 23, 27)

Mineralogical evolution for this case is similar to the case with pH 10.5 and Mg-containing secondary minerals. The only difference is the larger amount of precipitation of brucite and Ca-saponite that seals the fracture. For all flow values there is sealing of the fracture inlet since early times.

5.2.5. $Q = 3154, 631, 158, 32 \text{ l/a, pH 12, no Mg-containing secondary minerals}$

(Mineral contents and pH; Figs. 24, 26)

The mineralogical evolution for this case shows that the precipitation of C-S-H ($\text{Ca/Si} = 1.2$) at the fracture inlet causes the sealing of the fracture. The precipitation of this phase only happens with the pH 12 input solution and is more important when flow is slower (larger surface areas and reactivity of primary minerals; Table 5).

There is precipitation of mesolite too. The advance of the mesolite reaction front is faster when flow is also faster. Notice also that in these cases the magnitude of calcite

dissolution is very small compared with the previous cases. This effect is due to the fact that the incoming pH 12 solution is already close to equilibrium with respect to calcite.

As in the other cases, the rock is not reactive enough to change in any substantial measure the pH of the incoming solution.

5.2.6. $Q = 3154, 631, 158, 32 \text{ l/a}$, pH 12, with Mg-containing secondary minerals

(Mineral contents and pH; Figs. 25,27)

This case is very similar to the previous one, but sealing of the fracture inlet is caused by brucite and Ca-saponite in addition to C-S-H ($\text{Ca/Si} = 1.2$).

5.2.7. Conclusions

The results show that for pH 10.5 and 11 incoming solutions, there is an increase in porosity at the fracture inlet if Mg secondary minerals are not taken into account. However, there is a sealing of the fracture inlet, caused by the precipitation of brucite (mainly) and Ca-saponite, if Mg secondary minerals are included.

For a pH 12 incoming solution there is sealing of the fracture inlet regardless of the inclusion or not of Mg-containing secondary minerals. The precipitation of C-S-H ($\text{Ca/Si} = 1.2$) is responsible for the sealing.

For all cases, there is faster sealing of fracture and faster calcite dissolution at inlet when flow is faster. In addition, there is locally more primary mineral dissolution and secondary mineral precipitation when flow is slower, due to the larger reactive surface areas of primary minerals (related to the smaller fracture aperture).

The results show that the rock is not reactive enough to neutralize the high pH of the incoming solutions in any of the cases. At most, a minor reduction in pH can be observed when flow is slowest.

Figure 20a - Volumetric mineral content and porosity for the case with input pH equal to 10.5 and without including Mg-containing secondary minerals. $t = 1000$ a. The plot represents the first 15 meters of the fracture.

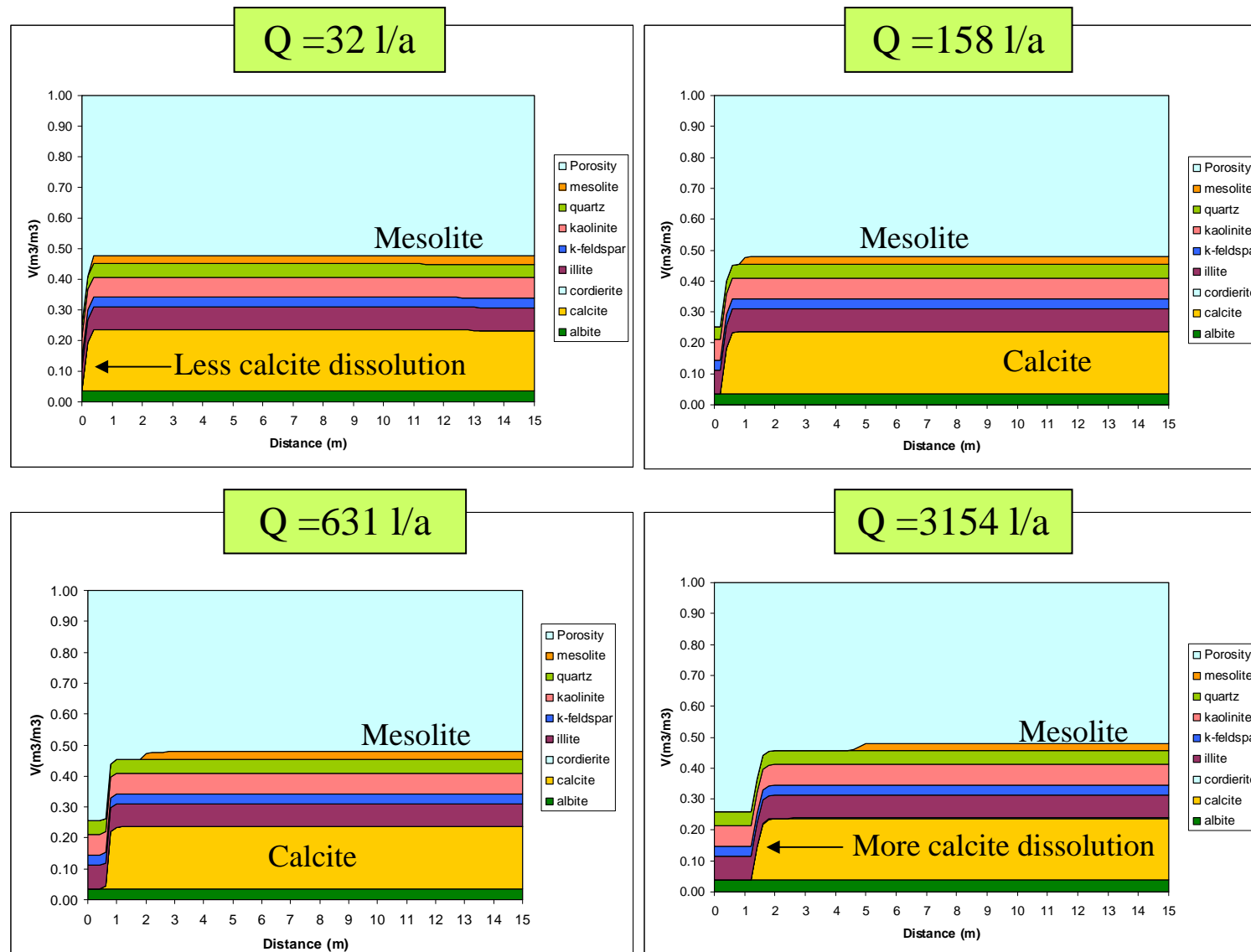


Figure 20b - Volumetric mineral content and porosity for the case with input pH equal to 10.5 and without including Mg-containing secondary minerals. $t = 10000$ a. The plot represents the first 15 meters of the fracture.

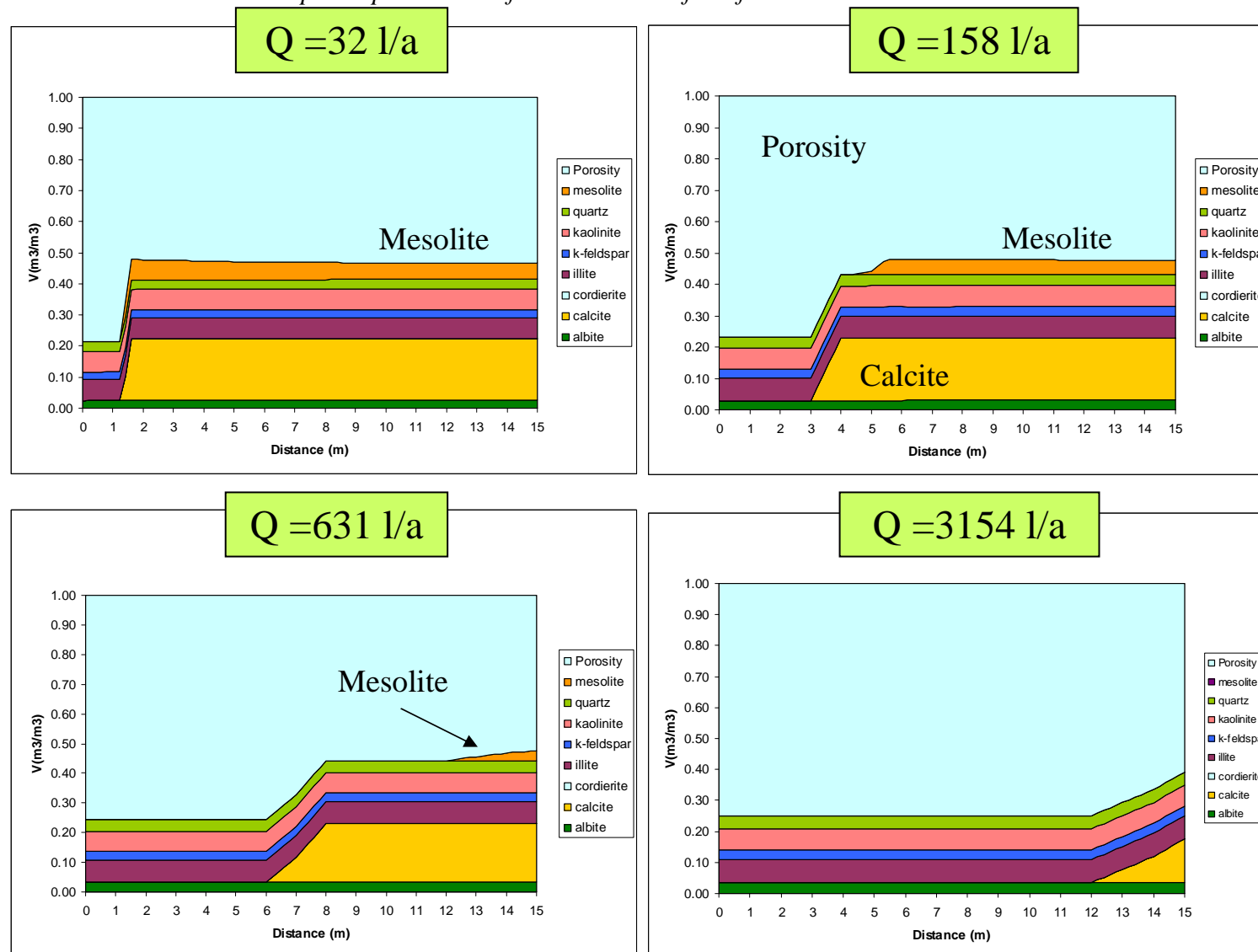


Figure 20c - Volumetric mineral content and porosity for the case with input pH equal to 10.5 and without including Mg-containing secondary minerals. $t = 10000$ a.

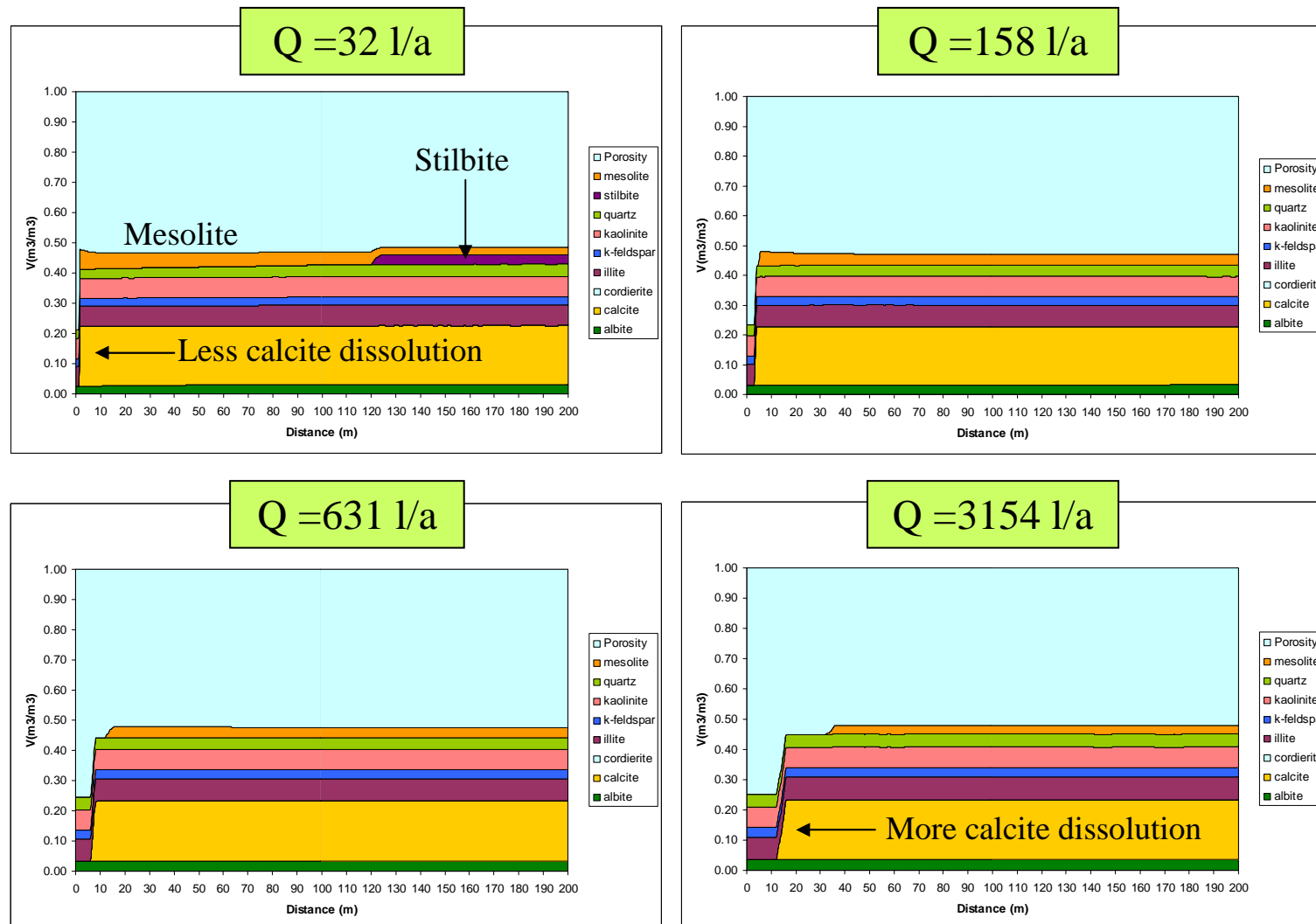


Figure 21a - Volumetric mineral content and porosity for the case with input pH equal to 10.5 and including Mg-containing secondary minerals. $t = 1000$ a. The plot represents the first 15 meters of the fracture

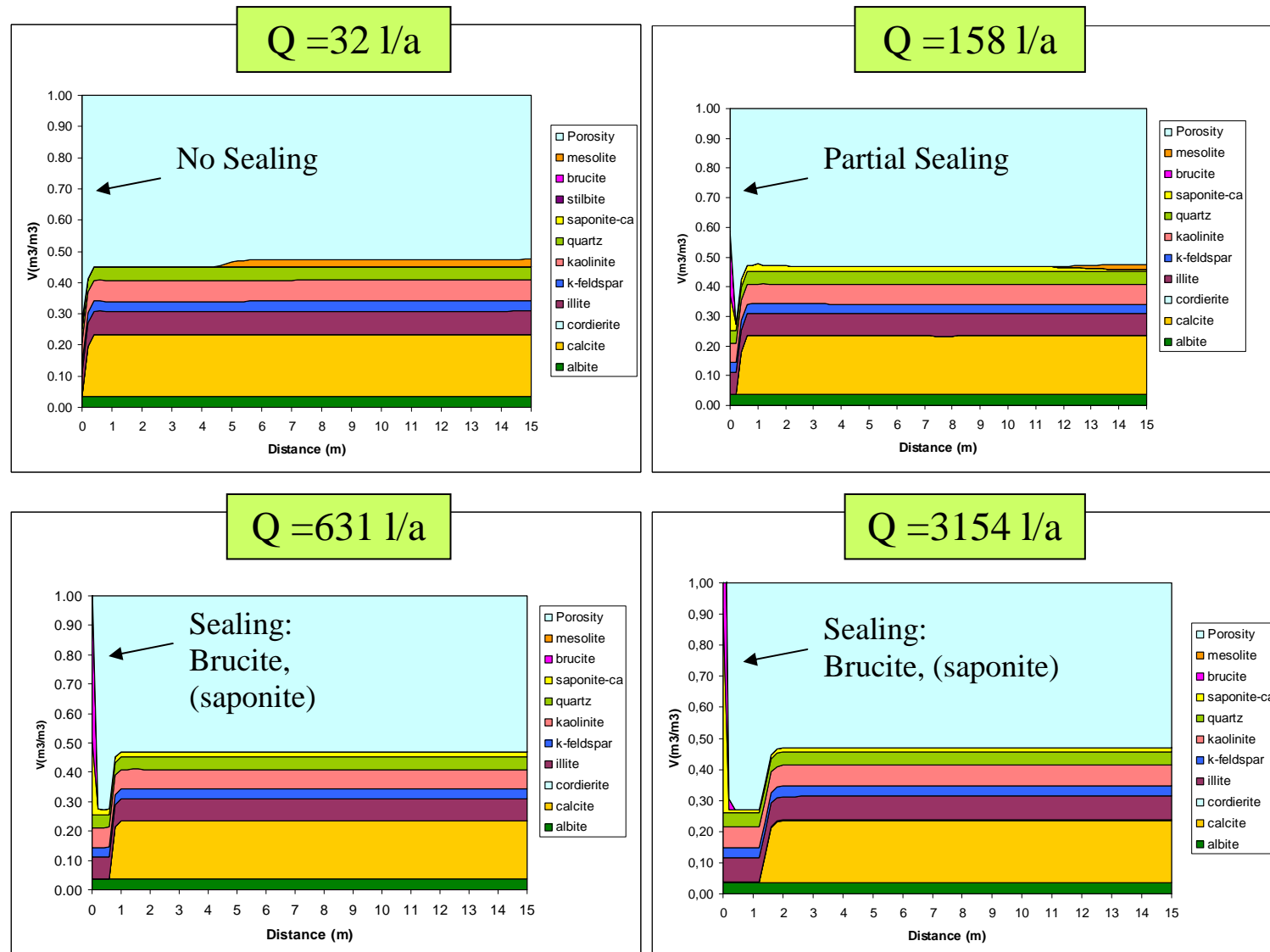


Figure 21b - Volumetric mineral content and porosity for the case with input pH equal to 10.5 and including Mg-containing secondary minerals. $t = 10000$ a. The plot represents the first 15 meters of the fracture.

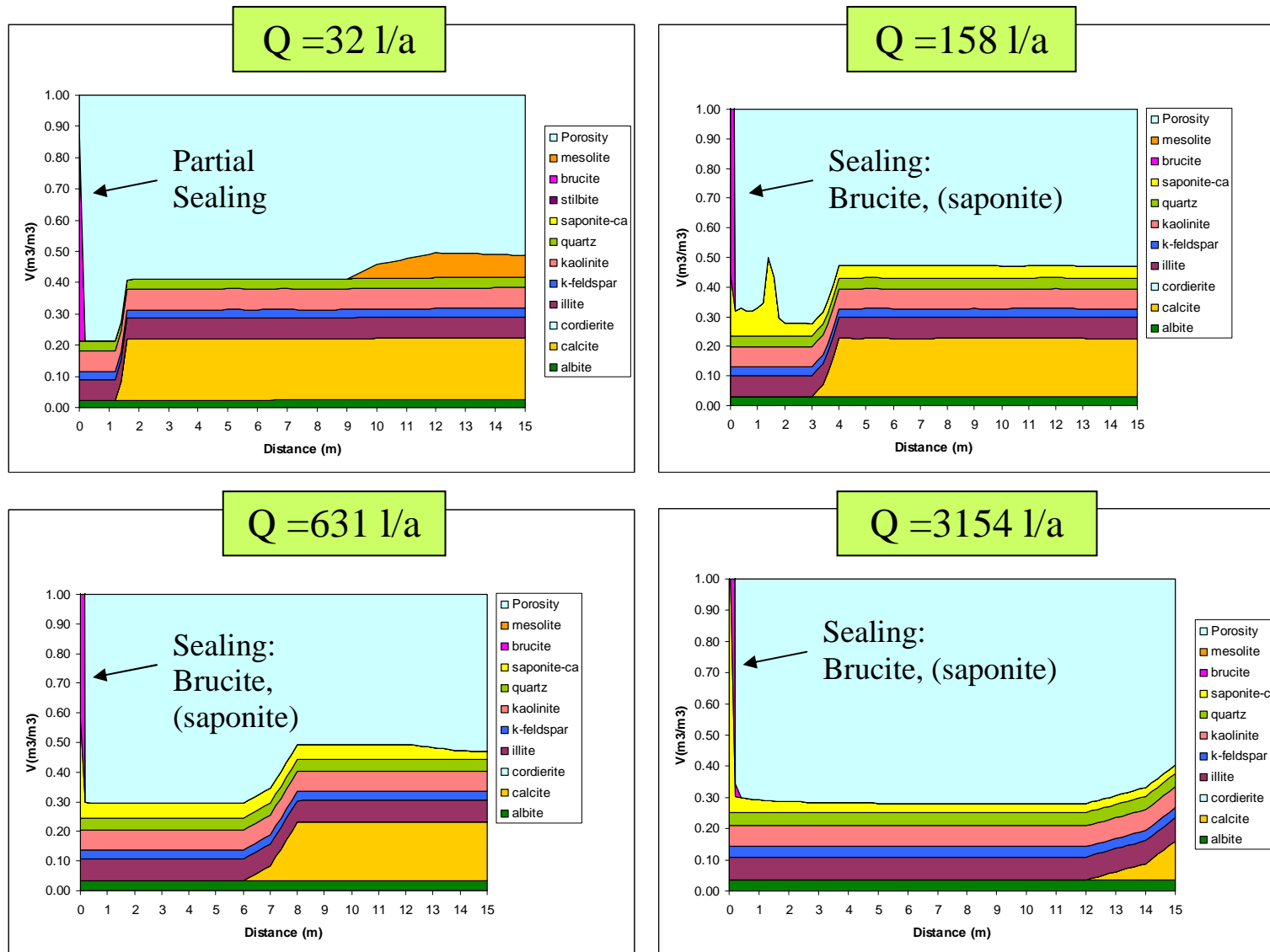


Figure 21c - Volumetric mineral content and porosity for the case with input pH equal to 10.5 and including Mg-containing secondary minerals. $t = 10000$ a.

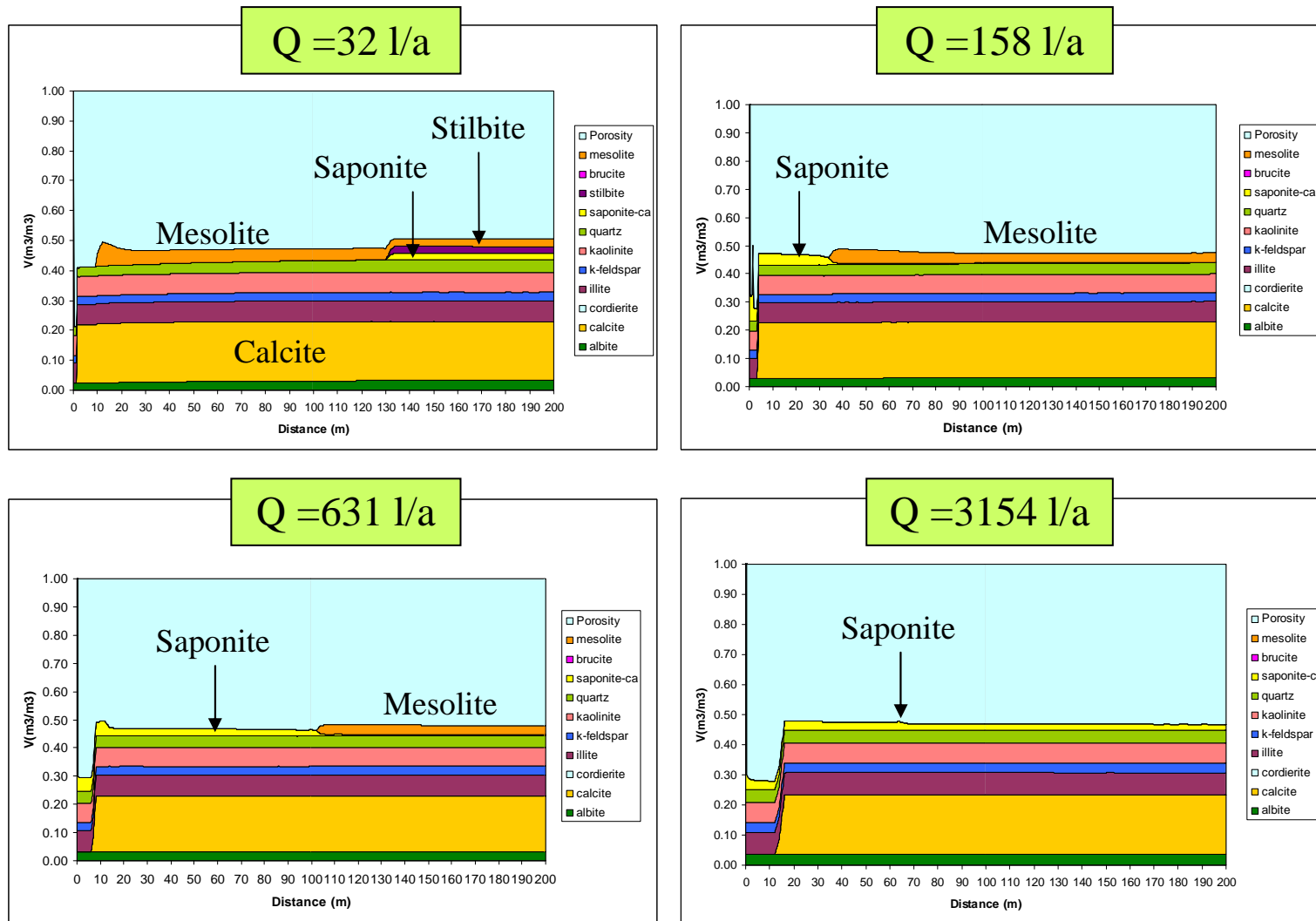


Figure 22a - Volumetric mineral content and porosity for the case with input pH equal to 11 and without including Mg-containing secondary minerals. $t = 1000$ a. The plot represents the first 15 meters of the fracture.

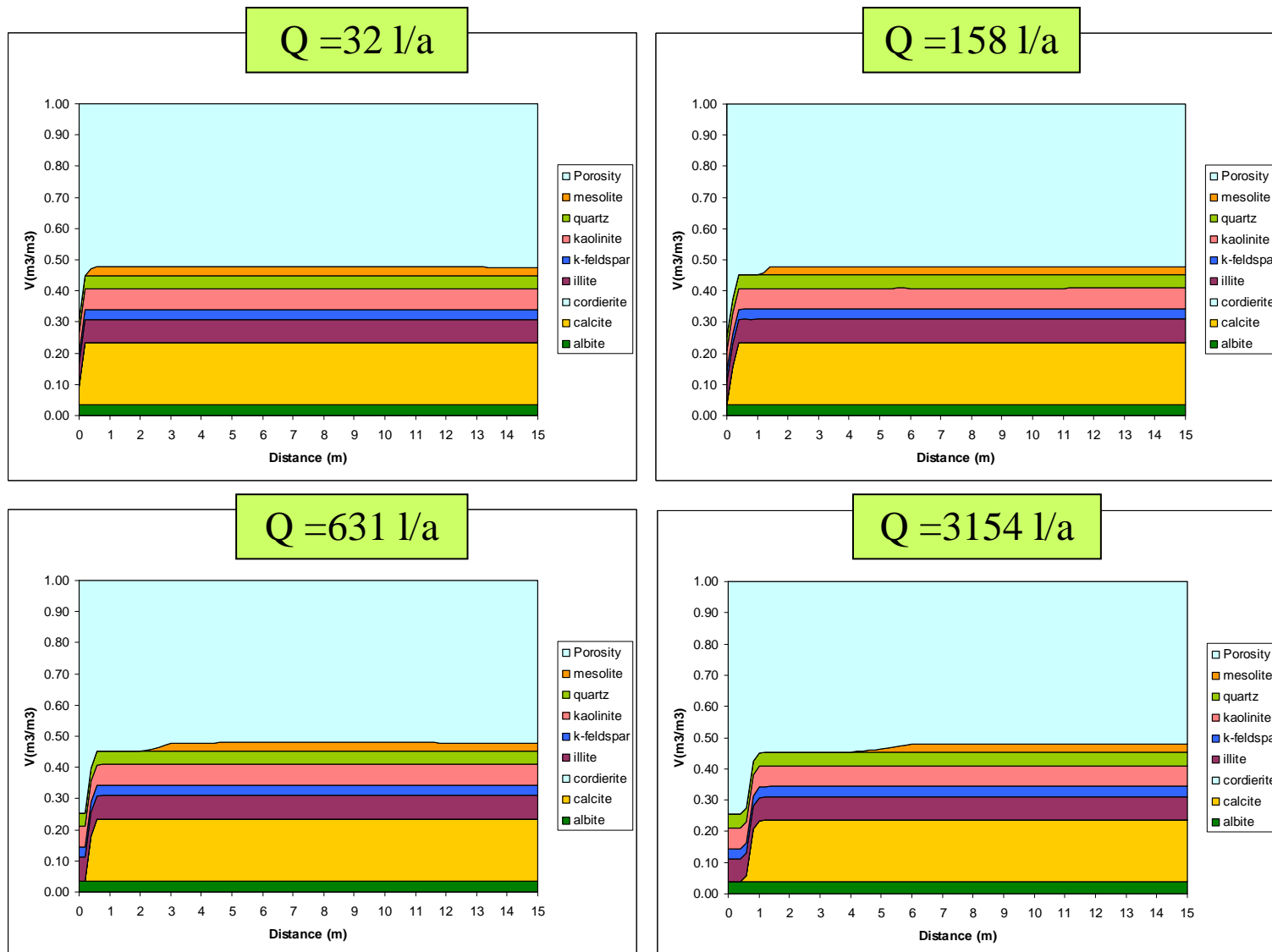


Figure 22b - Volumetric mineral content and porosity for the case with input pH equal to 11 and without including Mg-containing secondary minerals. $t = 10000$ a. The plot represents the first 15 meters of the fracture.

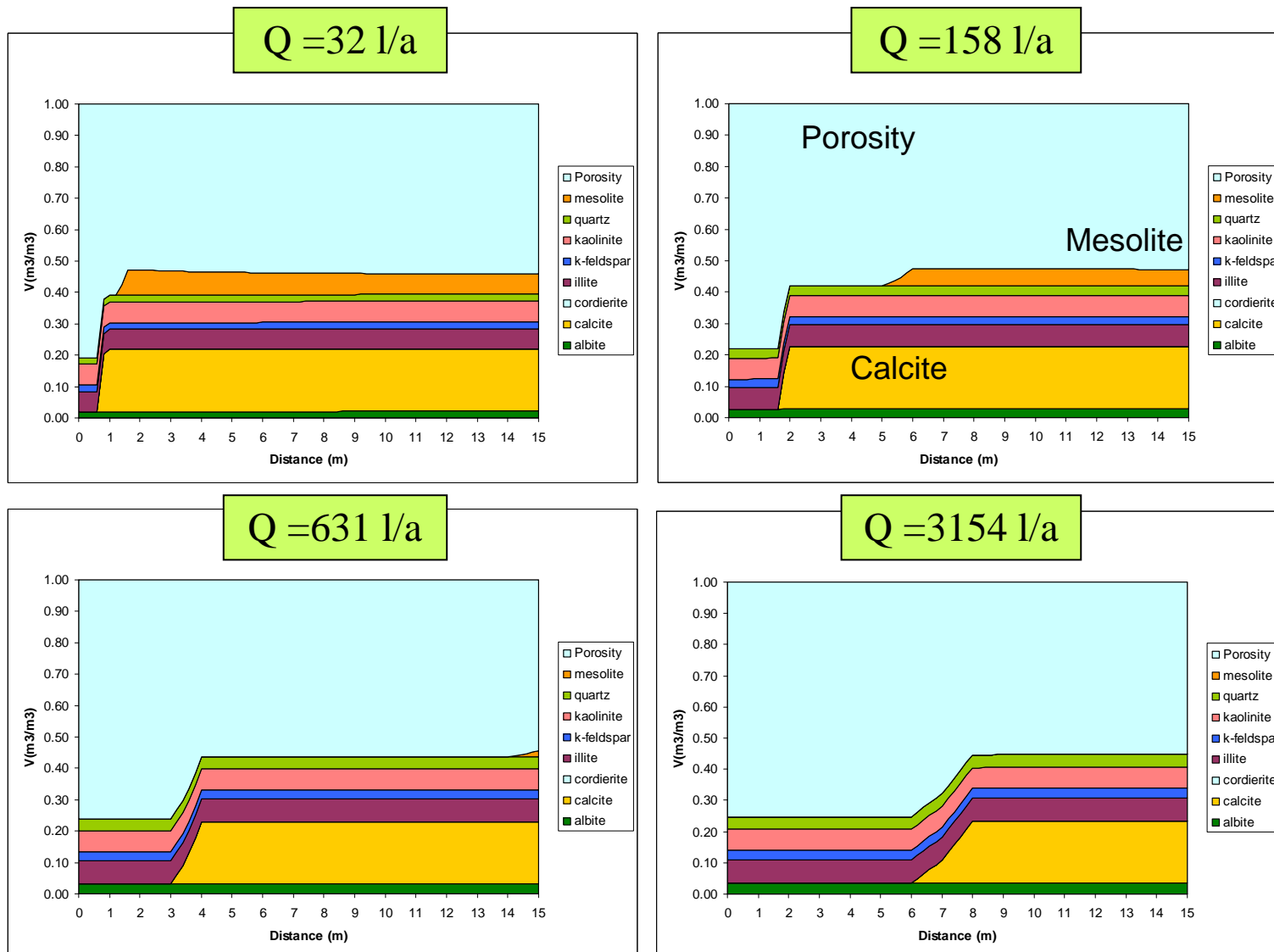


Figure 22c - Volumetric mineral content and porosity for the case with input pH equal to 11 and without including Mg-containing secondary minerals. $t = 10000$ a.

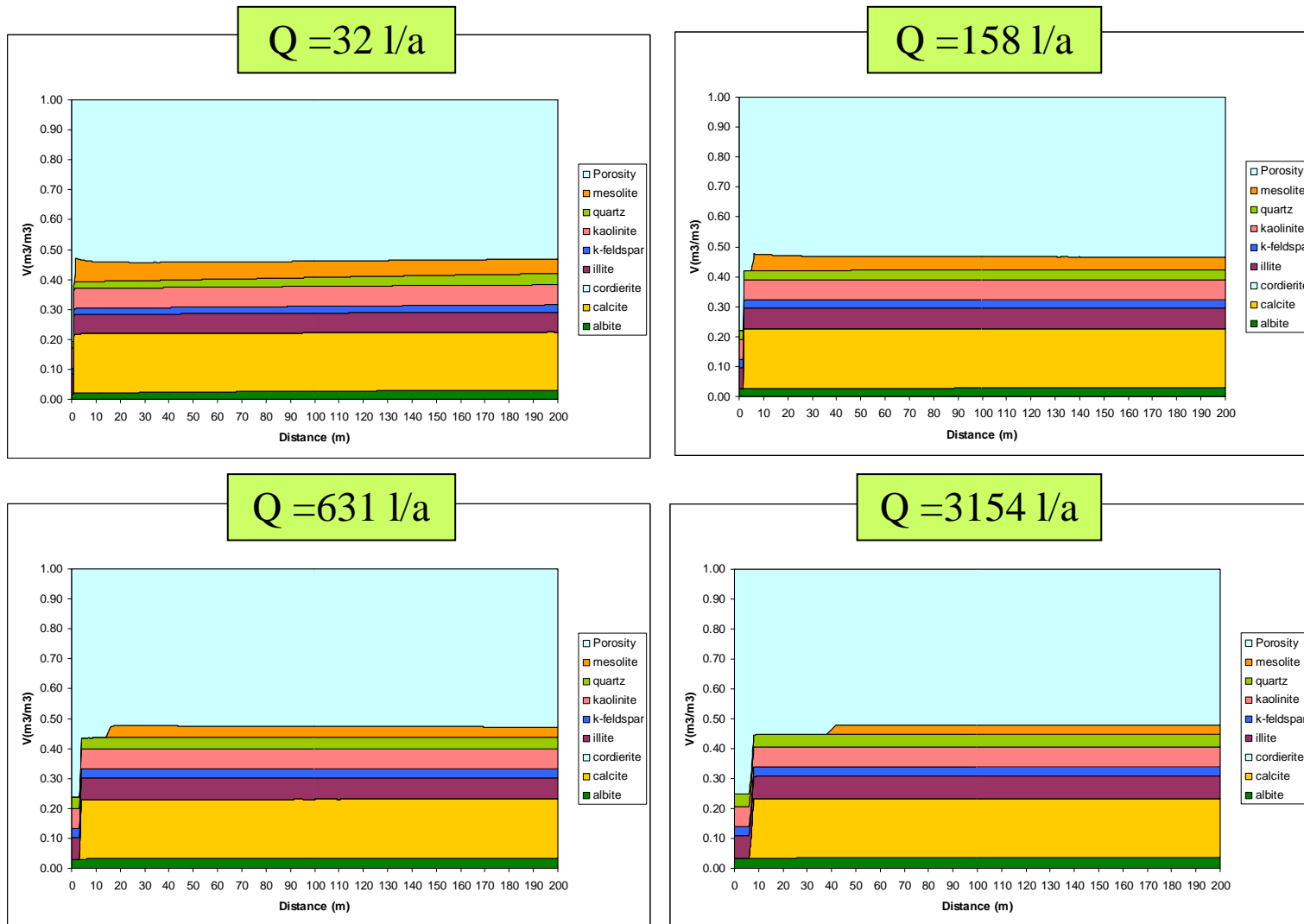


Figure 23a - Volumetric mineral content and porosity for the case with input pH equal to 11 and including Mg-containing secondary minerals. $t = 1000$ a. The plot represents the first 15 meters of the fracture.

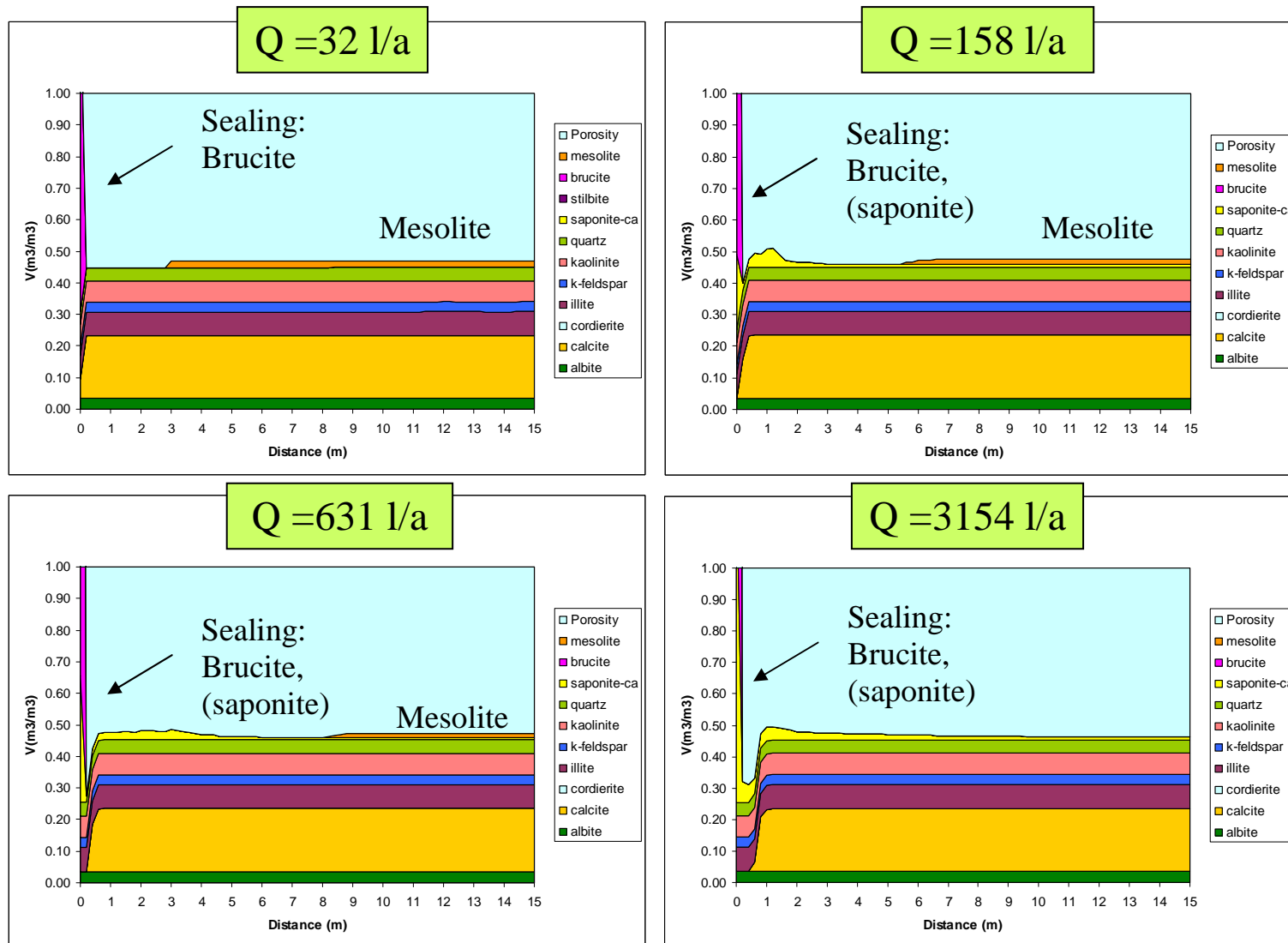


Figure 23b - Volumetric mineral content and porosity for the case with input pH equal to 11 and including Mg-containing secondary minerals. $t = 10000$ a. The plot represents the first 15 meters of the fracture.

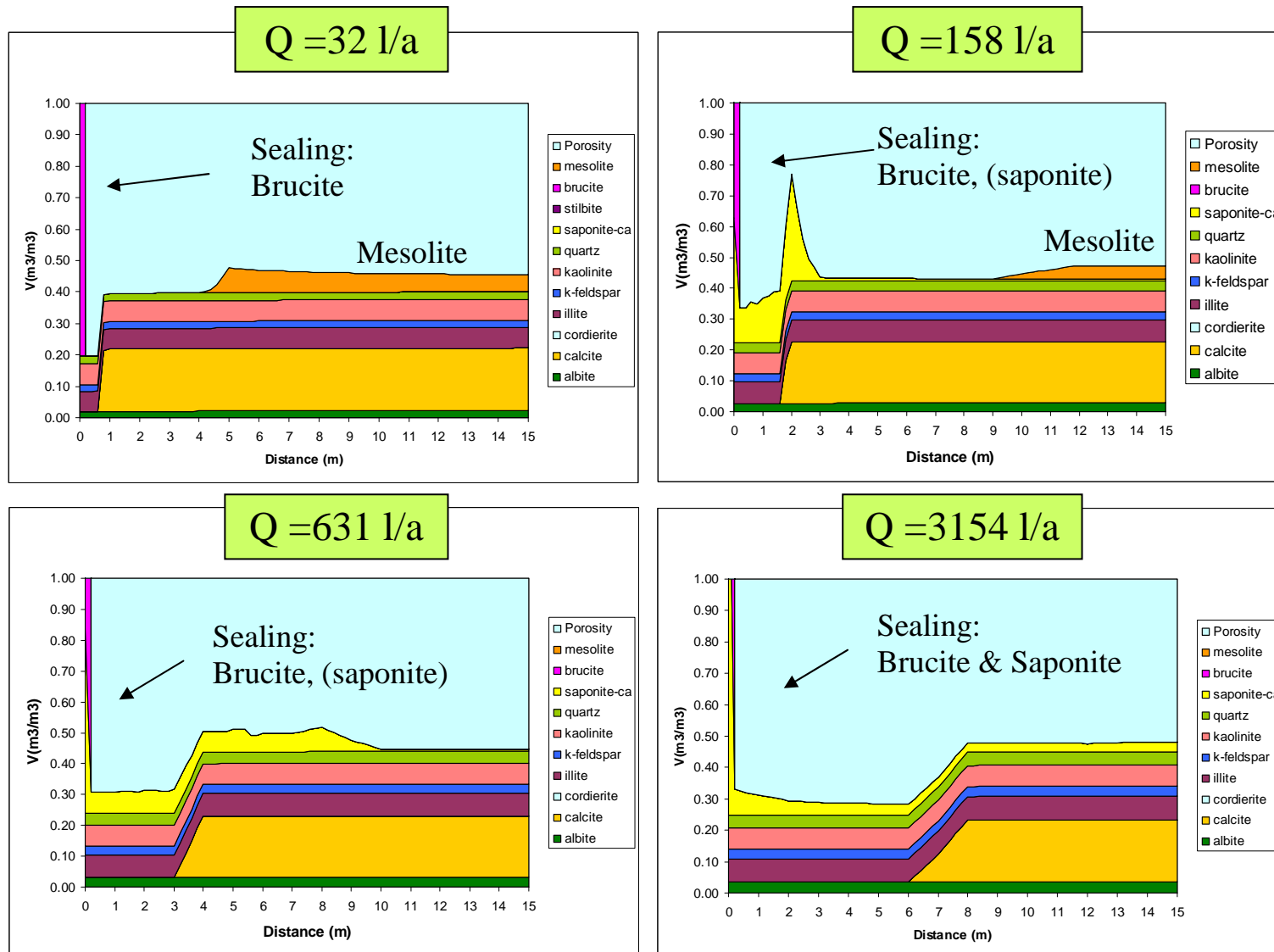


Figure 23c - Volumetric mineral content and porosity for the case with input pH equal to 11 and including Mg-containing secondary minerals. $t = 10000$ a.

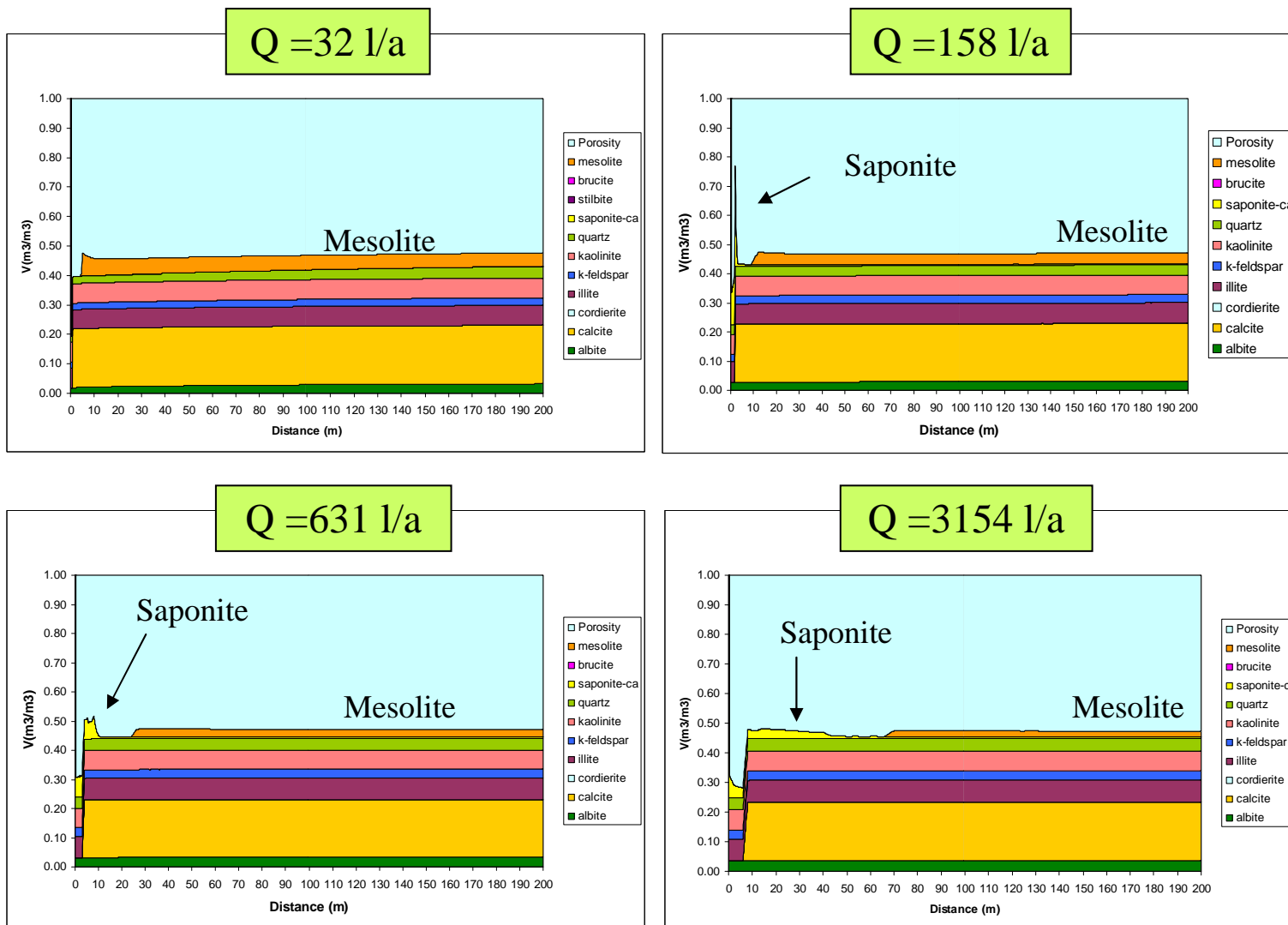


Figure 24a - Volumetric mineral content and porosity for the case with input pH equal to 12 and without including Mg-containing secondary minerals. $t = 1000$ a.

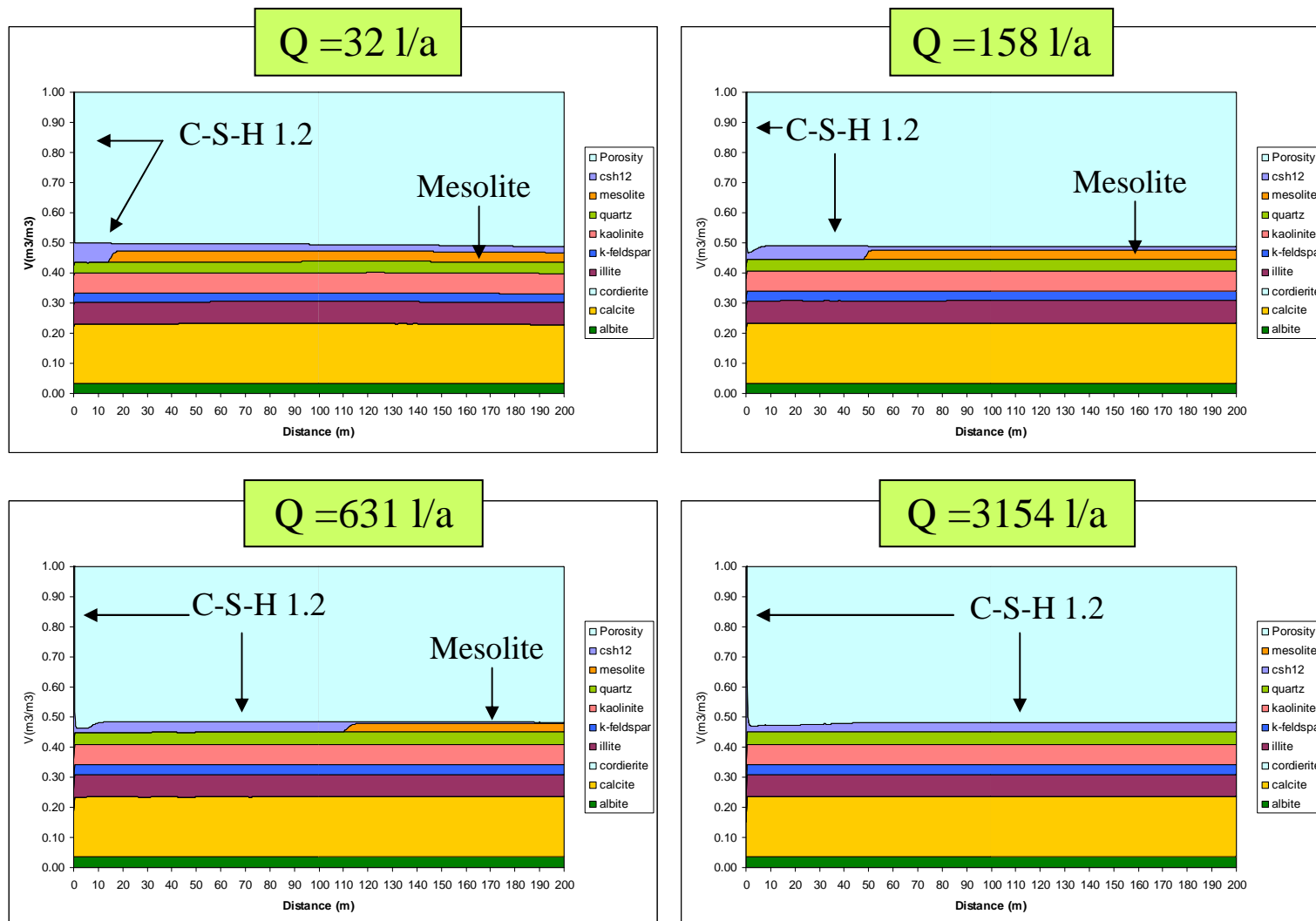


Figure 24b - Volumetric mineral content and porosity for the case with input pH equal to 12 and without including Mg-containing secondary minerals. $t = 10000$ a.

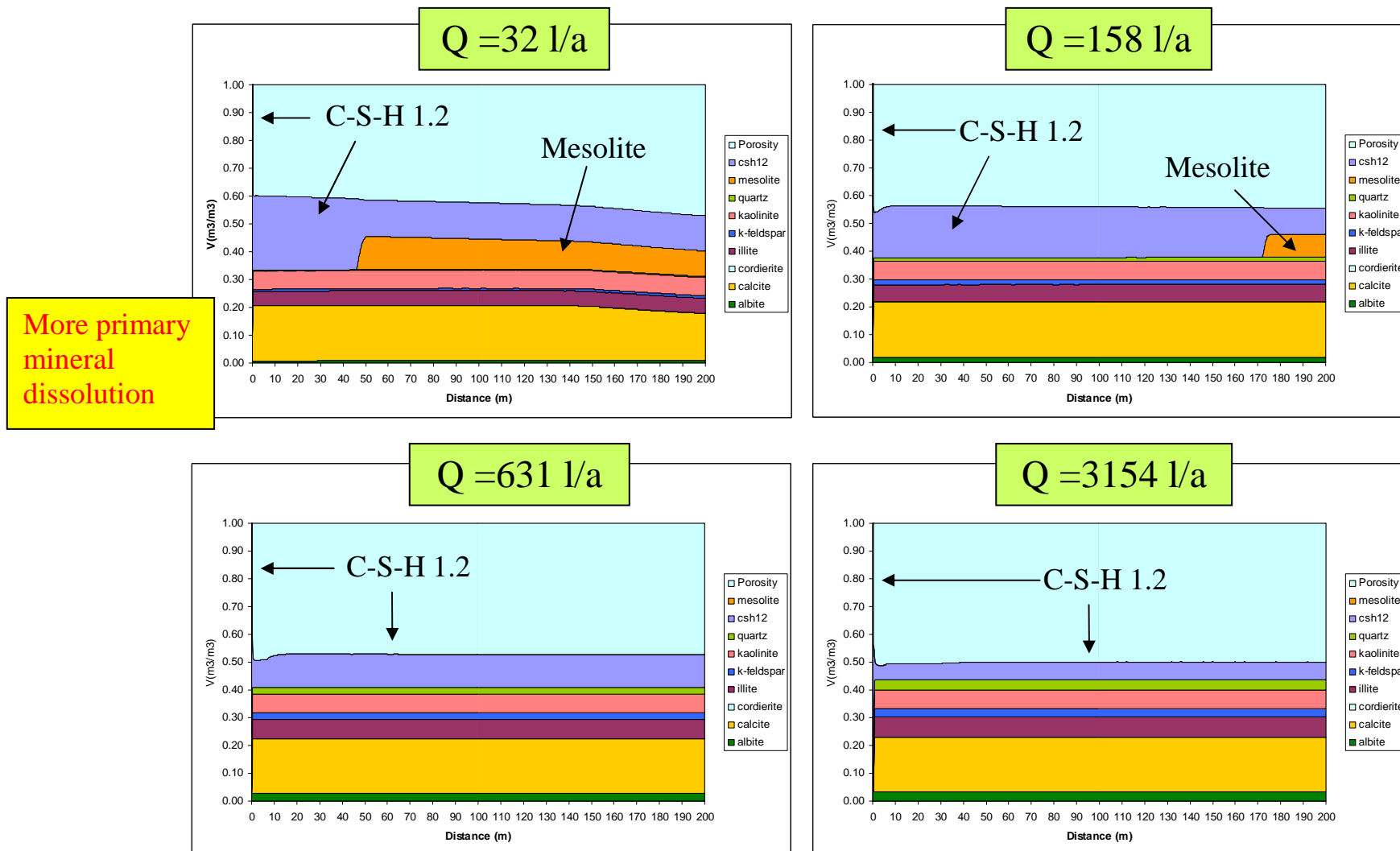


Figure 24c - Volumetric mineral content and porosity for the case with input pH equal to 12 and without including Mg-containing secondary minerals. $t = 10000$ a. The plot represents the first 15 meters of the fracture.

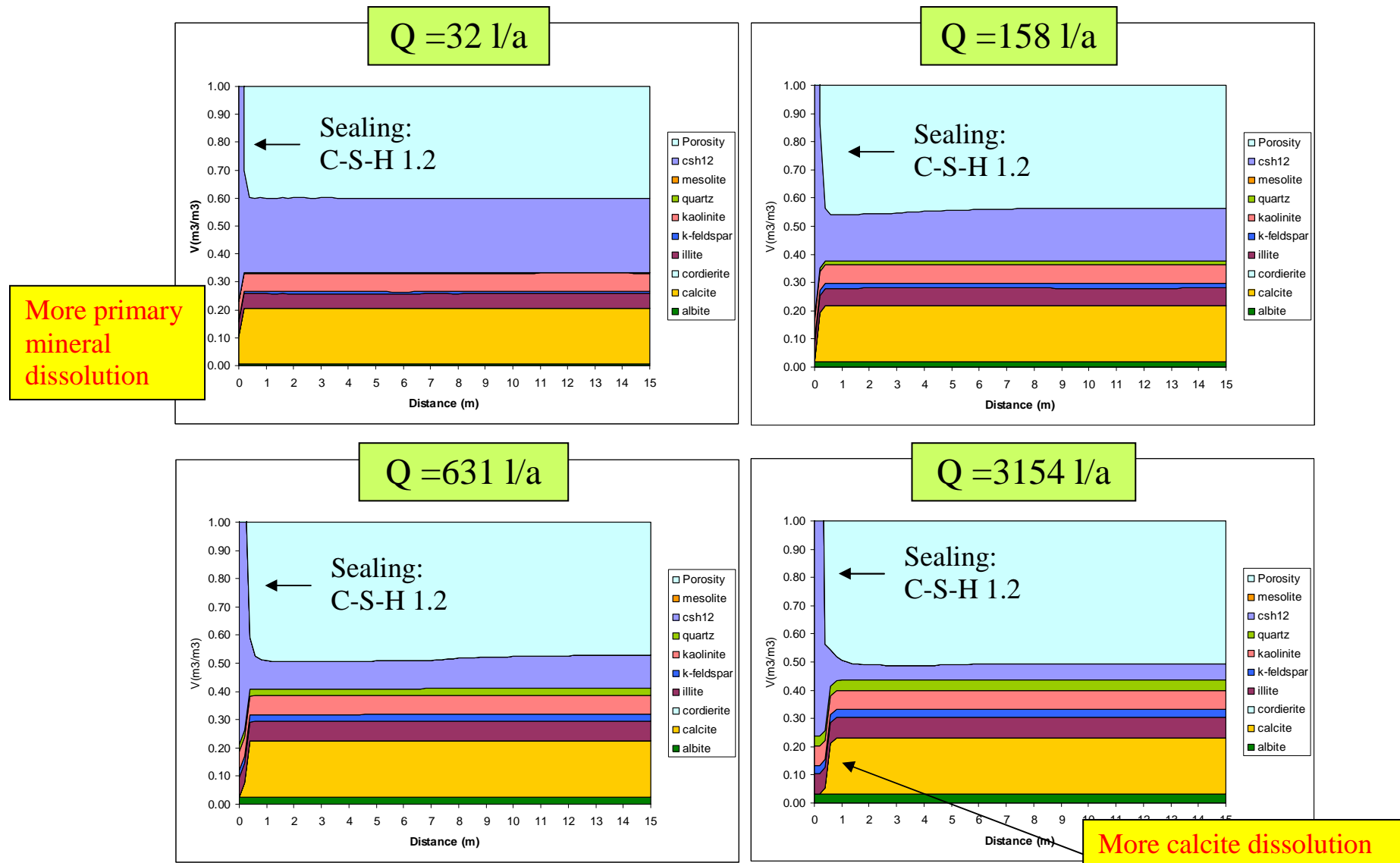


Figure 25a - Volumetric mineral content and porosity for the case with input pH equal to 12 and including Mg-containing secondary minerals. $t = 1000$ a.

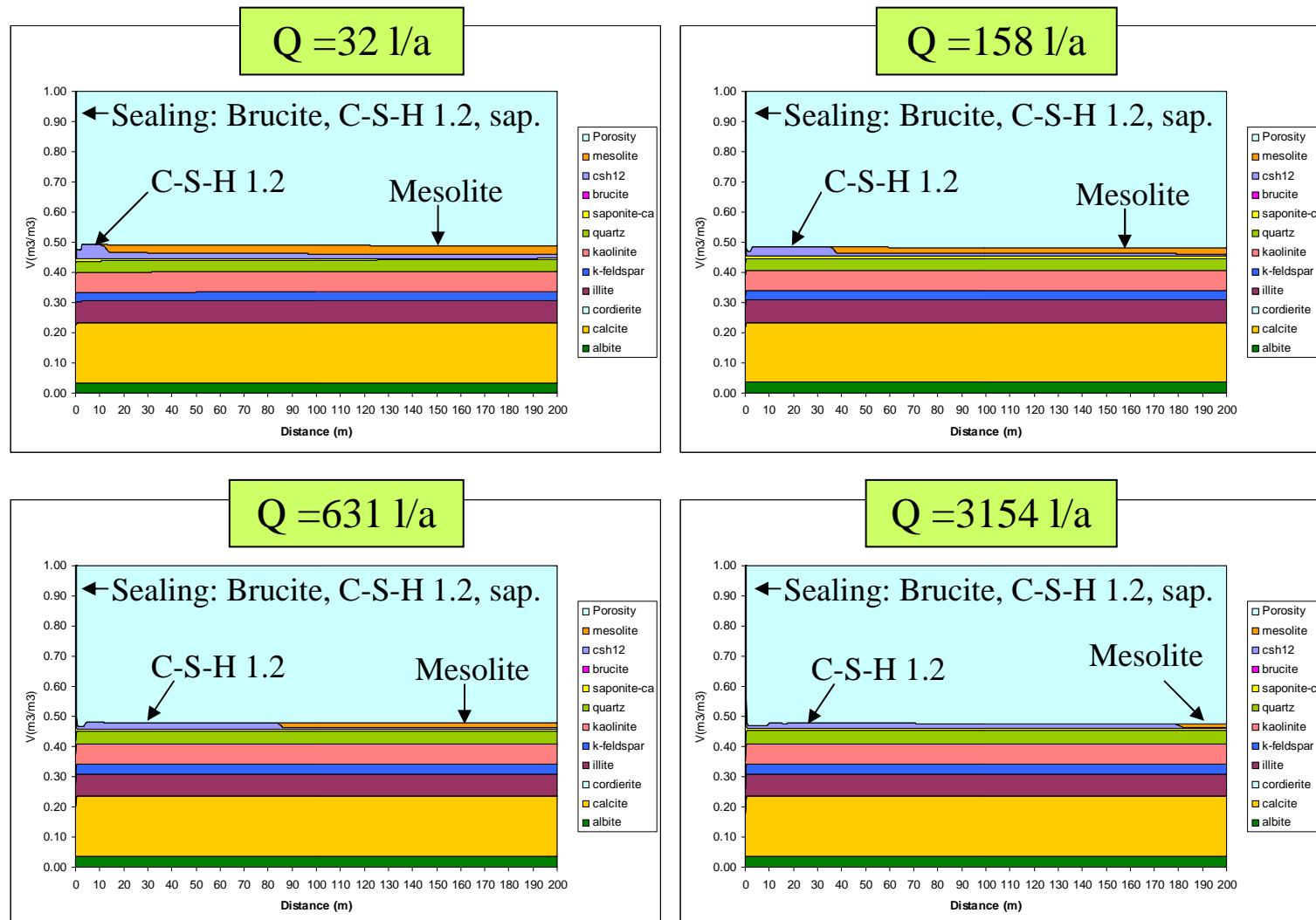


Figure 25b - Volumetric mineral content and porosity for the case with input pH equal to 12 and including Mg-containing secondary minerals. $t = 10000$ a.

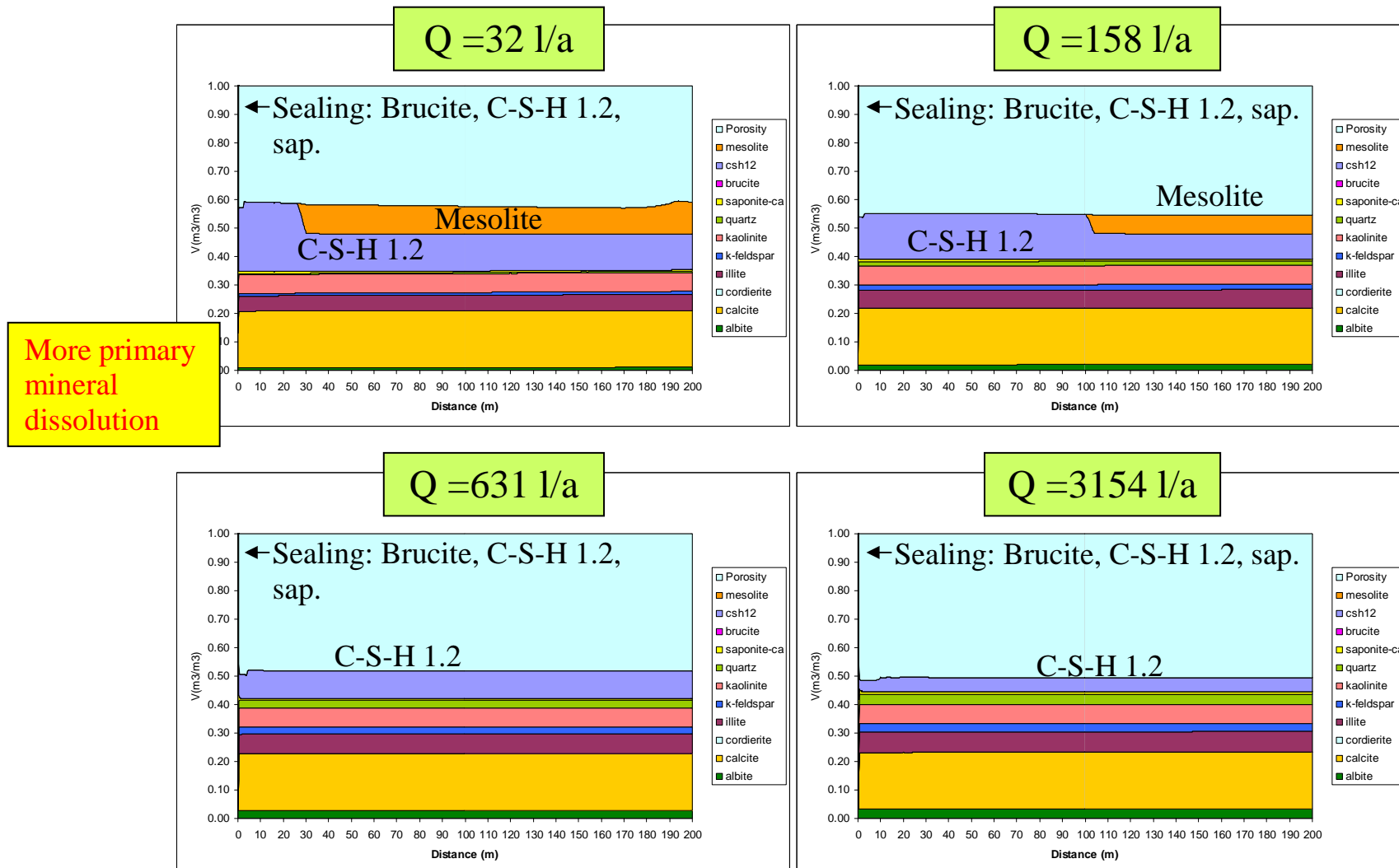


Figure 25c - Volumetric mineral content and porosity for the case with input pH equal to 12 and including Mg-containing secondary minerals. $t = 10000$ a. The plot represents the first 15 meters of the fracture.

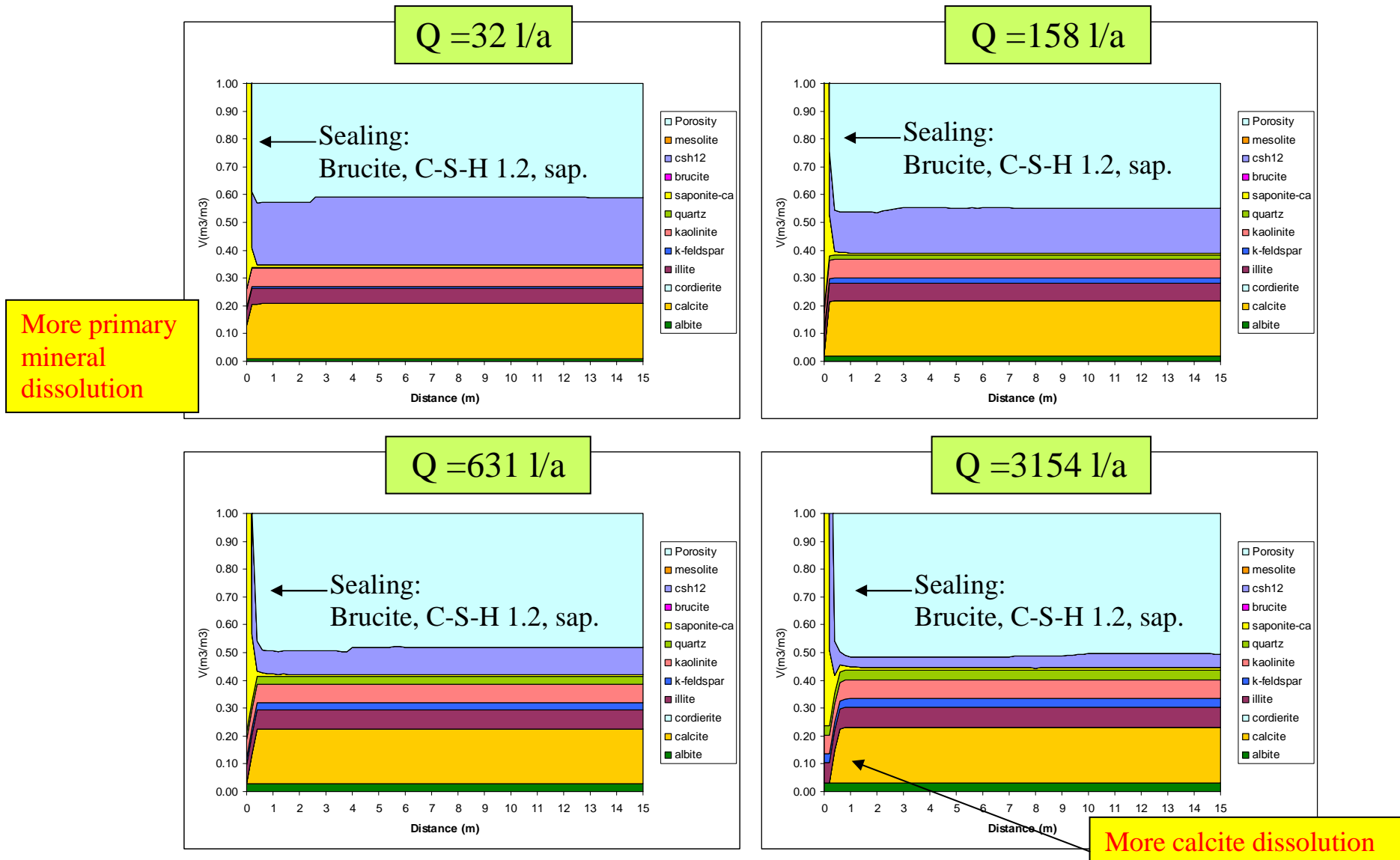


Figure 26 - Solution pH vs. distance for all the cases (without including Mg-containing secondary minerals).

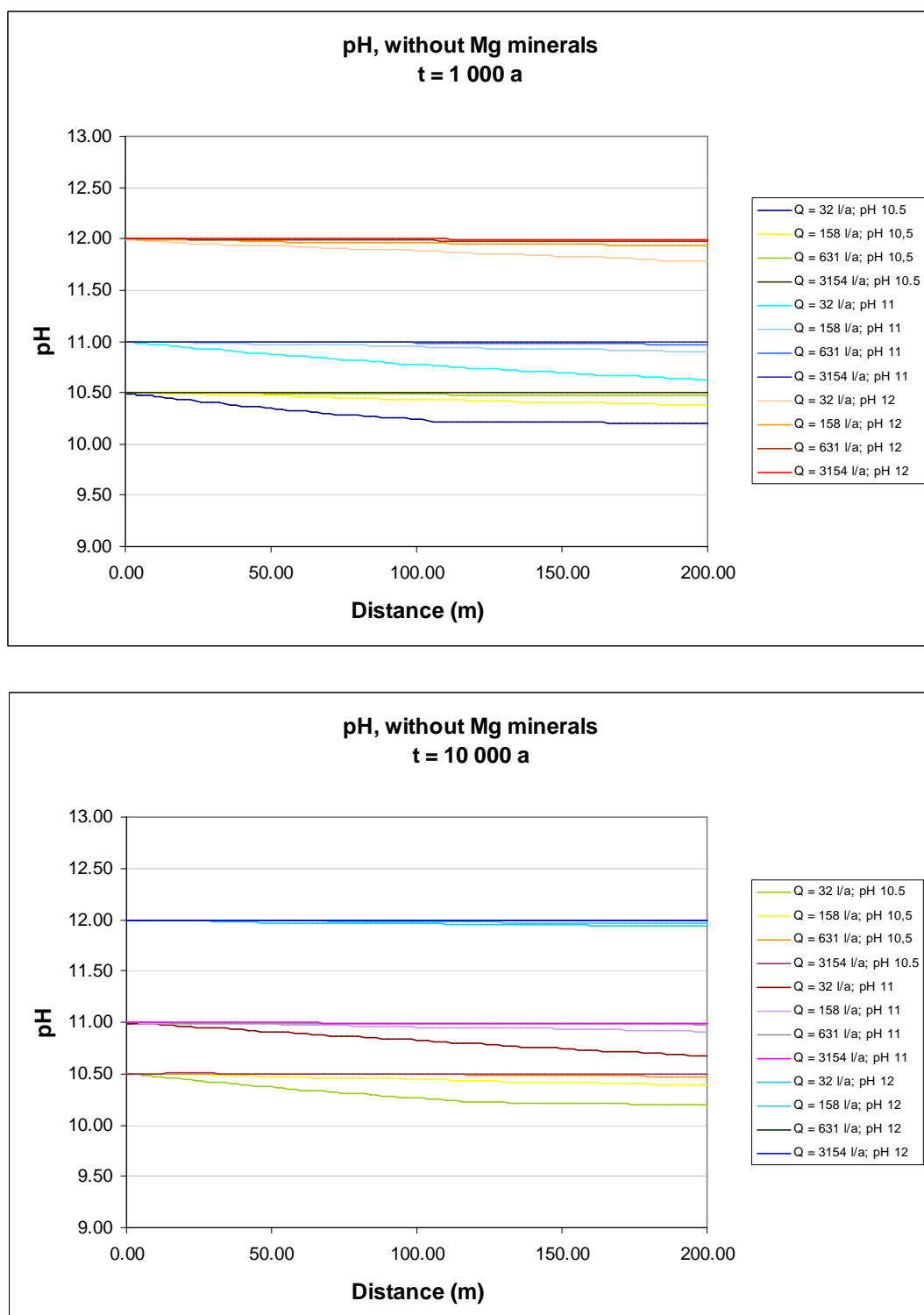
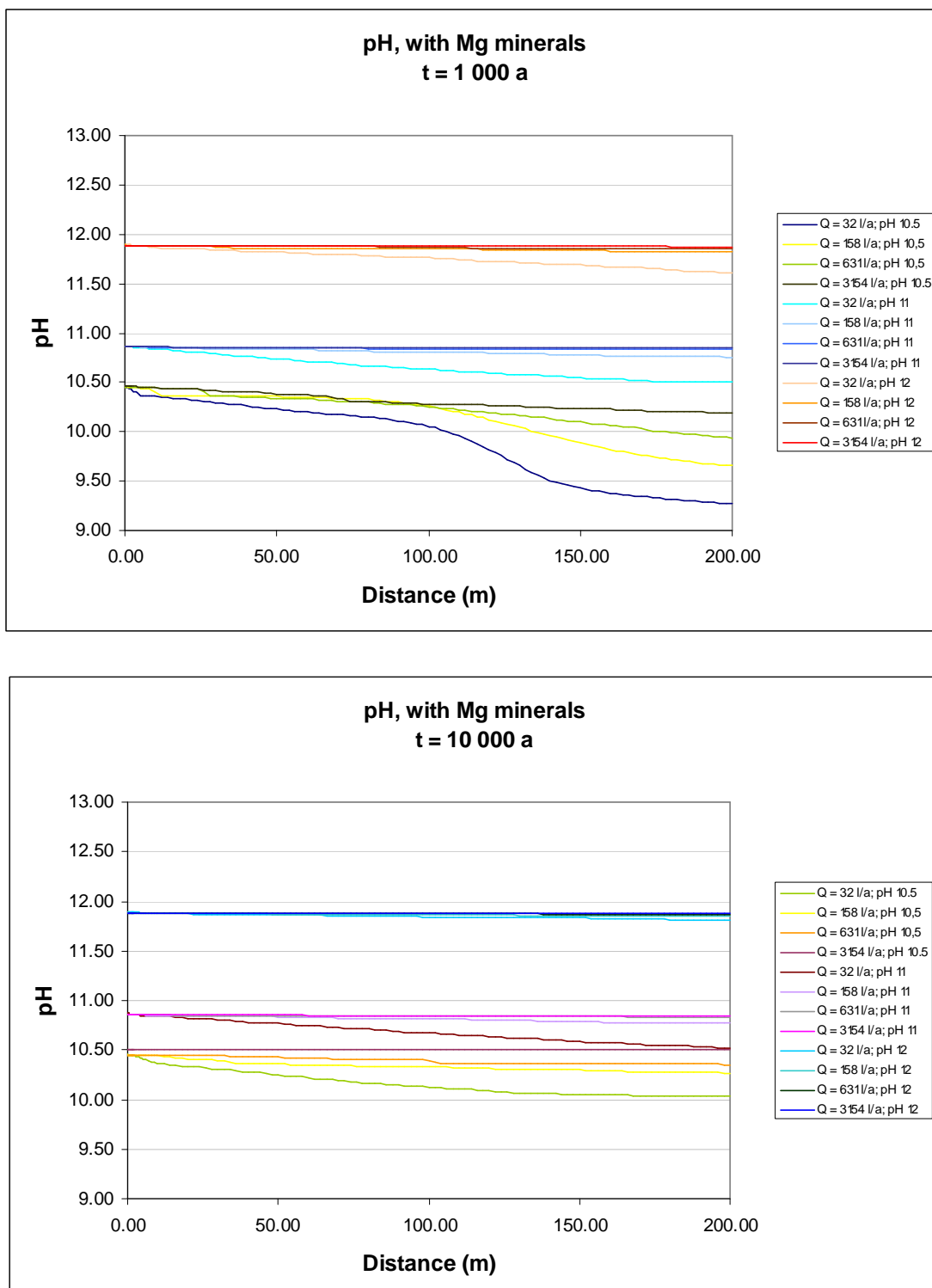


Figure 27 - Solution pH vs. distance for all the cases (including Mg-containing secondary minerals).



5.3. Q=631 l/a. Comparison of (A) High-pH solution 1 ($T = 25^\circ\text{C}$), (B) High-pH solution 1 (Variable T), (C) High-pH solution 2 (Experimental, $T = 25^\circ\text{C}$) and (D) High-pH solution 3 (Experimental, $T = 25^\circ\text{C}$)

In this chapter the results for a reference case ($Q = 631 \text{ l/a}$) with constant or variable temperature and those corresponding to high-pH solutions derived from leaching experiments (leaching with OL-SR saline solution and ALL-MR fresh solution at 12°C) will be compared. Two simulations are associated with each case; one including Mg-containing secondary minerals (brucite, sepiolite, saponites) and another one without including them.

Figure 28 shows the evolution of temperature in the domain for the case with variable temperature.

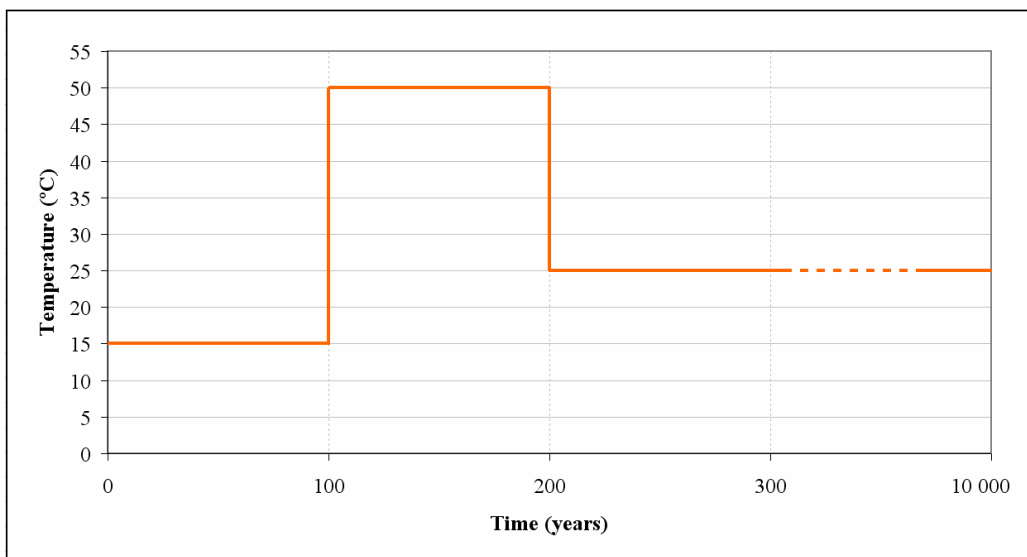


Figure 28 - Evolution of temperature used in the cases with variable temperature.

The results from the cases with constant or variable temperature (high-pH solution 1) are almost identical. On the other hand, the behavior of the model including the experimental high-pH solutions shows some definite particularities. There are no major variations of pH along the domain in any of the cases (Figs. 26, 27).

5.3.1. Q=631 l/a, lower pH cases, no Mg-containing secondary minerals

(Mineral contents and pH; Figs. 29, 35, 36)

The cases with variable temperature and constant temperature are very similar. In both cases, as in the previous chapter, there is an increase in porosity at the fracture inlet caused by the dissolution of calcite, precipitation of mesolite further down the fracture, quick dissolution of cordierite and minor dissolution of other primary minerals.

The case using the high-pH solution from leaching tests using a saline leaching solution (pH 9.7) shows a very significant difference with respect to the other cases. The intense precipitation of mesolite right at the fracture inlet causes the sealing of the fracture. This precipitation is due to the composition of this boundary water (high-pH solution 2), which is richer in Ca, Na, Si and Al than the initial solution (high-pH solution 1). High-pH solution 2 is already supersaturated with respect to several zeolites (Table 3a). This water is richer in carbonate too; in consequence, there is less dissolution of calcite than in the other two cases (the calcite dissolution front advances more slowly).

In the same way, the case with the experimental high-pH solution from leaching tests using a fresh leaching solution (pH 10.6) also shows intense mineral precipitation right at the fracture inlet, which causes the sealing of the fracture. In this case the mineral is stilbite. This precipitation is due to the composition of this boundary water (high-pH solution 3), which is richer in Na, Si and Al than the initial solution (high-pH solution 1). The small increase in pH at early times (Fig. 36; small step in pH at about 80 m) is due to the dissolution of previously precipitated mesolite combined with the precipitation of stilbite (advance of a stilbite-mesolite reaction front). In addition, this case also shows minor quartz precipitation (the incoming high-pH solution is slightly supersaturated with respect to quartz).

5.3.2. Q=631 l/a, lower pH cases, with Mg-containing secondary minerals

(Mineral contents and pH; Figs. 30,37,38)

The cases with variable temperature and constant temperature are very similar. Their main features are already described in section 5.2.2. (intense precipitation of brucite and Ca-saponite at the fracture inlet that causes the quick sealing of fracture porosity; precipitation of Ca-saponite further down the domain).

In the case with high-pH solution 2 (pH 9.7) the sealing of the fracture inlet by brucite and saponite occurs more slowly than in the other cases. Also, the calcite dissolution front advances more slowly.

For high-pH solution 3 (pH 10.60), the sealing of the fracture inlet also occurs more slowly than for high-pH solution 1 (pH 10.50), but in this case the minerals responsible for the sealing of porosity are stilbite and saponite. There is also minor precipitation of quartz. The small increase in pH at early times (Fig. 38; small step in pH at about 80 m) is due to the dissolution of previously precipitated mesolite combined with the precipitation of stilbite (advance of a stilbite-mesolite reaction front).

5.3.3. Q=631 l/a, intermediate pH cases, no Mg-containing secondary minerals

(Mineral contents and pH; Figs.31,35,36)

The cases with variable temperature and constant temperature are very similar. Their main features are already described in section 5.2.3. (increase in porosity at the fracture

inlet, precipitation of mesolite further down the fracture, fast dissolution of cordierite and minor dissolution of the other primary minerals). The cases with high-pH solution 2 (pH 11.6) and high-pH solution 3 (pH 11.9) show precipitation of C-S-H (Ca/Si = 1.2) but not at the fracture inlet (no sealing).

5.3.4. Q=631 l/a, intermediate pH cases, with Mg-containing secondary minerals

(Mineral contents and pH; Figs. 32,37,38)

The cases with variable temperature and constant temperature are very similar. Their main features are already described in section 5.4. The main difference shown by the case with high-pH solution 2 (pH 11.6) and high-pH solution 3 (pH 11.9) is in the fact that sealing of the fracture inlet occurs more slowly. Additionally, sealing in the case of high-pH solution 3 (pH 11.9) is caused by saponite instead of brucite, and it is not yet complete (porosity > 0) after 10000 a. There is also precipitation of C-S-H (Ca/Si = 1.2) further down the domain.

5.3.5. Q=631 l/a, higher pH cases, no Mg-containing secondary minerals

(Mineral contents and pH; Figs. 33,35,36)

The cases with variable temperature and constant temperature continue being very similar and the experimental case (high-pH solution 2 and 3) are substantially different. In the four cases there is a sealing of the fracture inlet. However, in the cases with high-pH solution 1 (pH 12) the sealing is caused by C-S-H 1.2 and in the case with high-pH solution 2 (pH 12.17) and 3 (pH 12.45) the sealing is caused by portlandite. Moreover, there is precipitation of C-S-H 1.667 further down the domain in the cases with high-pH solution 2 and 3. The advance of the calcite dissolution front is also faster, due to the fact that the high-pH solutions 2 and 3 are more undersaturated with respect to calcite than the pH 12 solution.

5.3.6. Q=631 l/a, higher pH cases, with Mg-containing secondary minerals

(Mineral contents and pH; Figs. 34,37,38)

These cases are similar to the ones shown in section 5.3.5, but they show precipitation of brucite (all cases) and saponite (only high-pH solution 1) at the fracture inlet in addition to C-S-H and portlandite.

Figure 29a - Volumetric mineral content and porosity for the case with lower pH and without including Mg-containing secondary minerals. $t = 1000$ a. The plot represents the first 15 meters of the fracture.

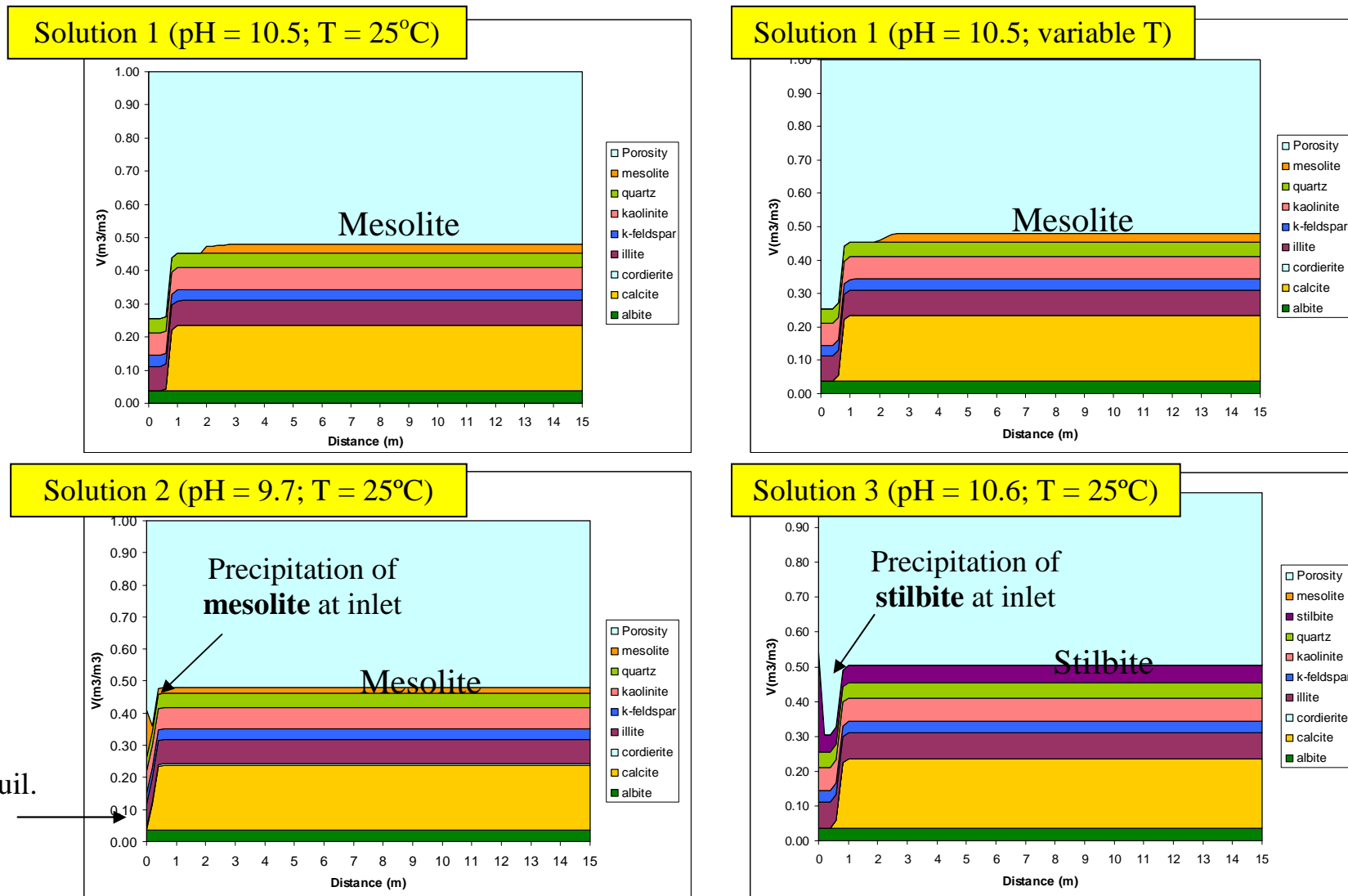


Figure 29b - Volumetric mineral content and porosity for the case with lower pH and without including Mg-containing secondary minerals. $t = 10000$ a. The plot represents the first 15 meters of the fracture.

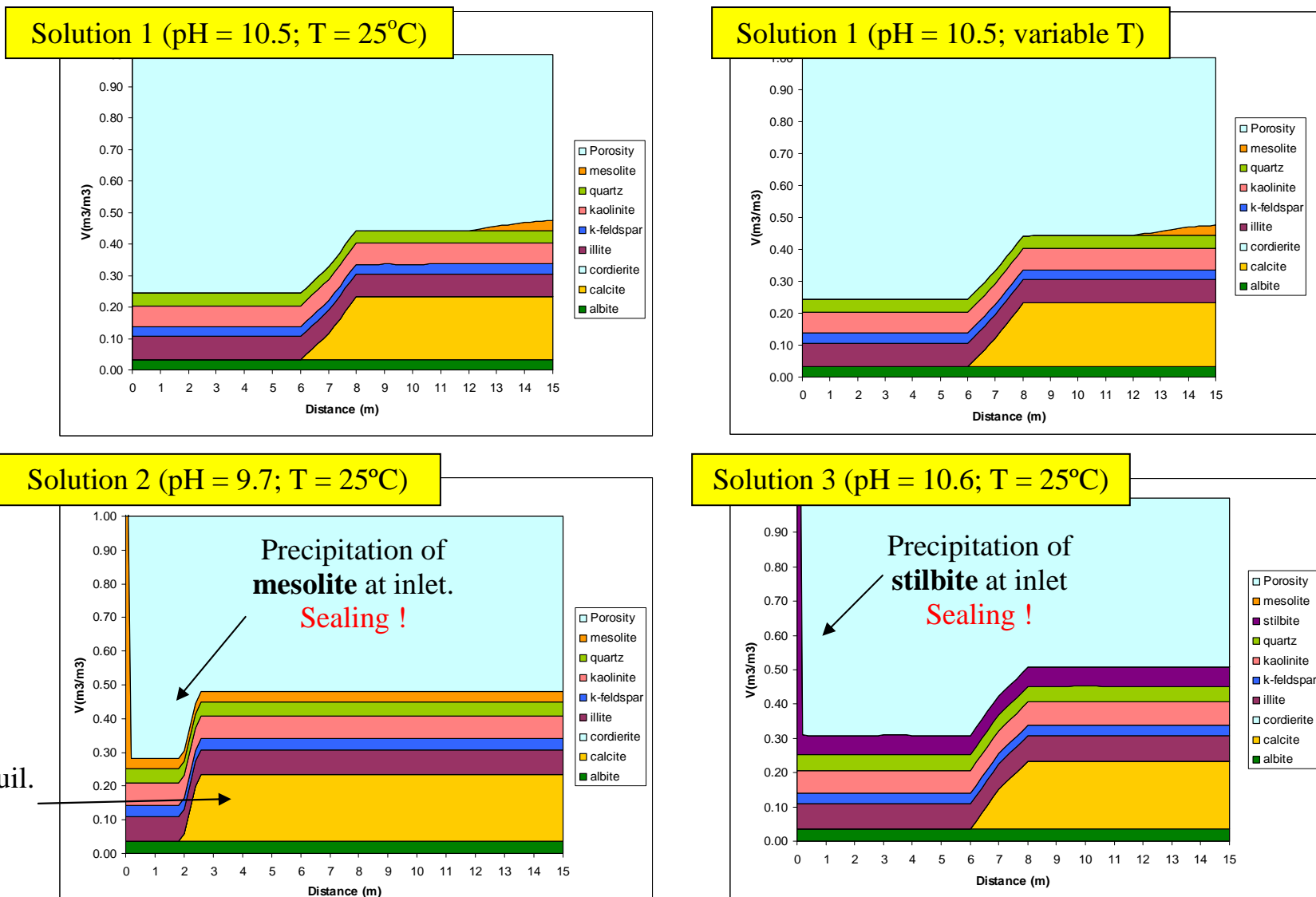


Figure 30a - Volumetric mineral content and porosity for the case with input lower pH and including Mg-containing secondary minerals. $t = 1000$ a. The plot represents the first 15 meters of the fracture.

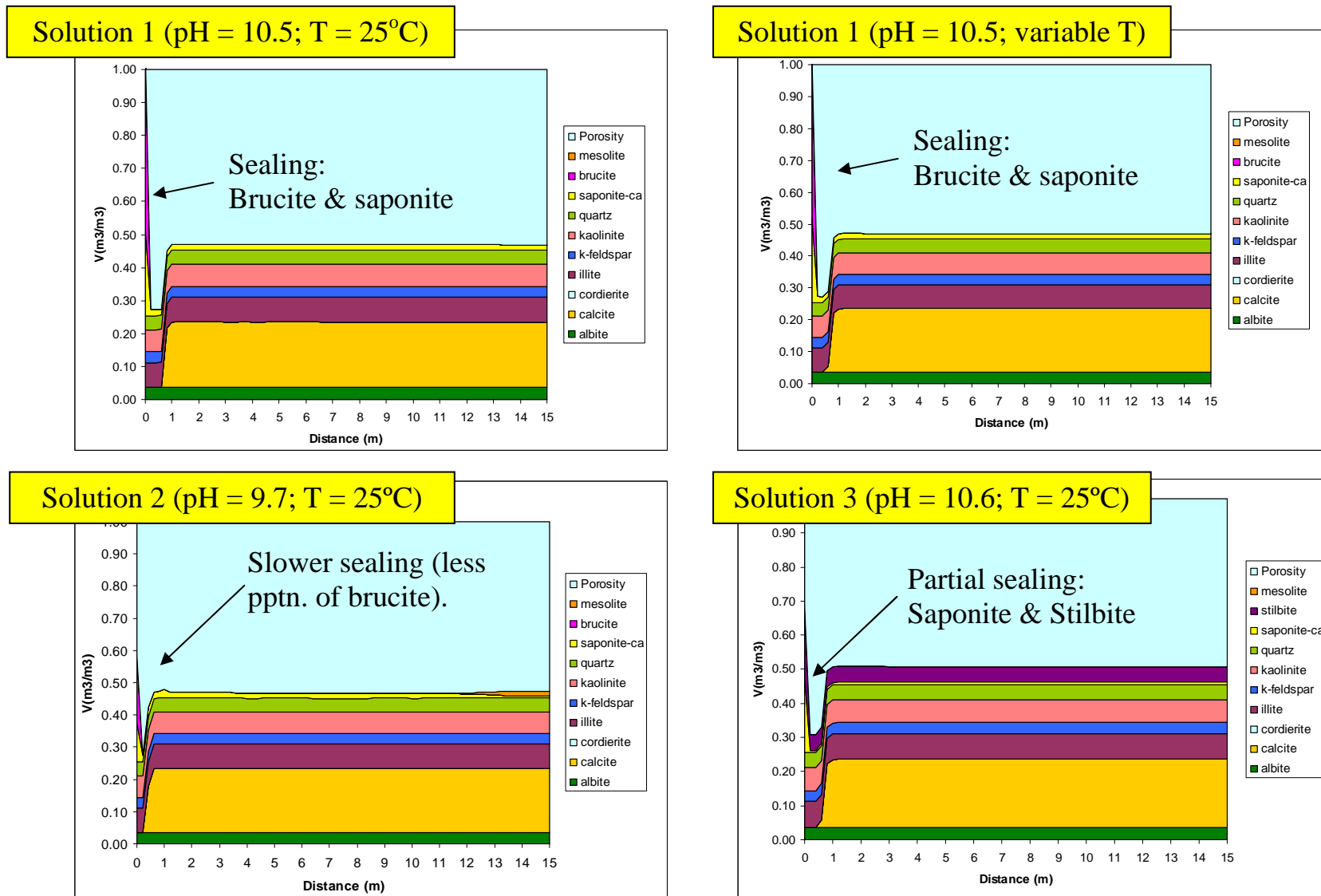


Figure 30b - Volumetric mineral content and porosity for the case with lower pH and including Mg-containing secondary minerals. $t = 5000$ a. The plot represents the first 15 meters of the fracture.

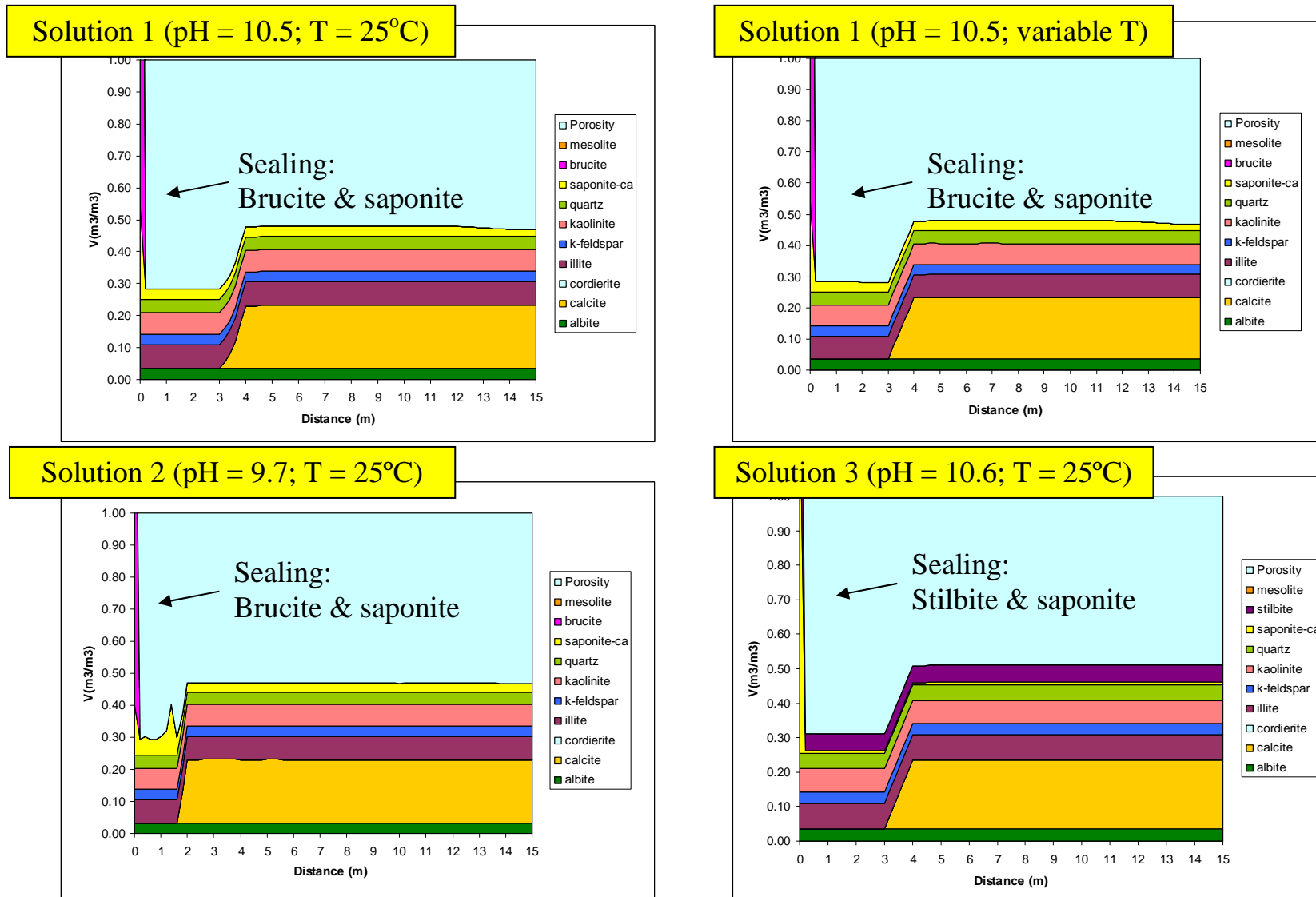


Figure 30c - Volumetric mineral content and porosity for the case with lower pH and including Mg²⁺-containing secondary minerals. $t = 5000$ a.

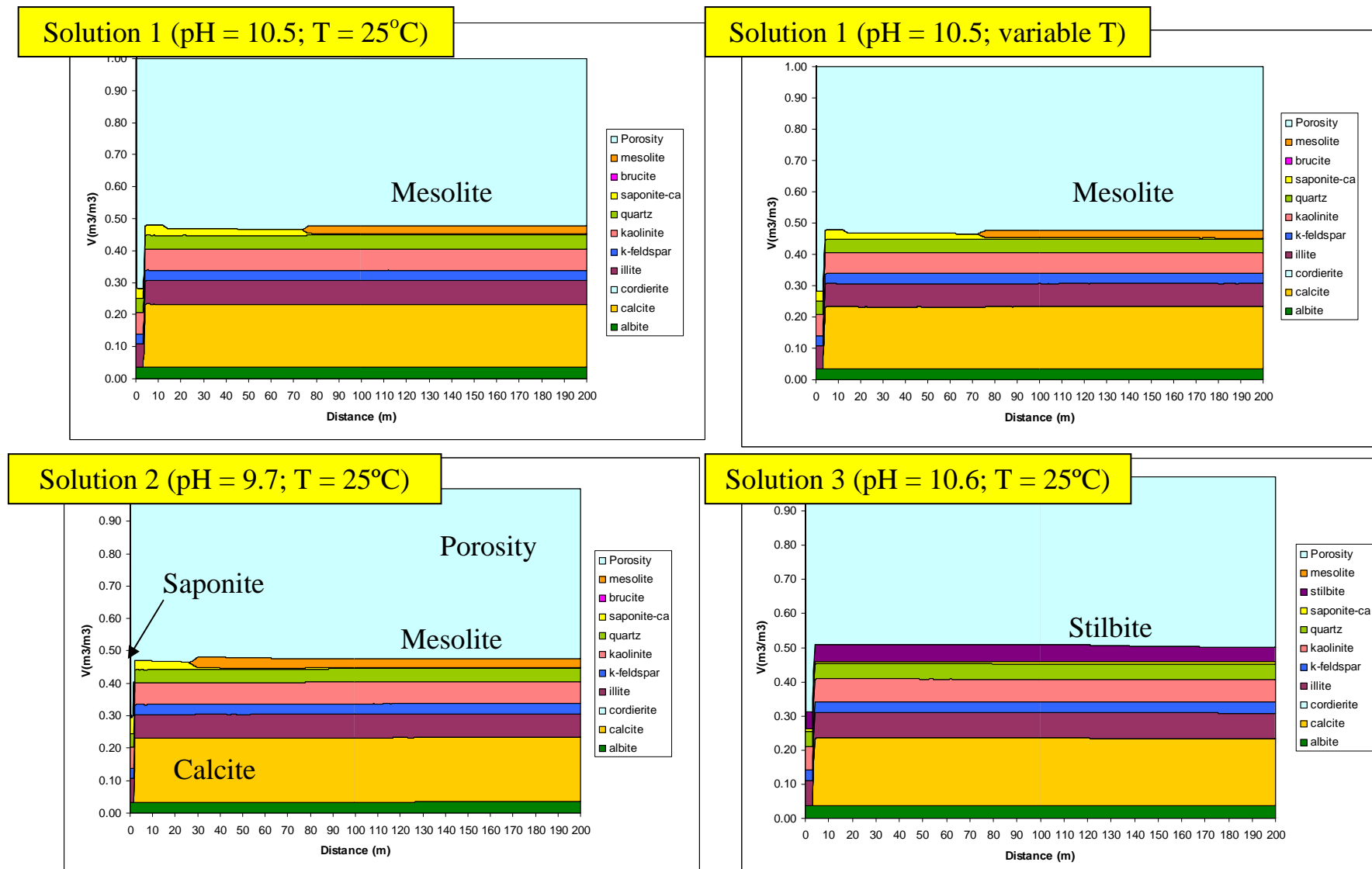


Figure 31a - Volumetric mineral content and porosity for the case with intermediate pH and without including Mg-containing secondary minerals. $t = 1000$ a.

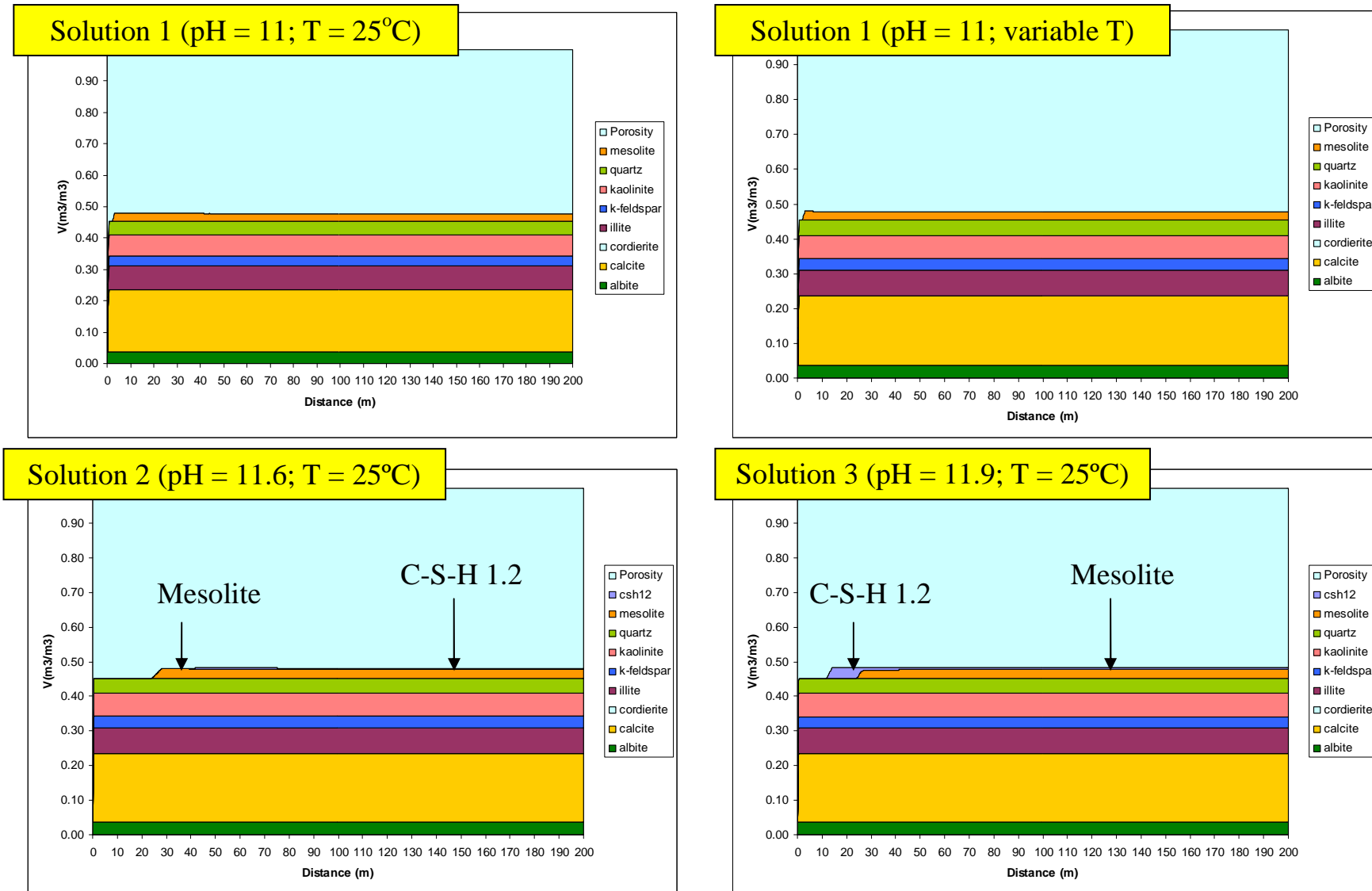


Figure 31b - Volumetric mineral content and porosity for the case with intermediate pH and without including Mg-containing secondary minerals. $t = 10000$ a.

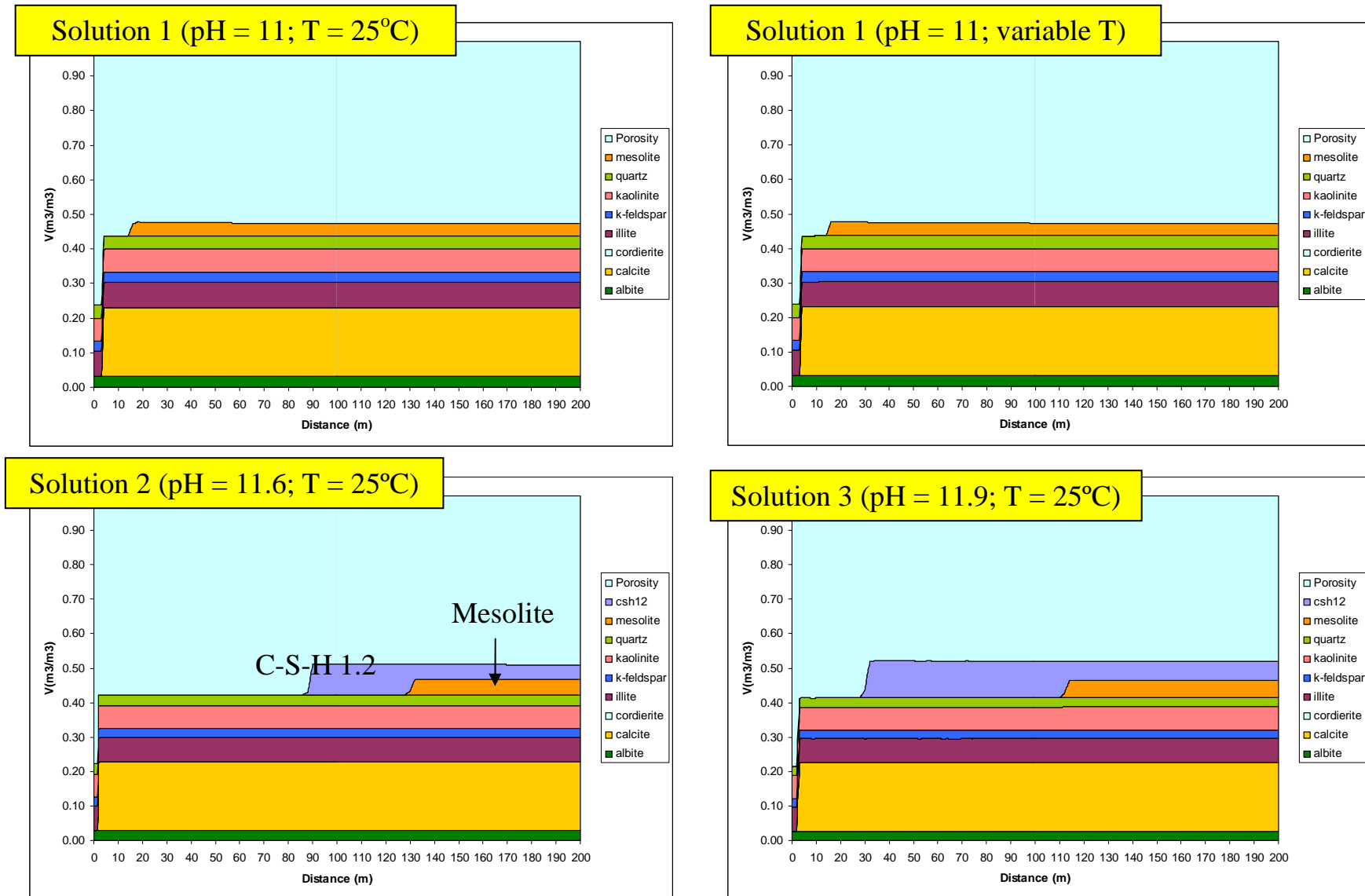


Figure 32a - Volumetric mineral content and porosity for the case with intermediate pH and including Mg-containing secondary minerals. $t = 1000$ a. The plot represents the first 15 meters of the fracture.

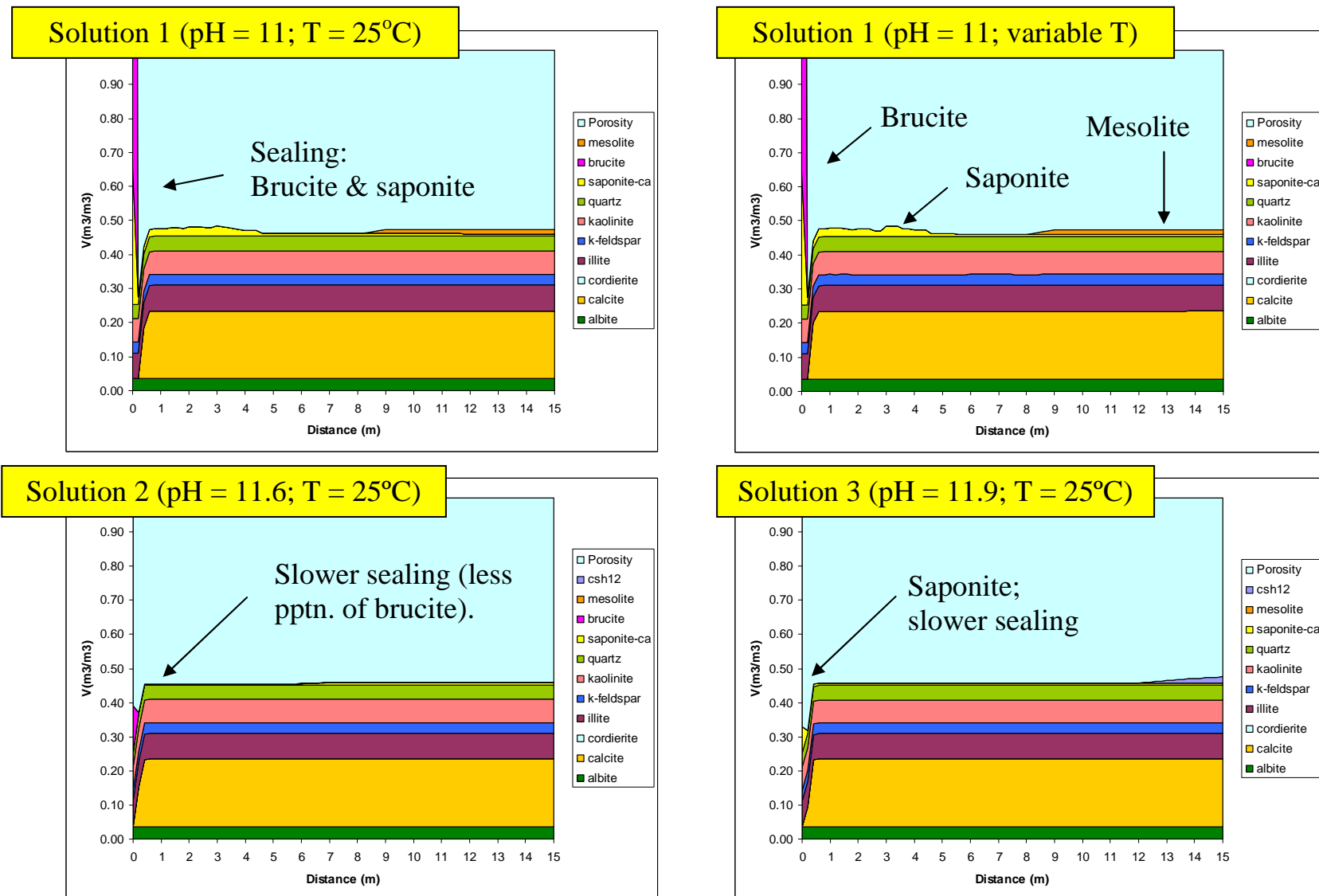


Figure 32b - Volumetric mineral content and porosity for the case with intermediate pH and including Mg-containing secondary minerals.
 $t = 10000$ a. The plot represents the first 15 meters of the fracture.

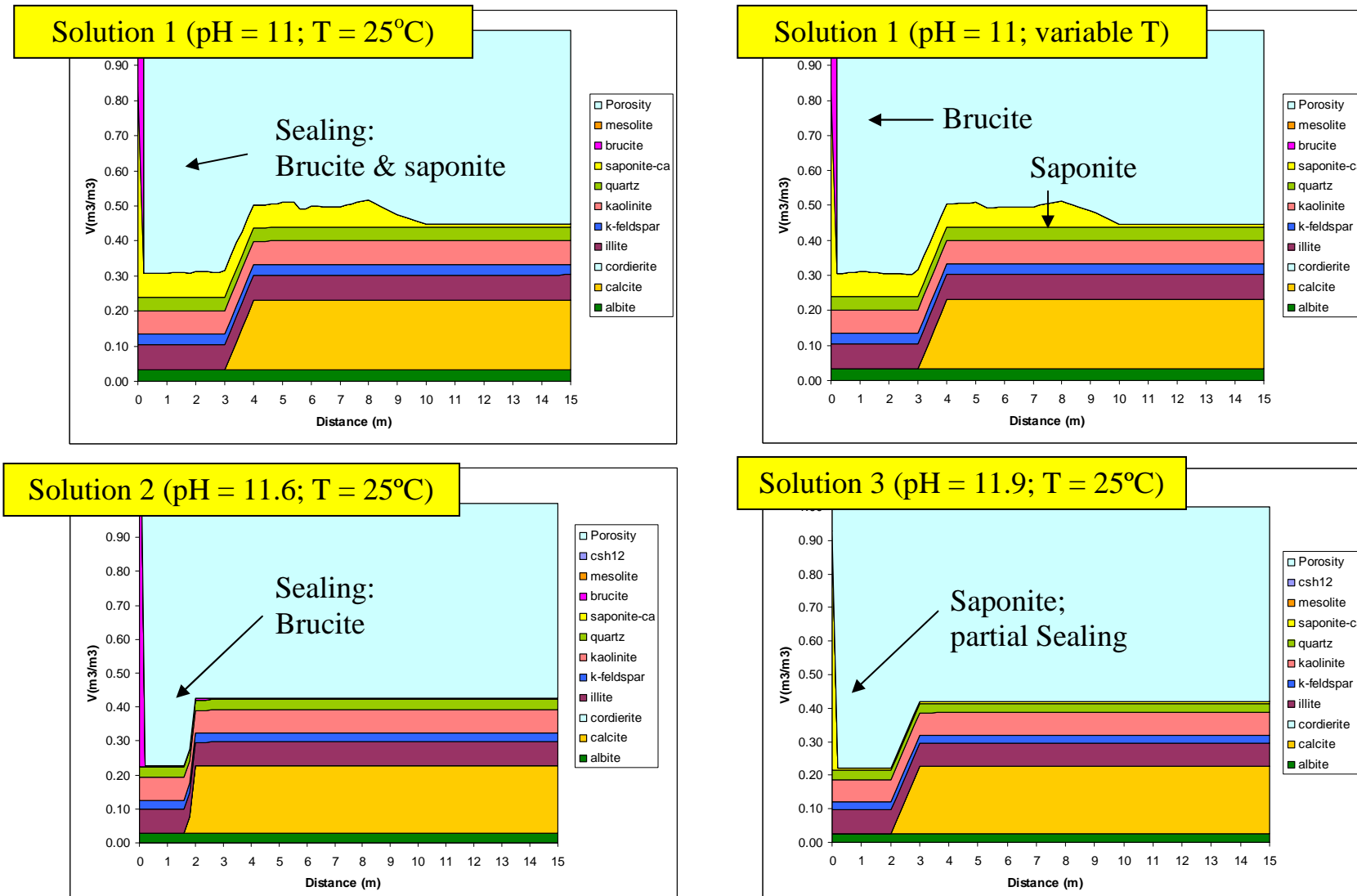


Figure 32c - Volumetric mineral content and porosity for the case with intermediate pH and including Mg -containing secondary minerals.
 $t = 10000$ a.

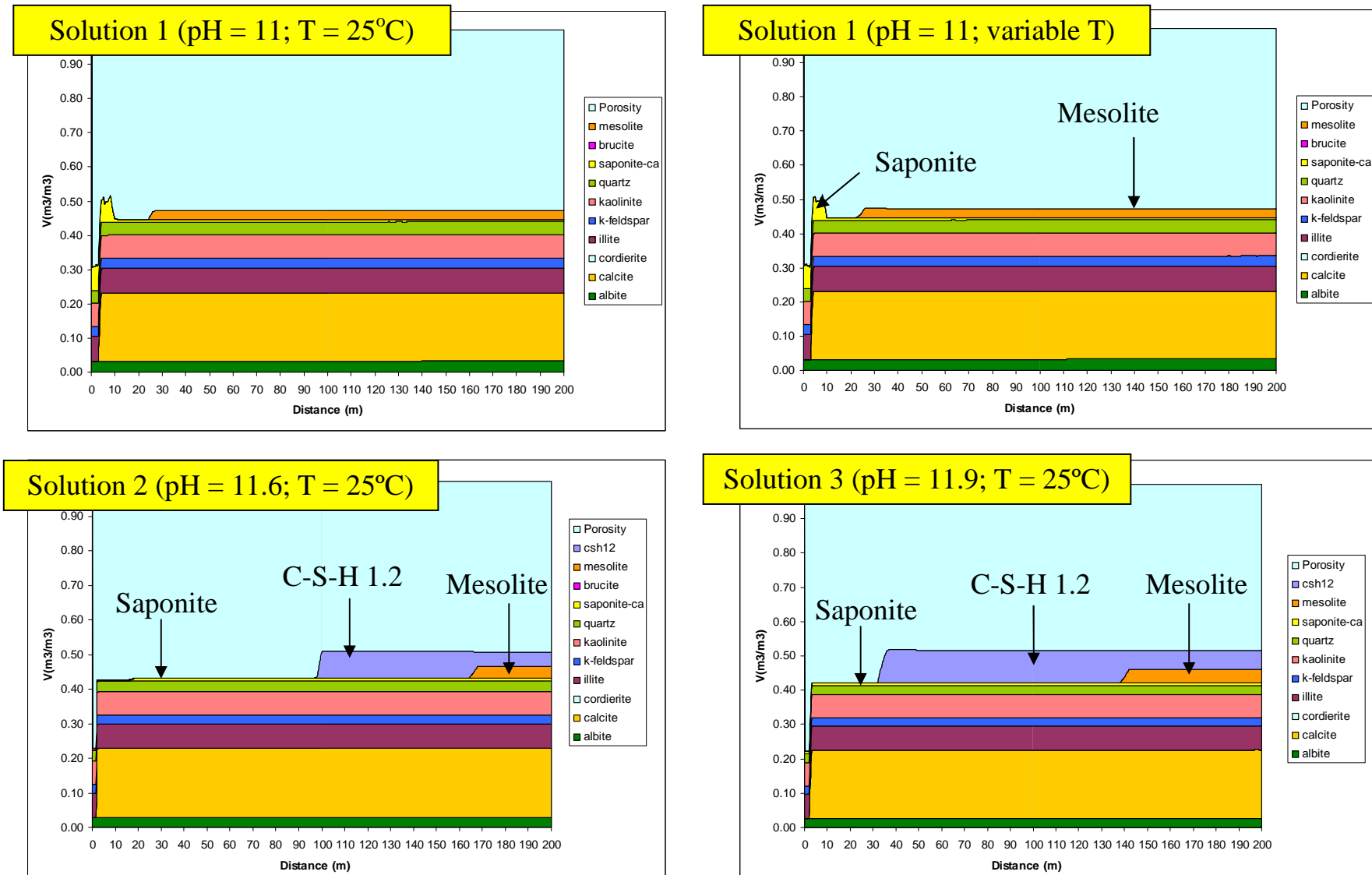


Figure 33a - Volumetric mineral content and porosity for the case with higher pH and without including Mg-containing secondary minerals. $t = 1000$ a.

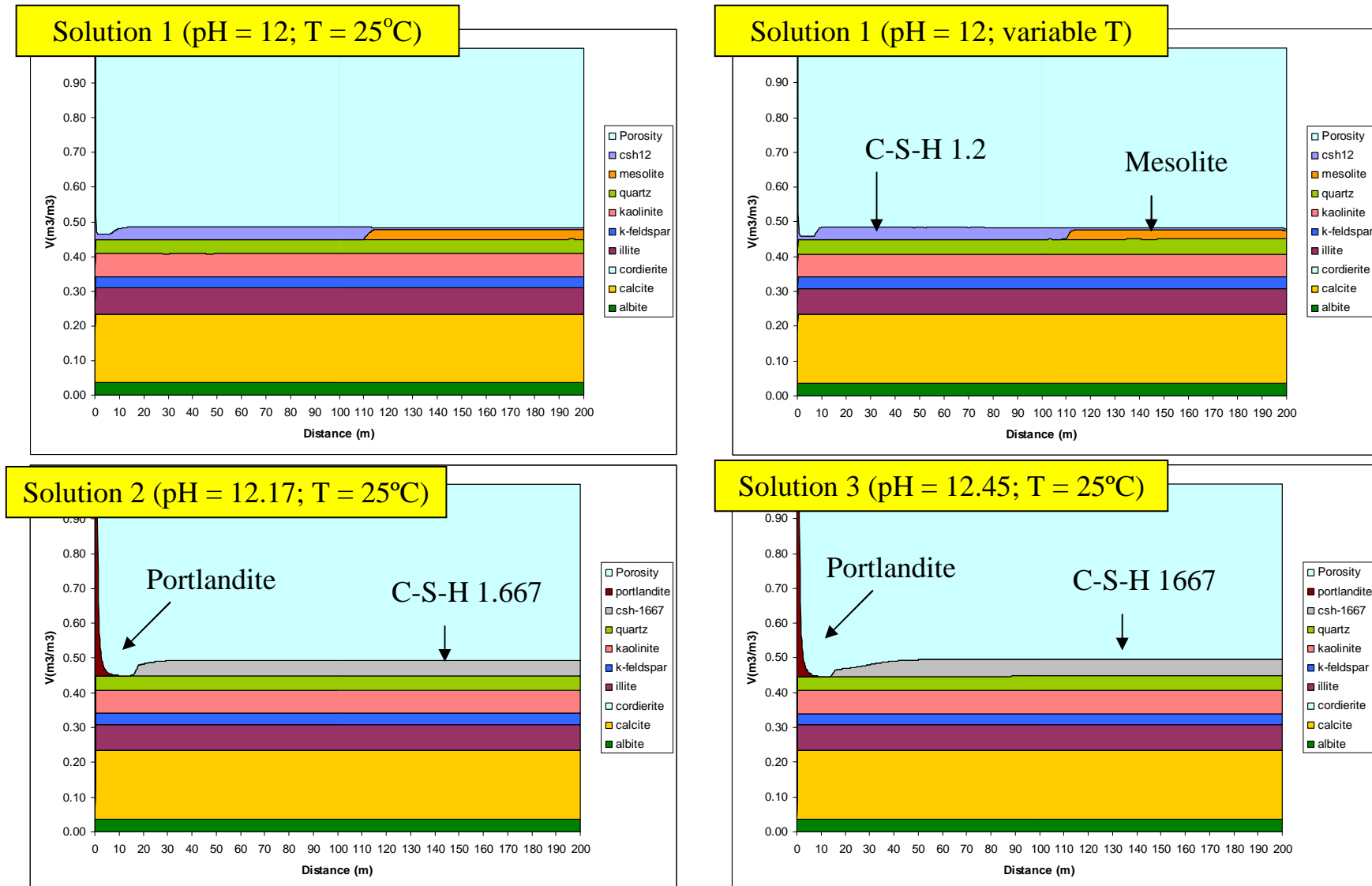


Figure 33b - Volumetric mineral content and porosity for the case with higher pH and without including Mg-containing secondary minerals. $t = 1000$ a. The plot represents the first 15 meters of the fracture.

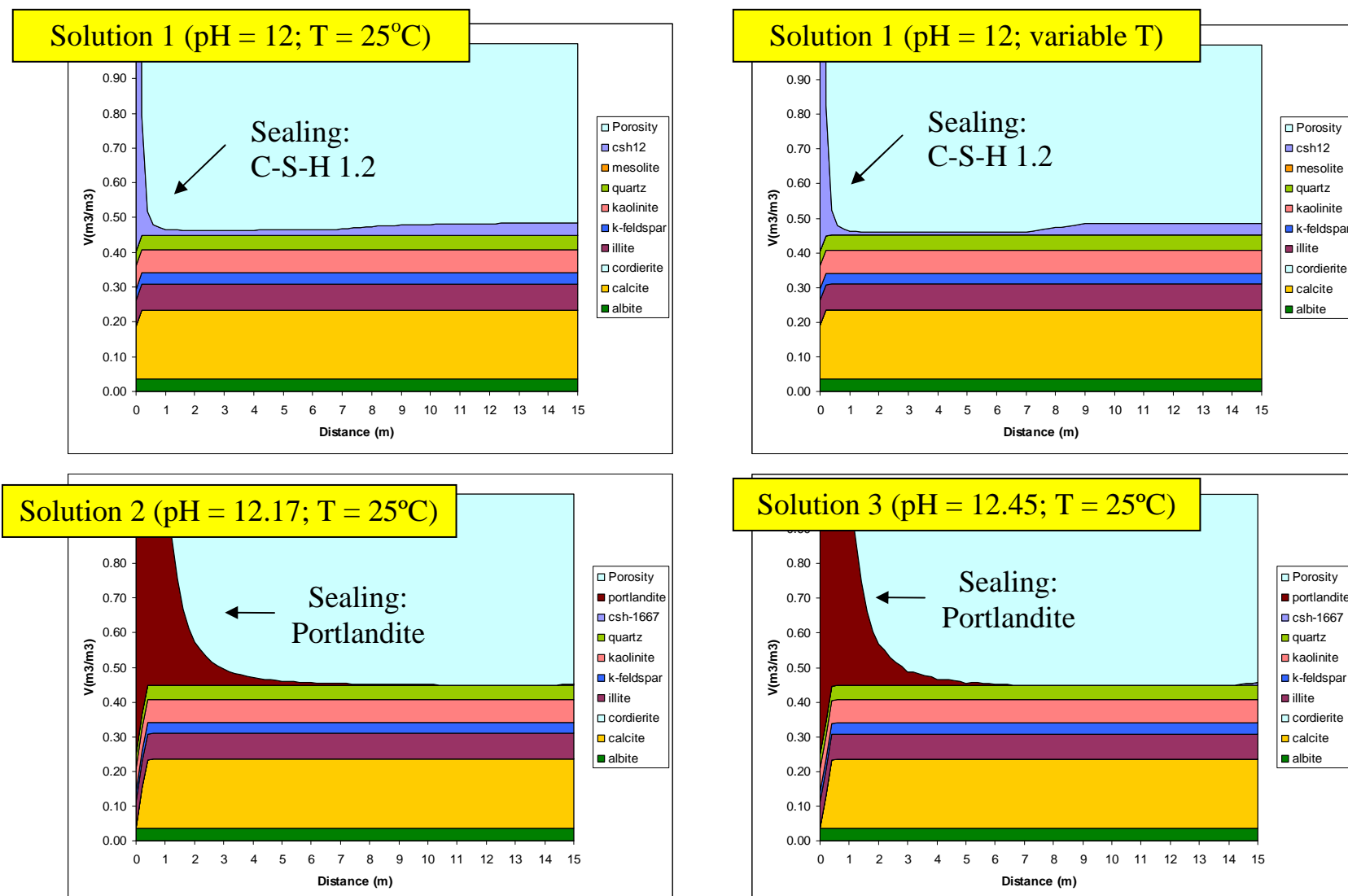


Figure 33c - Volumetric mineral content and porosity for the case with higher pH and without including Mg-containing secondary minerals. $t = 10000$ a.

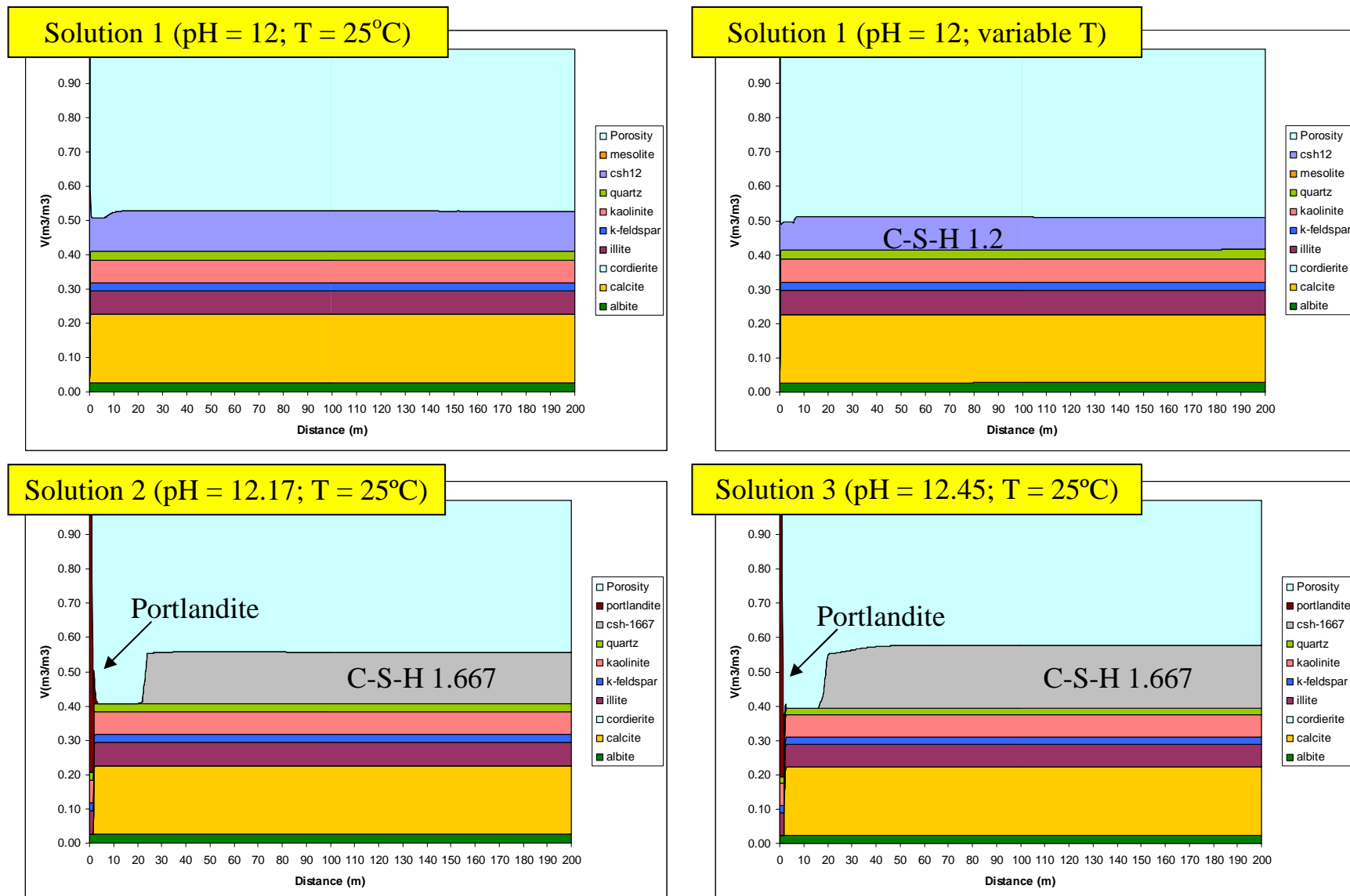


Figure 33d - Volumetric mineral content and porosity for the case with higher pH and without including Mg-containing secondary minerals. $t = 10000$ a. The plot represents the first 15 meters of the fracture.

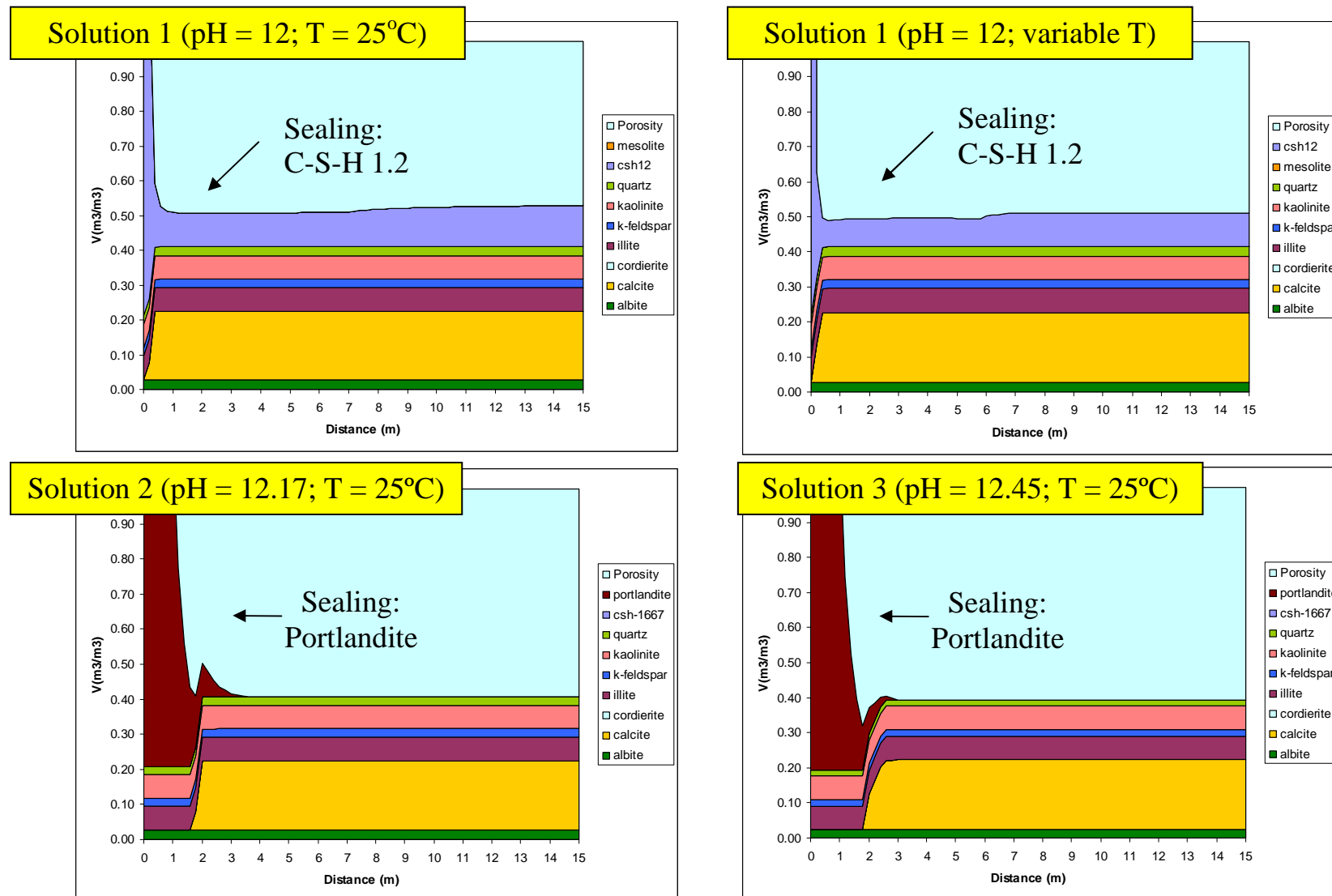


Figure 34a - Volumetric mineral content and porosity for the case with higher pH and including Mg-containing secondary minerals.
 $t = 1000$ a.

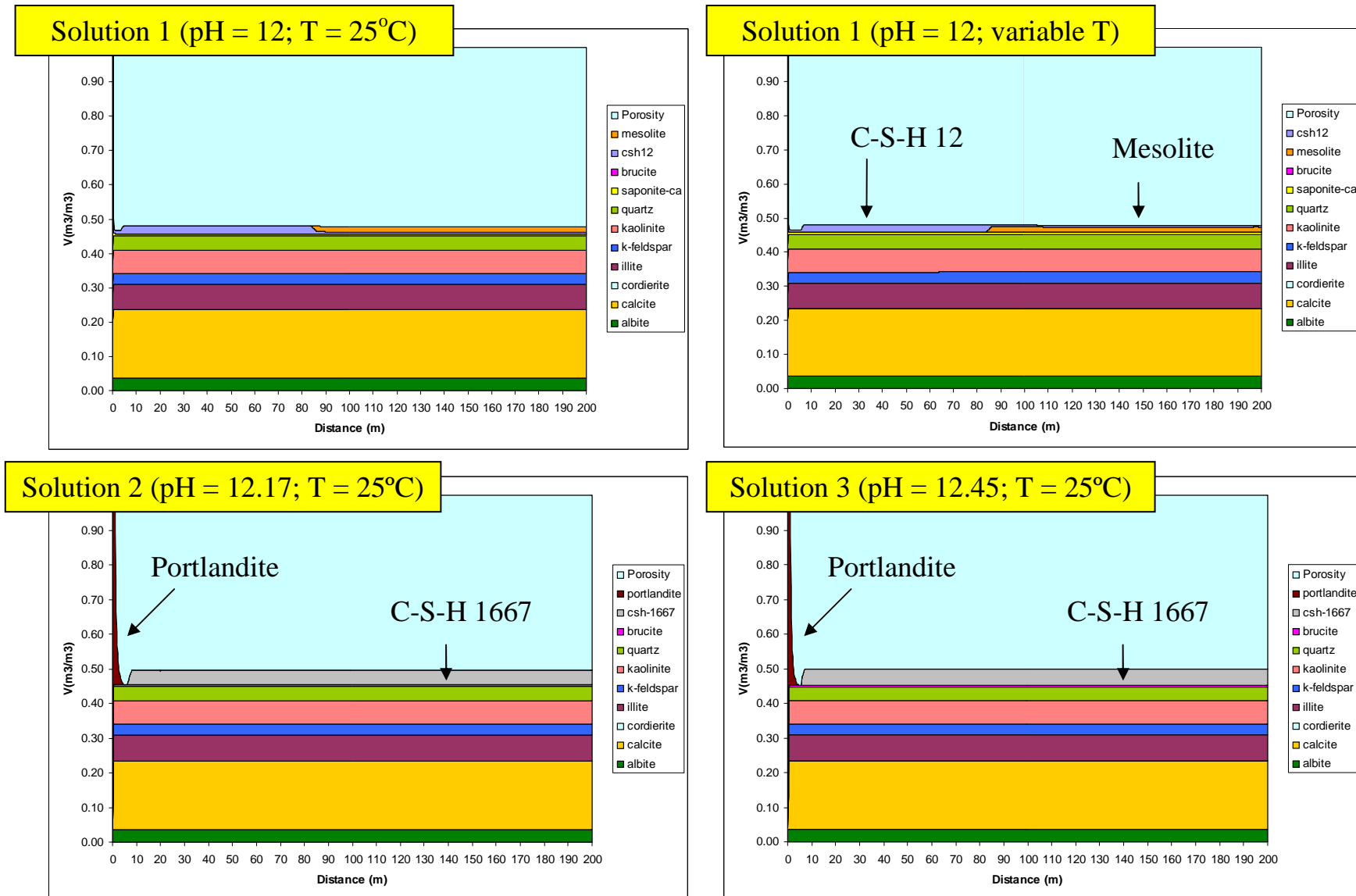


Figure 34b - Volumetric mineral content and porosity for the case with higher pH and including Mg-containing secondary minerals.
 $t = 1000$ a. The plot represents the first 15 meters of the fracture.

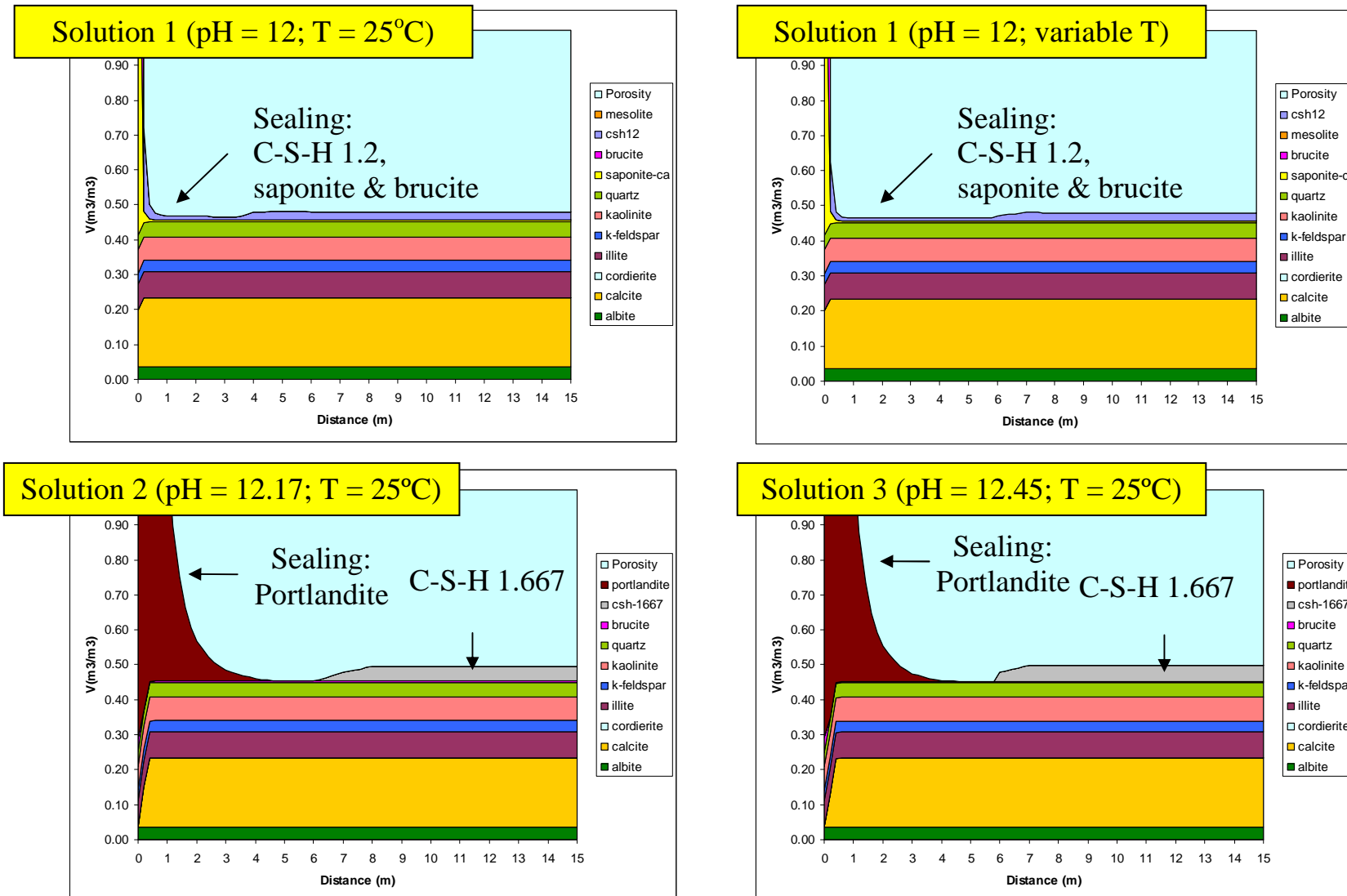


Figure 34c - Volumetric mineral content and porosity for the case with higher pH and including Mg-containing secondary minerals.
 $t = 10000$ a.

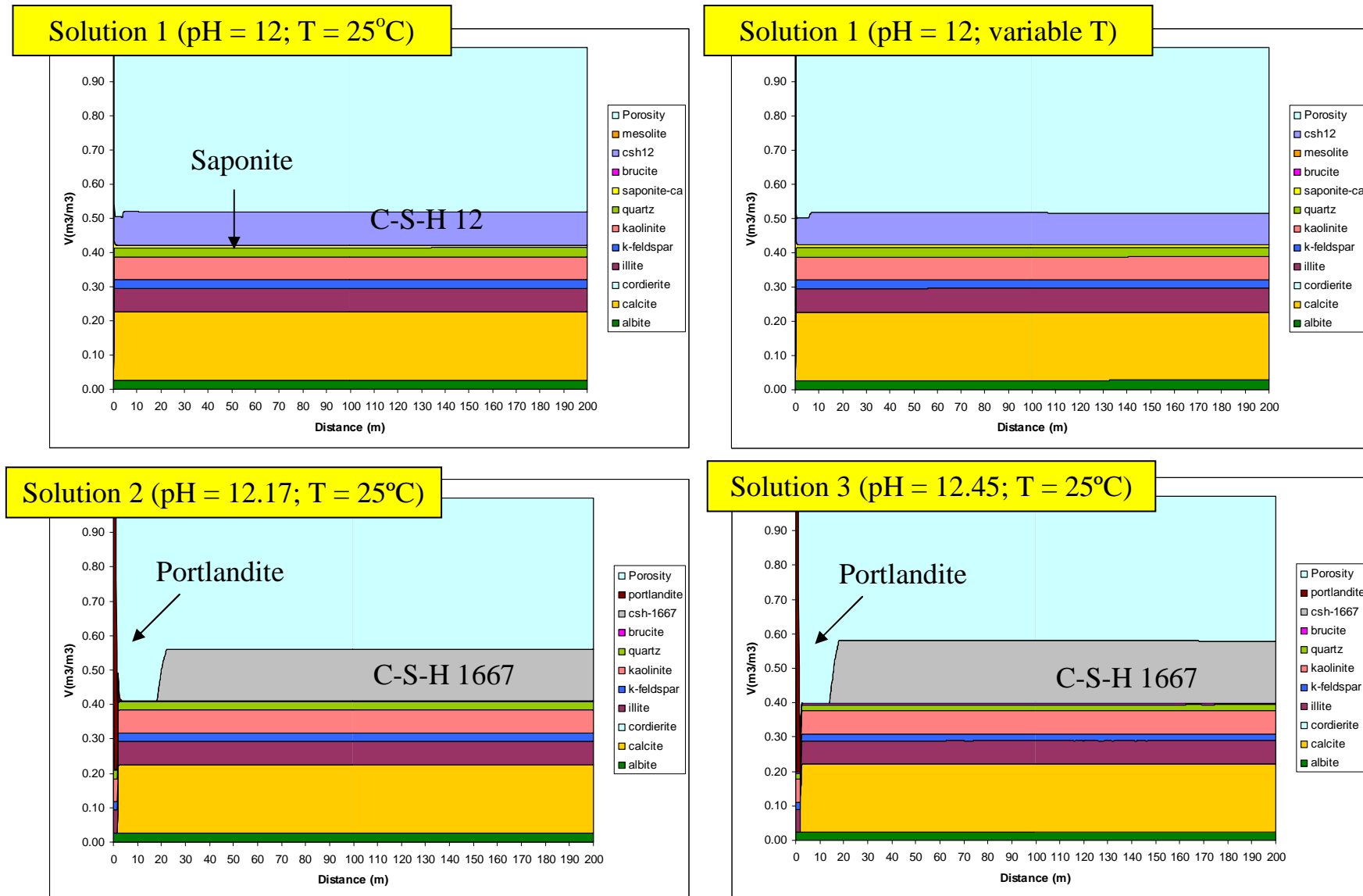


Figure 34d - Volumetric mineral content and porosity for the case with higher pH and including Mg-containing secondary minerals.
 $t = 10000$ a. The plot represents the first 15 meters of the fracture.

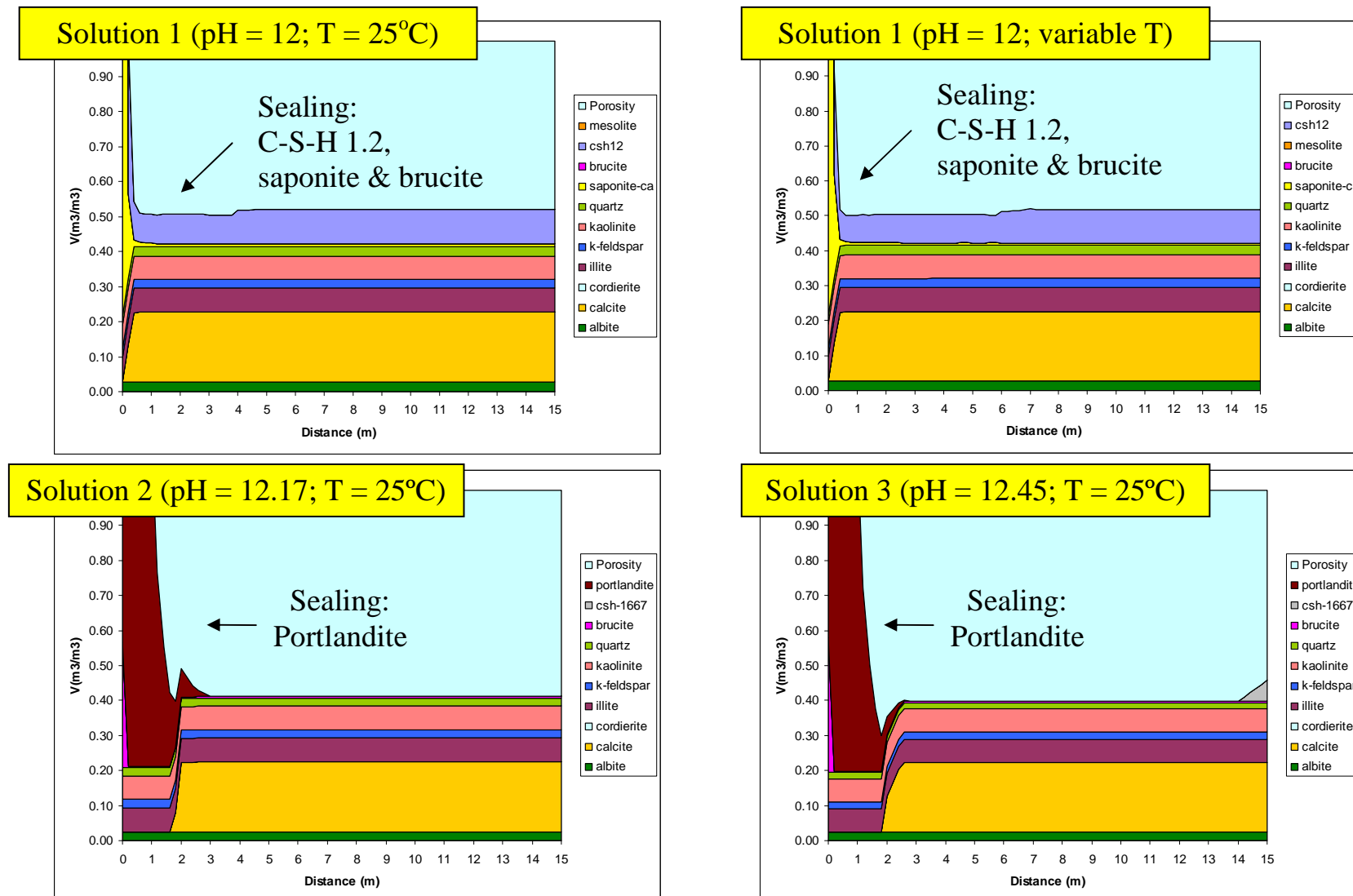


Figure 35 - Solution pH vs. distance for HIGH-pH SOLUTION 1 ($T = 25^{\circ}\text{C}$ and T variable). Without including Mg-containing secondary minerals.

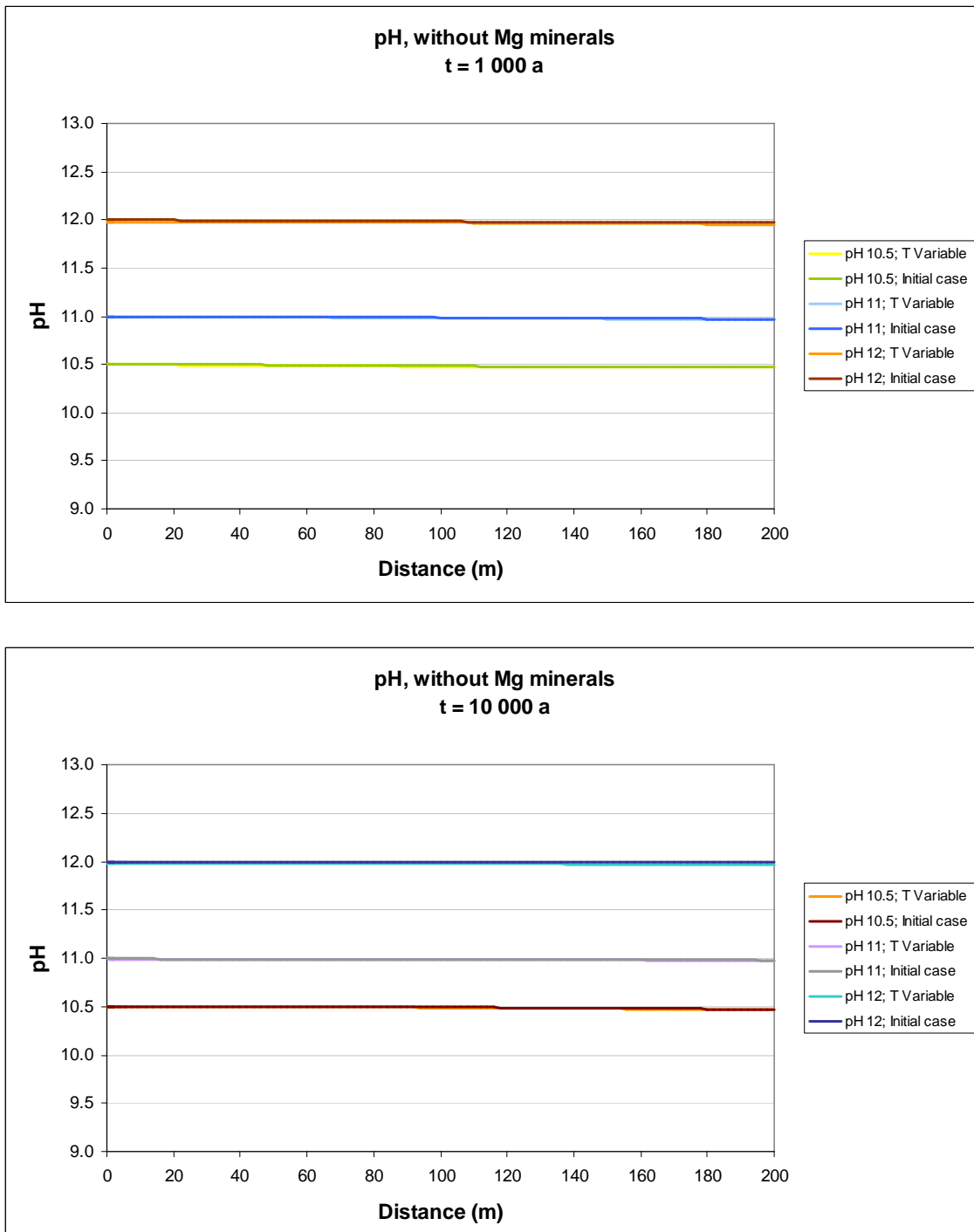


Figure 36 - Solution pH vs. distance for HIGH-pH SOLUTIONS 2 and 3. Without including Mg-containing secondary minerals.

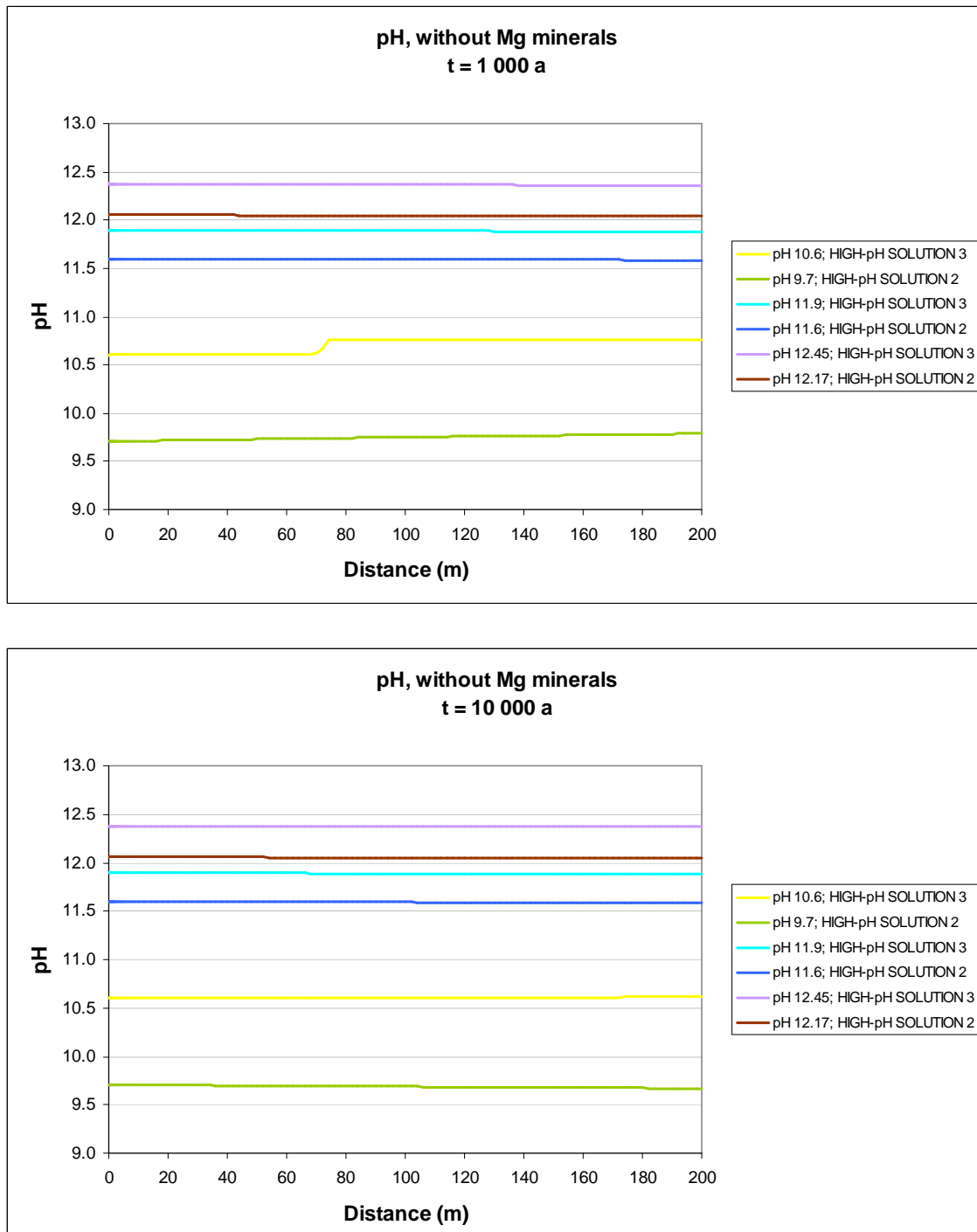


Figure 37 - Solution pH vs. distance for HIGH-pH SOLUTION 1 ($T = 25^{\circ}\text{C}$ and T variable). Including Mg-containing secondary minerals.

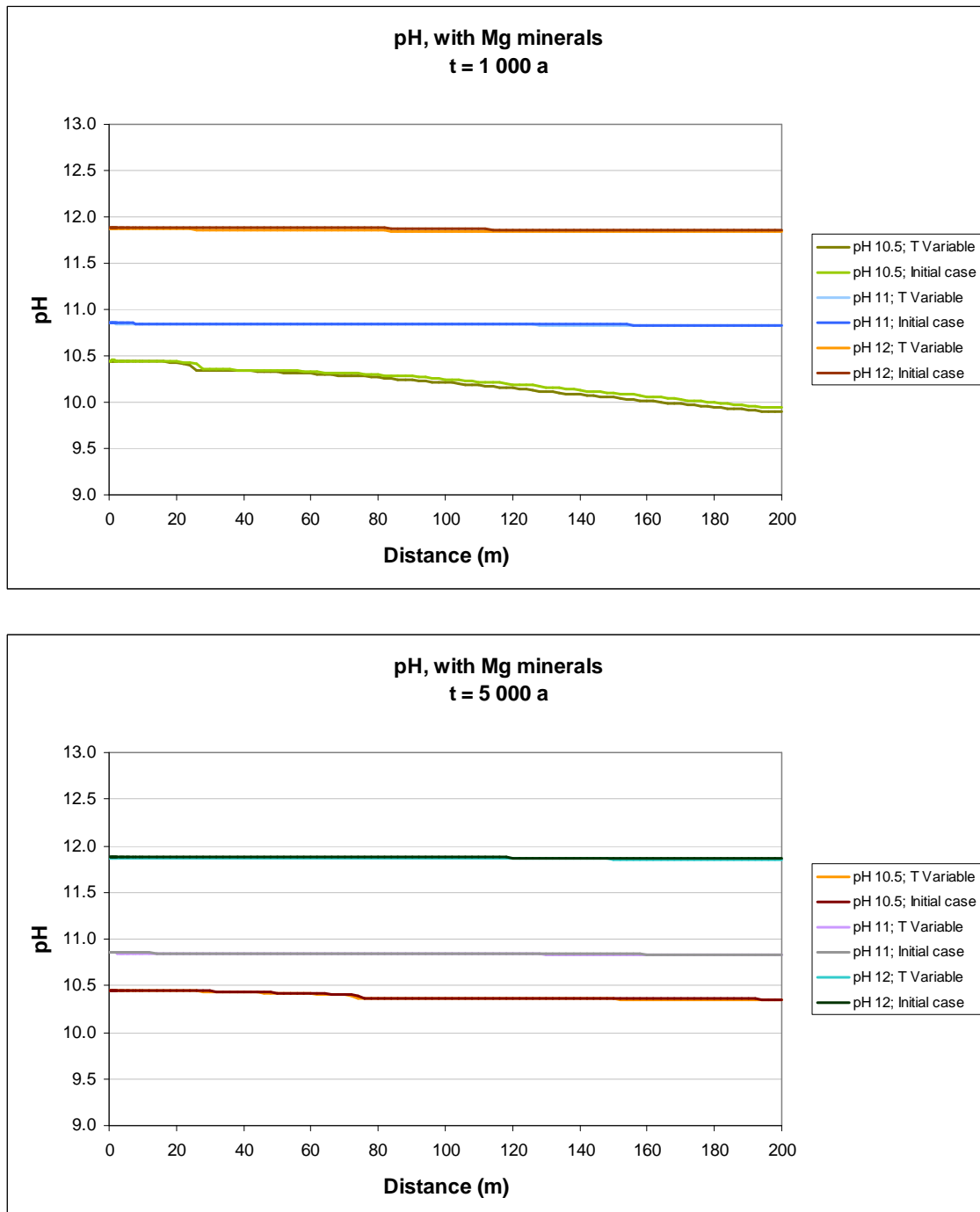
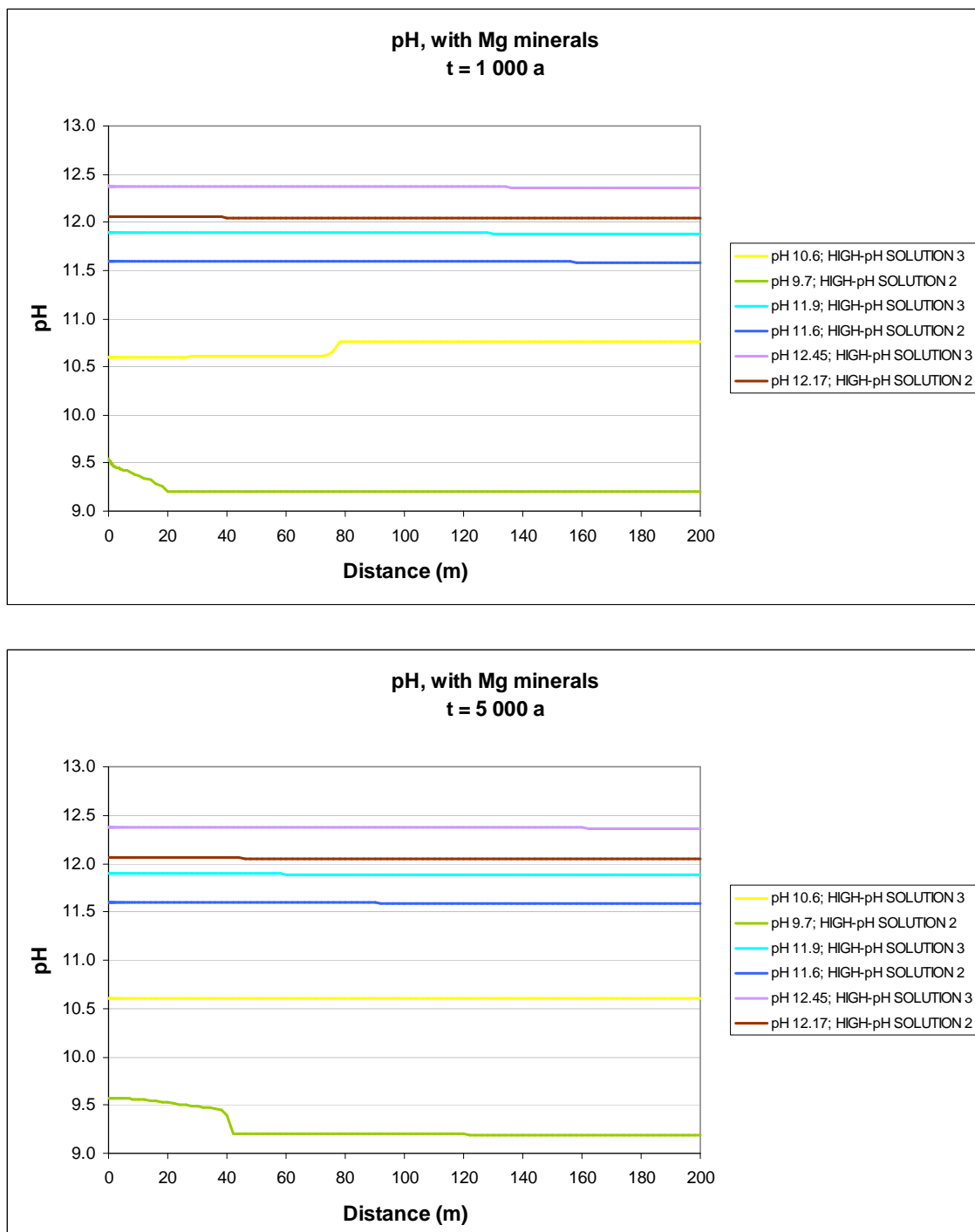


Figure 38 - Solution pH vs. distance for HIGH-pH SOLUTIONS 2 and 3. Including Mg-containing secondary minerals.



5.4. $Q = 631 \text{ l/a}$, $\text{pH} = 10.5$. Comparison of reference case with a case with large surface areas (X100) for primary minerals.

(Mineral contents and pH; Figs. 39 - 42)

In this chapter, a reference case with pH 10.5 input solution has been used to evaluate the potential effect of larger surface areas for primary minerals. These large surface areas could be caused, for instance, by the presence of a fault gouge.

Two simulations are associated with each case; one including Mg-containing secondary minerals (brucite, sepiolite, saponites) and another one without including them.

The results of large surface area cases follow the same trend as the reference cases, but the magnitude of the reactions is larger:

- More primary mineral dissolution (at $t = 10000 \text{ a}$ the only remaining primary minerals in the domain are calcite and kaolinite)
- More secondary mineral precipitation (saponite, mesolite, stilbite)
- Larger decrease of pH (not enough to neutralize the solution)

When Mg-containing secondary minerals are taken into account, the precipitation of brucite and saponite causes the sealing of the fracture inlet.

Figure 39a - Volumetric mineral content and porosity for the case with input pH equal to 10.5 and without including Mg-containing secondary minerals. $t = 1000$ a. The plots at the bottom represent the first 15 meters of the fracture.

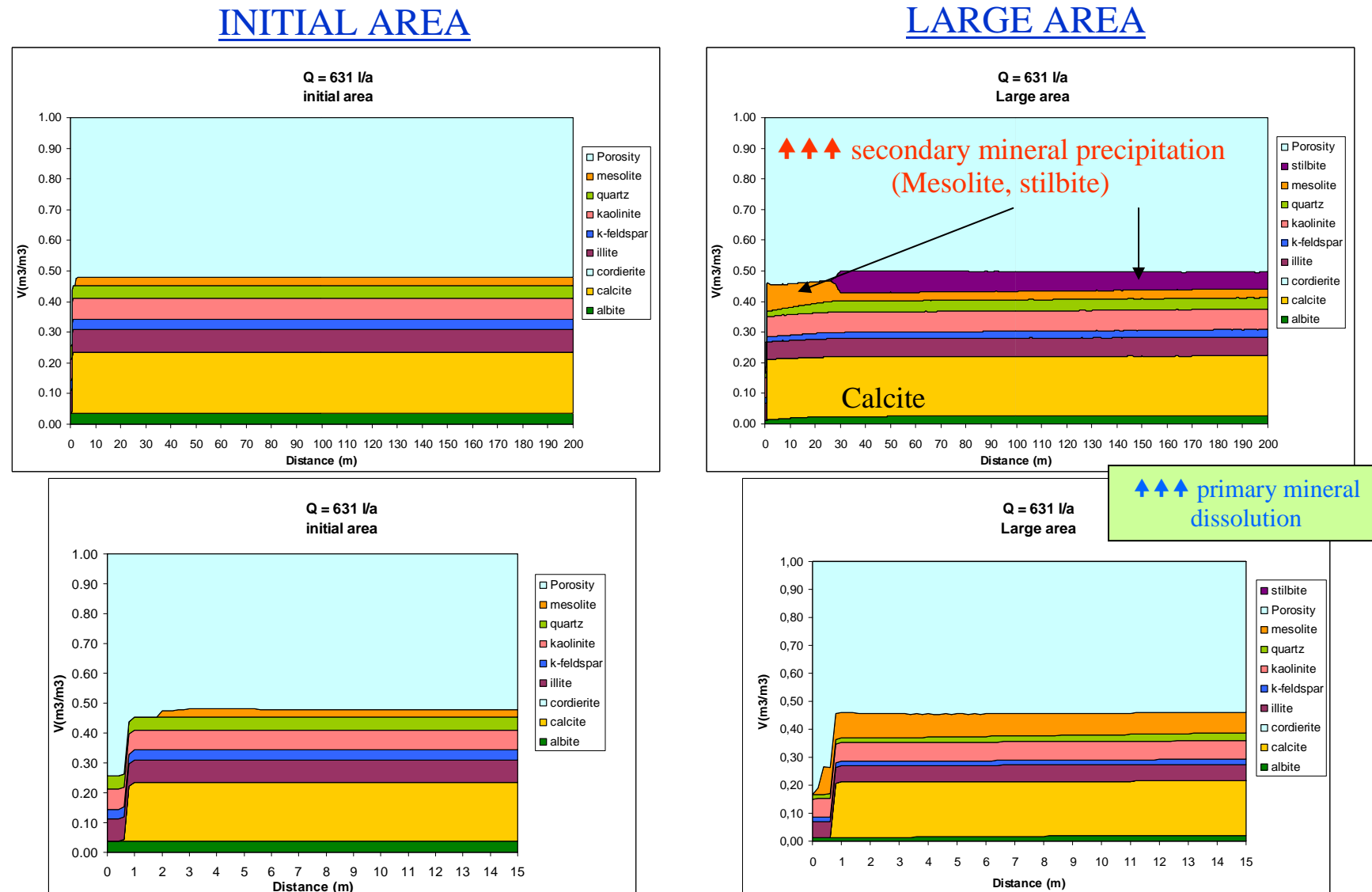


Figure 39b - Volumetric mineral content and porosity for the case with input pH equal to 10.5 and without including Mg-containing secondary minerals. $t = 10000$ a. The plots at the bottom represent the first 15 meters of the fracture.

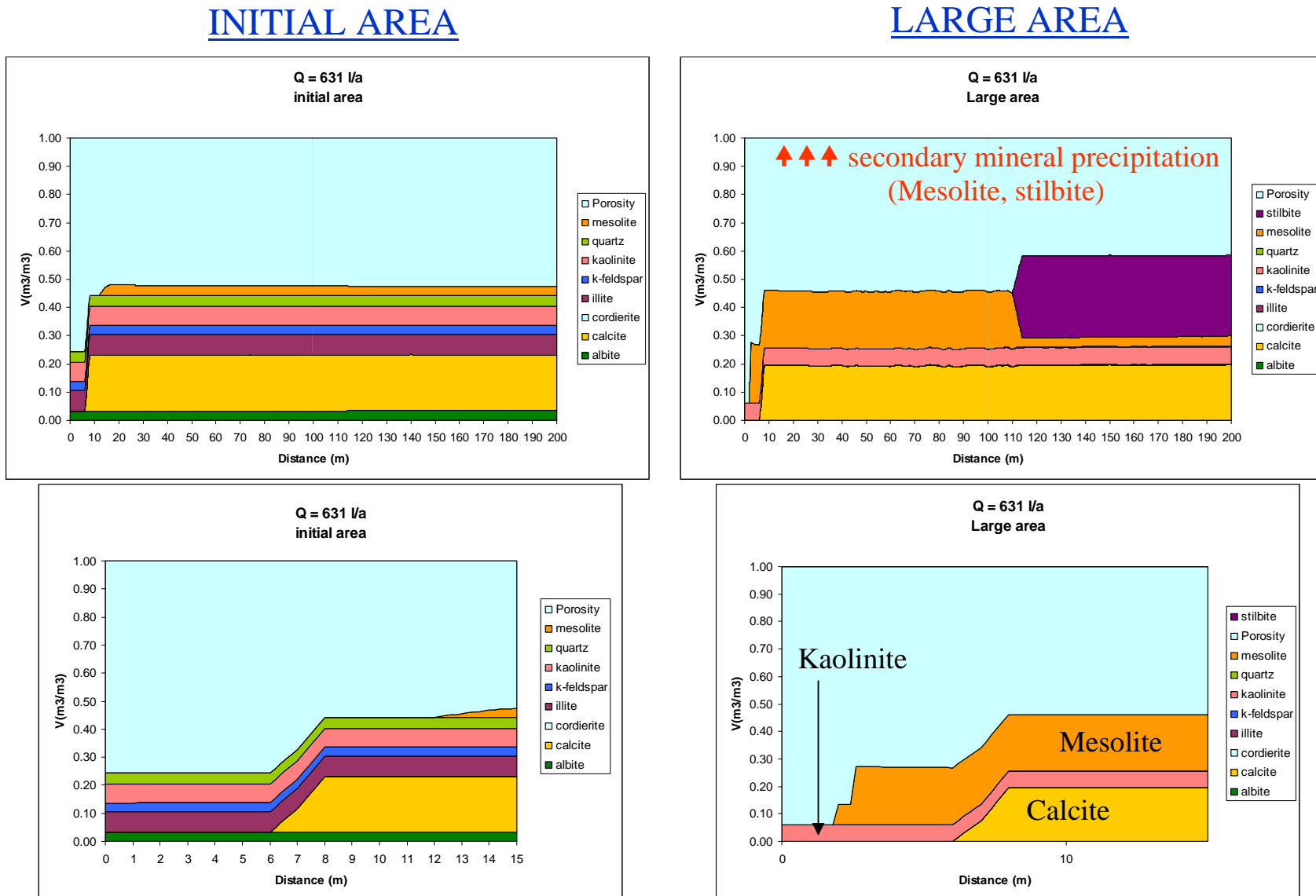


Figure 40b - Volumetric mineral content and porosity for the case with input pH equal to 10.5 and including Mg-containing secondary minerals. $t = 1000$ a. The plots at the bottom represent the first 15 meters of the fracture.

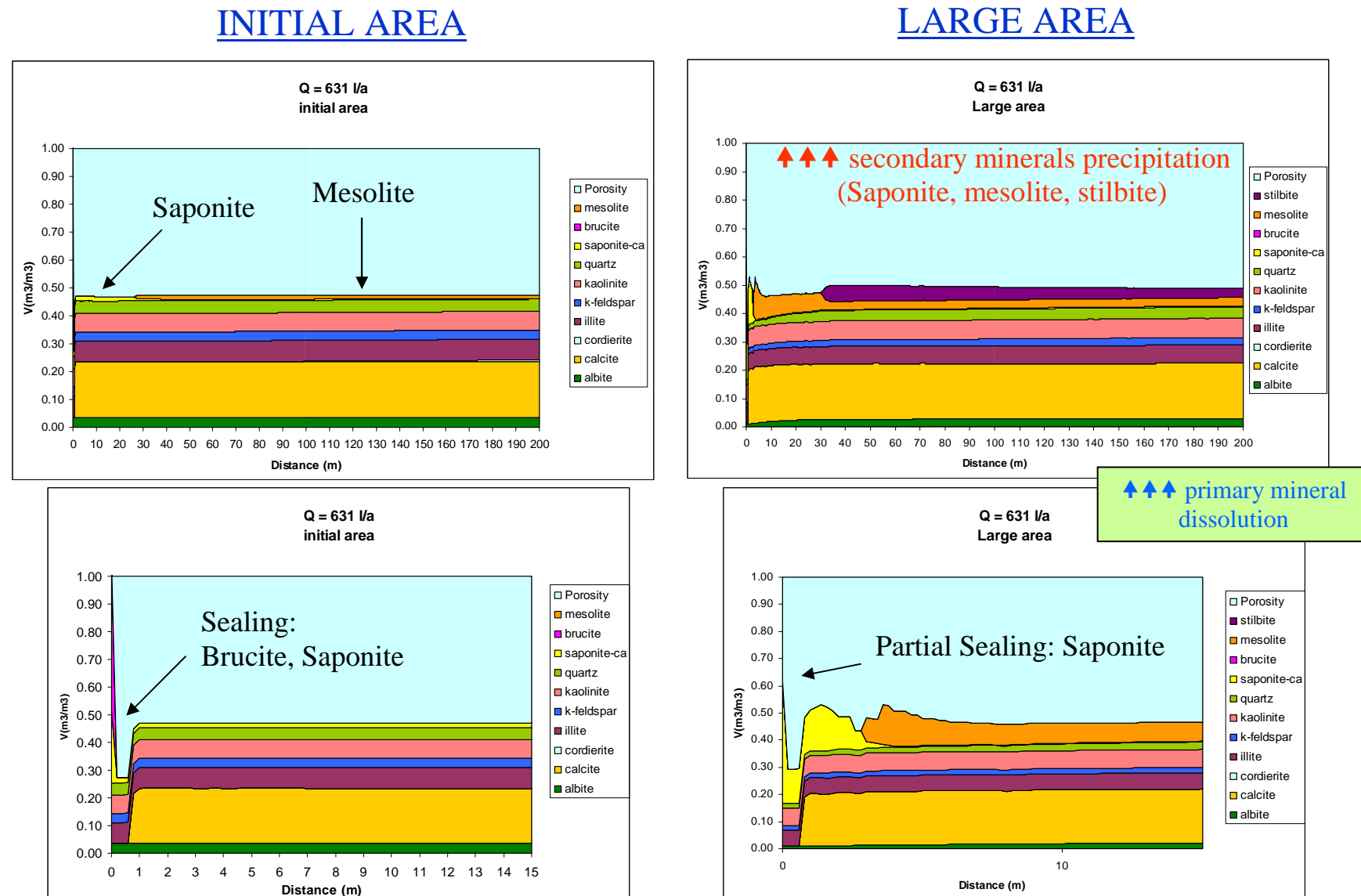


Figure 40b - Volumetric mineral content and porosity for the case with input pH equal to 10.5 and including Mg-containing secondary minerals. $t = 10000$ a. The plots at the bottom represent the first 15 meters of the fracture.

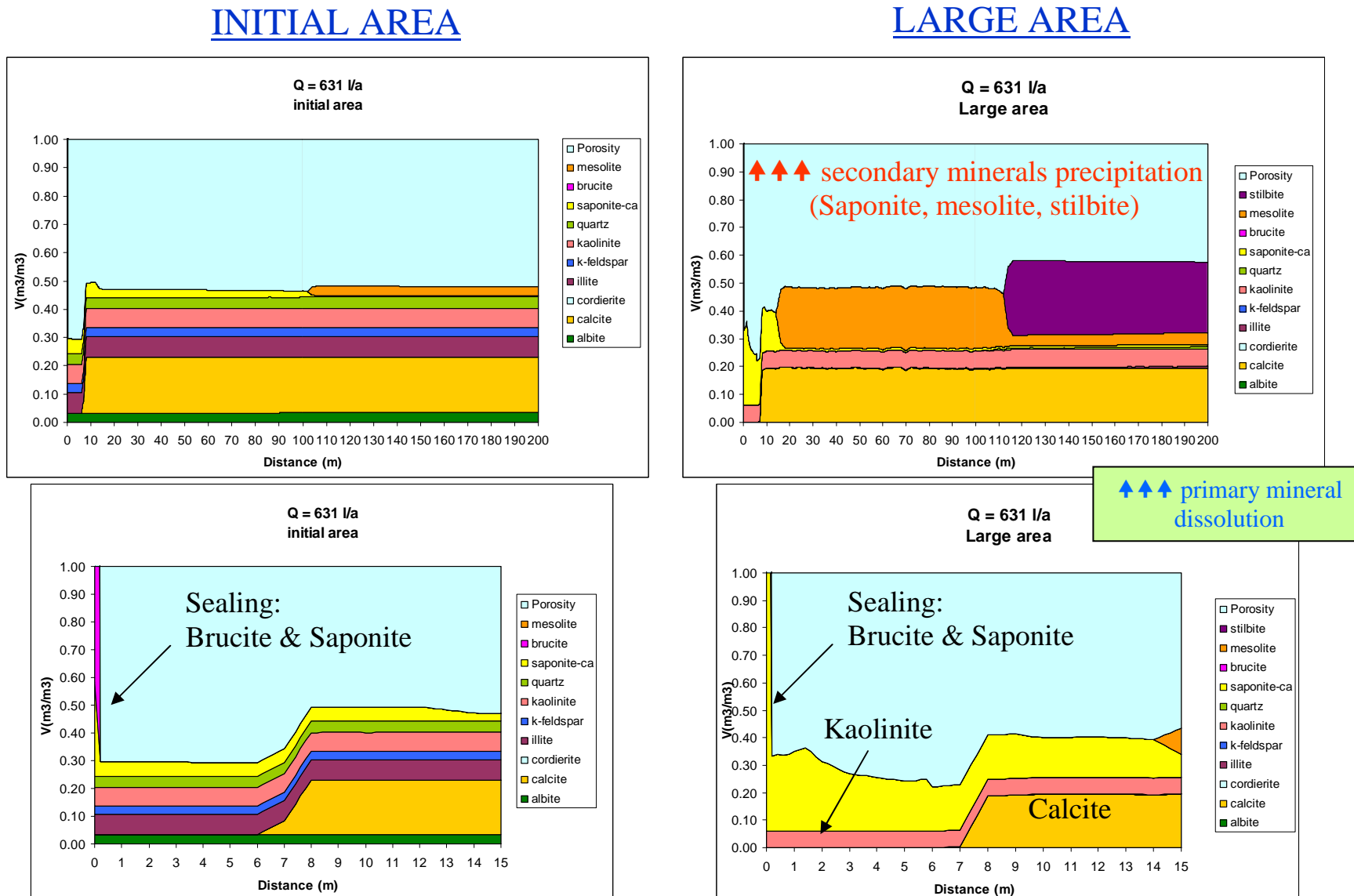


Figure 41 - Solution pH vs. distance for all the cases (without including Mg-containing secondary minerals).

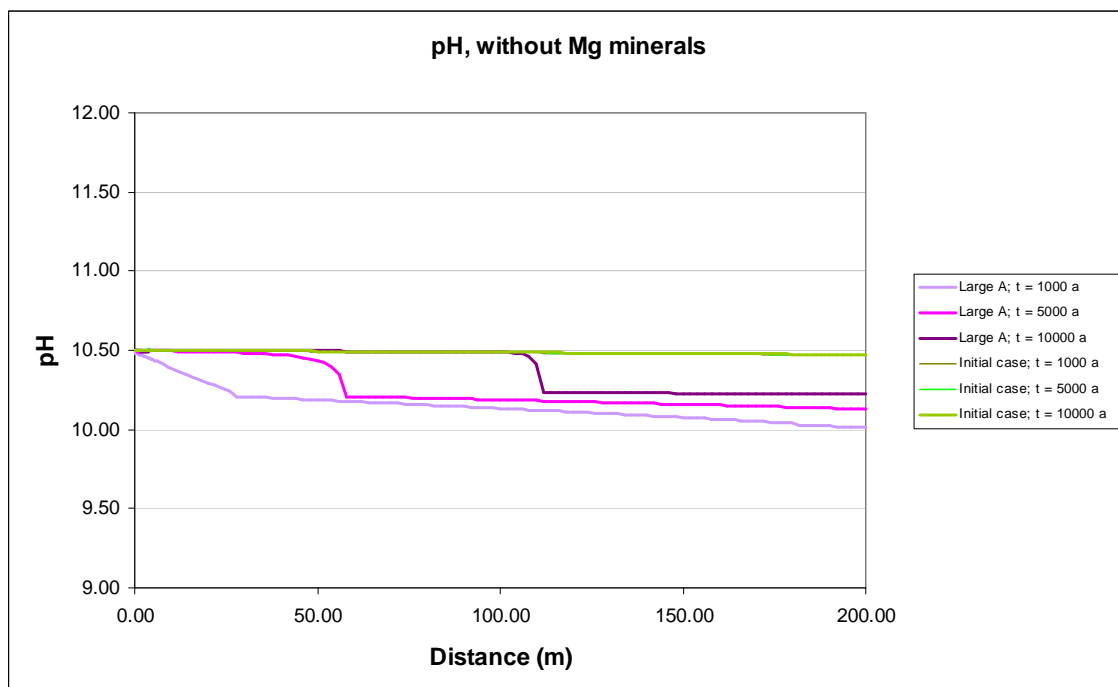
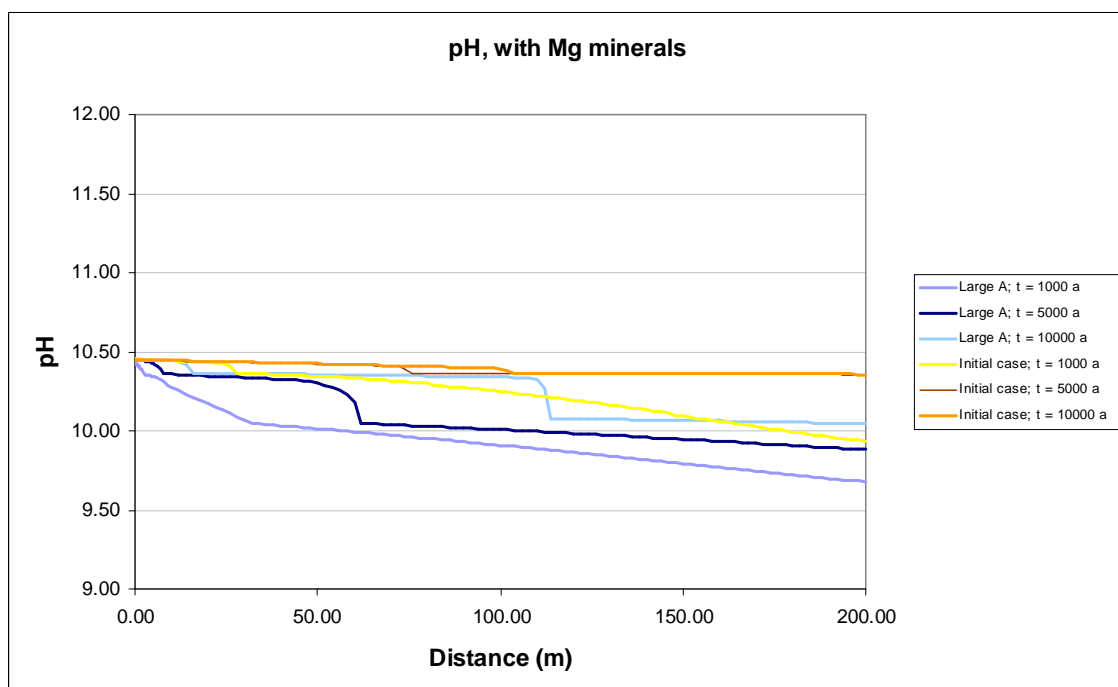


Figure 42 - Solution pH vs. distance for all the cases (including Mg-containing secondary minerals).



6. DISCUSSION AND CONCLUSIONS

One-dimensional reactive transport calculations have been performed to simulate the alteration of a fracture and the extension of the high-pH plume arising from the circulation of hyperalkaline solutions through the fracture. A series of scoping calculations covering a range of different high-pH solutions, flow velocities and primary mineral surface areas have been performed. The possible effect of a limited temperature anomaly (heat pulse) has also been evaluated. The calculations have been performed with the Retraso reactive transport code.

A conclusion that is common to all the cases is that the rock does not have sufficient buffering capacity to significantly reduce the pH of the circulating solutions within the calculation domain. However, there is some reduction of pH for (i) the slowest flow conditions, (ii) the lowest pH cases (pH 10.5, 9.7), (iii) when Mg-containing secondary minerals are included in the calculations, and (iv) when reactive surface areas of the primary minerals are larger (due, for instance, to the presence of fault gouge).

Another important observation is that there is a significantly different result depending on the inclusion or not of Mg-containing secondary minerals (brucite, saponite) in the calculations. In most cases, if Mg secondary minerals are included, the precipitation of brucite and saponite causes a sealing of porosity at the fracture inlet. On the other hand, if the modeling is performed without Mg secondary minerals, there is an increase in porosity at the fracture inlet for the cases with incoming solutions with pH less than 12. This increase in porosity is caused by the dissolution of calcite. For the highest pH cases, there is sealing of the fracture inlet by C-S-H with Ca/Si = 1.2 (pH 12 solution) or portlandite (pH 12.17 and pH 12.45 solutions, derived from leaching experiments), regardless of the inclusion of Mg-containing secondary minerals.

For the lower pH cases using solution compositions derived from leaching experiments using a low-pH cement (pH 9.7 and 10.6) there is sealing of the fracture inlet even without including Mg-containing secondary minerals. In these cases, mesolite (Na-Ca zeolite) and stilbite (Ca-Na-K zeolite) are responsible for this sealing, respectively.

Table 12 shows the total amounts (number of moles) of primary species that have entered the domain with the incoming high-pH solution and the net balance between mineral precipitation (+) and dissolution (-) for the different cases and for different times. For the cases with intense precipitation of Mg-containing secondary minerals, the amounts of Mg precipitated are very similar to the amounts that have entered the domain. The Mg in the secondary minerals is dominated by the Mg entering the domain, rather than by the Mg initially present in the rock (in cordierite and illite). In the cases when there is a net dissolution of Mg (negative values), this Mg comes essentially from the dissolution of cordierite. Only in the case with larger surface areas (x100) is there a significant contribution from the dissolution of illite.

In relation to the study of the effect of variable temperature, there are no significant differences between this case and the reference case. The temperature anomaly (heat pulse) is too short-lived to cause any significant and lasting effects. Only for the case without Mg-minerals and pH 12, the sealing of the fracture inlet during the heat pulse is

caused by C-S-H with a larger Ca/Si ratio (1.667). This C-S-H with Ca/Si = 1.667 is transformed into C-S-H with Ca/Si = 1.2 after temperature goes down to 25°C.

Notice that only a few discrete C-S-H phases with fixed Ca/Si ration have been taken into account in the calculations. The use of a solid solution model, which would allow a continuum of Ca/Si ratios, would probably give C-S-H precipitates with a range of compositions, rather than a unique phase with a given value of Ca/Si.

In view of all the results, the possibility of sealing of the fracture by the high-pH solutions seems to be a very definite possibility. This sealing would be consistent with the results of the laboratory and field (Grimsel Test Site) experiments conducted within the GTS-HPF project (Mäder et al., 2006; Pfingsten et al., 2006; Soler et al., 2006; Soler and Mäder, 2005, 2007) and with previous studies of the effects of high-pH plumes on different types of rocks (Steefel and Lichtner, 1994; Lichtner and Eikenberg, 1995; Adler, 2001; Read et al., 2001; Pfingsten, 2002; Savage et al., 2002; Soler, 2003; Gaucher et al., 2004).

The sealing of fracture porosity would mean that flow of solution through the fracture would slow down or stop rather quickly in the modeled one-dimensional system. Flow could bypass the sealed section of the fracture in a two- or three-dimensional calculation. No feedback between porosity and permeability changes has been implemented in the calculations. The results can be considered as an estimate of the possible chemical evolution of the system in the case that fluid flow would continue despite the sealing of porosity at the fracture inlet (uncoupling of chemical and physical properties).

Table 12 - Total number of moles of primary species that has entered the domain (entry) or reacted (precipitation(+) / dissolution(-)) for the different cases and for different times.

Q [l/a]	pH	with / without Mg	time (a)	Number of moles	Al	Ca	CO3	Si	K	Mg	Na
32	10.5	without Mg	1000	Entry	2.5E-04	1.5E+01	5.1E-03	1.8E-01	2.1E-01	1.7E+00	3.3E+01
			5000	pptr/dsln	-8.4E+00	-2.1E+00	-2.2E+01	-4.7E+00	-1.8E+00	-3.2E+01	1.8E+01
				Entry	1.2E-03	7.4E+01	2.5E-02	9.1E-01	1.0E+00	8.4E+00	1.6E+02
			10000	pptr/dsln	-8.6E+00	1.4E+00	-2.6E+01	-3.2E+01	-8.6E+00	-3.3E+01	1.8E+01
				Entry	2.5E-03	1.5E+02	5.1E-02	1.8E+00	2.1E+00	1.7E+01	3.3E+02
		with Mg	1000	pptr/dsln	-8.8E+00	5.4E+00	-3.1E+01	-6.5E+01	-1.7E+01	-3.4E+01	1.7E+01
				Entry	2.5E-04	1.5E+01	5.1E-03	1.8E-01	2.1E-01	1.7E+00	3.3E+01
			5000	pptr/dsln	-1.2E+01	1.3E+01	-4.6E+00	2.3E-01	-1.0E+00	-2.1E+01	1.6E+01
				Entry	1.2E-03	7.4E+01	2.5E-02	9.1E-01	1.0E+00	8.4E+00	1.6E+02
			10000	pptr/dsln	-1.2E+01	1.6E+01	-9.3E+00	-1.9E+01	-7.3E+00	-1.5E+01	1.6E+01
				Entry	2.5E-03	1.5E+02	5.1E-02	1.8E+00	2.1E+00	1.7E+01	3.3E+02
	11	without Mg	1000	pptr/dsln	-1.2E+01	1.9E+01	-1.4E+01	-4.5E+01	-1.5E+01	-6.6E+00	1.6E+01
				Entry	8.3E-04	4.9E+01	1.7E-02	6.0E-01	6.9E-01	5.6E+00	1.1E+02
			5000	pptr/dsln	-8.9E+00	2.1E+00	-1.8E+01	-1.7E+01	-2.9E+00	-3.2E+01	1.9E+01
				Entry	4.1E-03	2.5E+02	8.4E-02	3.0E+00	3.5E+00	2.8E+01	5.5E+02
		with Mg	10000	pptr/dsln	-8.9E+00	1.0E+01	-2.0E+01	-9.2E+01	-1.4E+01	-3.3E+01	2.1E+01
				Entry	8.3E-03	4.9E+02	1.7E-01	6.0E+00	6.9E+00	5.6E+01	1.1E+03
			10000	pptr/dsln	-8.7E+00	1.9E+01	-2.3E+01	-1.8E+02	-2.7E+01	-3.5E+01	2.3E+01
				Entry	8.3E-04	4.9E+01	1.7E-02	6.0E-01	6.9E-01	5.6E+00	1.1E+02
	12	without Mg	1000	pptr/dsln	-1.2E+01	1.8E+01	-1.4E+00	-2.9E+00	-1.8E+00	-1.6E+01	1.7E+01
				Entry	5.9E-02	3.5E+03	1.2E+00	4.3E+01	5.0E+01	4.0E+02	7.8E+03
			5000	pptr/dsln	-2.6E+01	4.6E+02	-2.5E+01	-1.2E+01	-3.7E+01	-3.6E+01	1.2E+01
				Entry	1.2E-01	7.0E+03	2.4E+00	8.6E+01	9.9E+01	8.0E+02	1.6E+04
		with Mg	10000	pptr/dsln	-5.4E+01	7.1E+02	-2.7E+01	-2.1E+01	-6.5E+01	-3.9E+01	6.3E+00
				Entry	1.2E-02	7.0E+02	2.4E-01	8.6E+00	9.9E+00	8.0E+01	1.6E+03
			10000	pptr/dsln	-2.0E+01	9.5E+01	-2.8E-03	4.4E+00	-7.1E+00	7.1E+01	1.3E+01
				Entry	5.9E-02	3.5E+03	1.2E+00	4.3E+01	5.0E+01	4.0E+02	7.8E+03

Table 12 (continued) - Total number of moles of primary species that has entered the domain (entry) or reacted (precipitation(+) / dissolution(-)) for the different cases and for different times.

Q [l/a]	pH	with / without Mg	time (a)	Number of moles	Al	Ca	CO3	Si	K	Mg	Na
158	10.5	without Mg	1000	Entry	1.2E-03	7.3E+01	2.5E-02	9.0E-01	1.0E+00	8.3E+00	1.6E+02
				pptr/dsln	-1.7E+01	1.6E+01	-2.2E+01	-1.1E+01	-2.2E+00	-6.3E+01	3.7E+01
			5000	Entry	6.1E-03	3.6E+02	1.2E-01	4.5E+00	5.1E+00	4.1E+01	8.1E+02
				pptr/dsln	-1.7E+01	8.2E+00	-3.9E+01	-7.8E+01	-1.1E+01	-6.4E+01	3.7E+01
			10000	Entry	1.2E-02	7.3E+02	2.5E-01	9.0E+00	1.0E+01	8.3E+01	1.6E+03
				pptr/dsln	-1.7E+01	-2.6E+00	-6.0E+01	-1.6E+02	-2.1E+01	-6.6E+01	3.7E+01
	11	with Mg	1000	Entry	1.2E-03	7.3E+01	2.5E-02	9.0E-01	1.0E+00	8.3E+00	1.6E+02
				pptr/dsln	-3.3E+01	1.8E+01	-1.1E+01	1.1E+00	-1.3E+00	-2.6E+01	2.7E+01
			5000	Entry	6.1E-03	3.6E+02	1.2E-01	4.5E+00	5.1E+00	4.1E+01	8.1E+02
				pptr/dsln	-3.6E+01	1.1E+01	-3.0E+01	-3.5E+01	-8.9E+00	5.5E+00	2.7E+01
			10000	Entry	1.2E-02	7.3E+02	2.5E-01	9.0E+00	1.0E+01	8.3E+01	1.6E+03
				pptr/dsln	-3.6E+01	-1.9E+00	-5.3E+01	-8.2E+01	-1.8E+01	4.6E+01	2.5E+01
	12	without Mg	1000	Entry	4.1E-03	2.4E+02	8.3E-02	3.0E+00	3.4E+00	2.8E+01	5.4E+02
				pptr/dsln	-1.8E+01	3.2E+01	-7.3E+00	-2.6E+01	-3.5E+00	-6.3E+01	3.7E+01
			5000	Entry	2.0E-02	1.2E+03	4.1E-01	1.5E+01	1.7E+01	1.4E+02	2.7E+03
				pptr/dsln	-1.8E+01	3.7E+01	-1.5E+01	-1.5E+02	-1.7E+01	-6.5E+01	3.6E+01
			10000	Entry	4.1E-02	2.4E+03	8.3E-01	3.0E+01	3.4E+01	2.8E+02	5.4E+03
				pptr/dsln	-1.9E+01	4.2E+01	-2.5E+01	-2.8E+02	-3.3E+01	-6.7E+01	3.6E+01
	12	with Mg	1000	Entry	4.1E-03	2.4E+02	8.3E-02	3.0E+00	3.4E+00	2.8E+01	5.4E+02
				pptr/dsln	-4.1E+01	2.8E+01	-3.5E+00	-5.4E+00	-2.4E+00	2.6E+00	2.7E+01
			5000	Entry	2.0E-02	1.2E+03	4.1E-01	1.5E+01	1.7E+01	1.4E+02	2.7E+03
				pptr/dsln	-4.1E+01	3.2E+01	-1.1E+01	-9.8E+01	-1.4E+01	1.1E+02	2.7E+01
			10000	Entry	4.1E-02	2.4E+03	8.3E-01	3.0E+01	3.4E+01	2.8E+02	5.4E+03
				pptr/dsln	-4.1E+01	3.6E+01	-2.1E+01	-2.1E+02	-2.8E+01	2.5E+02	2.6E+01
	12	without Mg	1000	Entry	5.8E-02	3.5E+03	1.2E+00	4.3E+01	4.9E+01	4.0E+02	7.7E+03
				pptr/dsln	-4.3E+01	2.1E+02	-2.0E-01	2.0E+01	-9.1E+00	-6.4E+01	2.8E+01
			5000	Entry	2.9E-01	1.7E+04	5.9E+00	2.1E+02	2.4E+02	2.0E+03	3.9E+04
				pptr/dsln	-1.5E+02	8.9E+02	-1.2E+00	9.7E+01	-4.3E+01	-6.7E+01	-8.2E+00
			10000	Entry	5.8E-01	3.5E+04	1.2E+01	4.3E+02	4.9E+02	4.0E+03	7.7E+04
				pptr/dsln	-2.9E+02	1.6E+03	-2.4E+00	1.9E+02	-7.9E+01	-7.1E+01	-5.5E+01
	12	with Mg	1000	Entry	5.8E-02	3.5E+03	1.2E+00	4.3E+01	4.9E+01	4.0E+02	7.7E+03
				pptr/dsln	-6.5E+01	1.6E+02	-5.5E-02	2.9E+01	-8.1E+00	3.9E+02	1.8E+01
			5000	Entry	2.9E-01	1.7E+04	5.9E+00	2.1E+02	2.4E+02	2.0E+03	3.9E+04
				pptr/dsln	-1.1E+02	7.2E+02	-4.7E-01	1.3E+02	-3.9E+01	2.0E+03	1.5E+00
			10000	Entry	5.8E-01	3.5E+04	1.2E+01	4.3E+02	4.9E+02	4.0E+03	7.7E+04
				pptr/dsln	-1.7E+02	1.3E+03	-1.0E+00	2.5E+02	-7.3E+01	3.9E+03	-1.8E+01

Table 12 (continued) - Total number of moles of primary species that has entered the domain (entry) or reacted (precipitation(+)/dissolution(-)) for the different cases and for different times.

Q [l/a]	pH	with / without Mg	time (a)	Number of moles	Al	Ca	CO3	Si	K	Mg	Na
631	10.5	without Mg	1000	Entry	4.9E-03	2.9E+02	1.0E-01	3.6E+00	4.1E+00	3.3E+01	6.5E+02
				pptr/dsln	-3.4E+01	5.4E+01	-2.1E+01	-6.0E+00	-2.3E+00	-1.3E+02	7.4E+01
			5000	Entry	2.5E-02	1.5E+03	5.0E-01	1.8E+01	2.1E+01	1.7E+02	3.2E+03
				pptr/dsln	-3.5E+01	-1.2E-01	-8.4E+01	-8.6E+01	-1.1E+01	-1.3E+02	7.2E+01
			10000	Entry	4.9E-02	2.9E+03	1.0E+00	3.6E+00	4.1E+01	3.3E+02	6.5E+03
				pptr/dsln	-3.7E+01	-6.7E+01	-1.6E+02	-1.8E+02	-2.2E+01	-1.3E+02	7.0E+01
	11	with Mg	1000	Entry	4.9E-03	2.9E+02	1.0E-01	3.6E+00	4.1E+00	3.3E+01	6.5E+02
				pptr/dsln	-9.2E+01	2.6E+00	-4.1E+01	3.7E+00	-1.5E+00	-2.6E+00	3.7E+01
			5000	Entry	2.5E-02	1.5E+03	5.0E-01	1.8E+01	2.1E+01	1.7E+02	3.2E+03
				pptr/dsln	-1.2E+02	-5.2E+01	-1.1E+02	1.8E+00	-9.6E+00	1.3E+02	3.4E+01
			10000	Entry	4.9E-02	2.9E+03	1.0E+00	3.6E+00	4.1E+01	3.3E+02	6.5E+03
				pptr/dsln	-1.4E+02	-1.3E+02	-1.9E+02	-3.0E+00	-2.0E+01	2.9E+02	2.2E+01
	12	without Mg	1000	Entry	1.6E-02	9.7E+02	3.3E-01	1.2E+01	1.4E+01	1.1E+02	2.2E+03
				pptr/dsln	-3.7E+01	6.7E+01	-7.8E+00	-2.4E+01	-3.6E+00	-1.3E+02	7.3E+01
			5000	Entry	8.2E-02	4.9E+03	1.7E+00	6.0E+01	6.8E+01	5.5E+02	1.1E+04
				pptr/dsln	-3.9E+01	4.9E+01	-3.9E+01	-1.6E+02	-1.8E+01	-1.3E+02	7.1E+01
			10000	Entry	1.6E-01	9.7E+03	3.3E+00	1.2E+02	1.4E+02	1.1E+03	2.2E+04
				pptr/dsln	-4.2E+01	2.6E+01	-7.7E+01	-3.2E+02	-3.5E+01	-1.3E+02	6.8E+01
	13	with Mg	1000	Entry	1.6E-02	9.7E+02	3.3E-01	1.2E+01	1.4E+01	1.1E+02	2.2E+03
				pptr/dsln	-1.1E+02	4.2E+01	-9.8E+00	3.9E-01	-2.8E+00	9.7E+01	4.2E+01
			5000	Entry	8.2E-02	4.9E+03	1.7E+00	6.0E+01	6.8E+01	5.5E+02	1.1E+04
				pptr/dsln	-1.1E+02	2.3E+01	-4.0E+01	-9.5E+01	-1.5E+01	5.4E+02	4.0E+01
			10000	Entry	1.6E-01	9.7E+03	3.3E+00	1.2E+02	1.4E+02	1.1E+03	2.2E+04
				pptr/dsln	-1.2E+02	-1.1E-01	-7.9E+01	-2.1E+02	-3.0E+01	1.1E+03	3.6E+01
	14	without Mg	1000	Entry	2.3E-01	1.4E+04	4.7E+00	1.7E+02	2.0E+02	1.6E+03	3.1E+04
				pptr/dsln	-1.7E+02	4.8E+02	-5.0E-01	8.3E+01	-9.4E+00	-1.3E+02	2.9E+01
			5000	Entry	1.2E+00	6.9E+04	2.4E+01	8.5E+02	9.8E+02	7.9E+03	1.5E+05
				pptr/dsln	-3.7E+02	1.7E+03	-2.9E+00	4.3E+02	-4.6E+01	-1.3E+02	-4.4E+01
			10000	Entry	2.3E+00	1.4E+05	4.7E+01	1.7E+03	2.0E+03	1.6E+04	3.1E+05
				pptr/dsln	-4.9E+02	2.9E+03	-5.6E+00	8.7E+02	-8.8E+01	-1.3E+02	-8.3E+01
	15	with Mg	1000	Entry	2.3E-01	1.4E+04	4.7E+00	1.7E+02	2.0E+02	1.6E+03	3.1E+04
				pptr/dsln	-1.8E+02	3.4E+02	-2.5E-01	1.1E+02	-8.4E+00	1.6E+03	2.0E+01
			5000	Entry	1.2E+00	6.9E+04	2.4E+01	8.5E+02	9.8E+02	7.9E+03	1.5E+05
				pptr/dsln	-3.5E+02	1.5E+03	-1.9E+00	5.4E+02	-4.1E+01	7.9E+03	-4.1E+01
			10000	Entry	2.3E+00	1.4E+05	4.7E+01	1.7E+03	2.0E+03	1.6E+04	3.1E+05
				pptr/dsln	-4.5E+02	2.8E+03	-4.1E+00	1.1E+03	-8.0E+01	1.6E+04	-7.7E+01

Table 12 (continued) - Total number of moles of primary species that has entered the domain (entry) or reacted (precipitation(+) / dissolution(-)) for the different cases and for different times.

Q [l/a]	pH	with / without Mg	time (a)	Number of moles	Al	Ca	CO3	Si	K	Mg	Na
3154	10.5	without Mg	1000	Entry	2.5E-02	1.5E+03	5.0E-01	1.8E+01	2.1E+01	1.7E+02	3.2E+03
				pptr/dsln	-7.7E+01	7.3E+01	-8.3E+01	4.7E+00	-2.3E+00	-2.7E+02	1.6E+02
			5000	Entry	1.2E-01	7.3E+03	2.5E+00	8.9E+01	1.0E+02	8.3E+02	1.6E+04
				pptr/dsln	-1.2E+02	-2.1E+02	-3.9E+02	-1.1E+02	-1.1E+01	-3.2E+02	1.7E+02
			10000	Entry	2.5E-01	1.5E+04	5.0E+00	1.8E+02	2.1E+02	1.7E+03	3.2E+04
				pptr/dsln	-1.6E+02	-5.9E+02	-7.7E+02	-2.8E+02	-2.3E+01	-3.2E+02	1.6E+02
	11	with Mg	1000	Entry	2.5E-02	1.5E+03	5.0E-01	1.8E+01	2.1E+01	1.7E+02	3.2E+03
				pptr/dsln	-2.7E+02	-4.9E+01	-1.1E+02	1.6E+01	-1.8E+00	1.5E+02	4.0E+01
			5000	Entry	1.2E-01	7.3E+03	2.5E+00	8.9E+01	1.0E+02	8.3E+02	1.6E+04
				pptr/dsln	-5.8E+02	-3.9E+02	-4.4E+02	5.5E+01	-1.0E+01	7.9E+02	-1.5E+01
			10000	Entry	2.5E-01	1.5E+04	5.0E+00	1.8E+02	2.1E+02	1.7E+03	3.2E+04
				pptr/dsln	-5.9E+02	-7.8E+02	-8.3E+02	1.4E+02	-2.1E+01	1.3E+03	-3.1E+01
	12	without Mg	1000	Entry	8.2E-02	4.9E+03	1.7E+00	6.0E+01	6.8E+01	5.5E+02	1.1E+04
				pptr/dsln	-8.7E+01	1.4E+02	-4.1E+01	-2.1E+00	-3.6E+00	-3.2E+02	1.8E+02
			5000	Entry	4.1E-01	2.4E+04	8.3E+00	3.0E+02	3.4E+02	2.8E+03	5.4E+04
				pptr/dsln	-1.3E+02	-9.5E+00	-1.9E+02	-2.0E+02	-1.8E+01	-3.2E+02	1.7E+02
			10000	Entry	8.2E-01	4.9E+04	1.7E+01	6.0E+02	6.8E+02	5.5E+03	1.1E+05
				pptr/dsln	-1.7E+02	-2.0E+02	-3.9E+02	-4.4E+02	-3.6E+01	-3.2E+02	1.5E+02
	12	with Mg	1000	Entry	8.2E-02	4.9E+03	1.7E+00	6.0E+01	6.8E+01	5.5E+02	1.1E+04
				pptr/dsln	-3.2E+02	7.3E+01	-3.9E+01	5.0E+01	-3.0E+00	5.5E+02	9.0E+01
			5000	Entry	4.1E-01	2.4E+04	8.3E+00	3.0E+02	3.4E+02	2.8E+03	5.4E+04
				pptr/dsln	-3.5E+02	-7.3E+01	-1.9E+02	-2.2E+01	-1.6E+01	2.8E+03	7.6E+01
			10000	Entry	8.2E-01	4.9E+04	1.7E+01	6.0E+02	6.8E+02	5.5E+03	1.1E+05
				pptr/dsln	-3.8E+02	-2.6E+02	-3.8E+02	-1.1E+02	-3.1E+01	5.5E+03	5.8E+01
	12	without Mg	1000	Entry	1.2E+00	6.9E+04	2.4E+01	8.5E+02	9.8E+02	7.9E+03	1.5E+05
				pptr/dsln	-6.5E+02	1.6E+03	-2.8E+00	4.0E+02	-9.6E+00	-3.2E+02	-8.2E+00
			5000	Entry	5.8E+00	3.5E+05	1.2E+02	4.3E+03	4.9E+03	3.9E+04	7.7E+05
				pptr/dsln	-7.5E+02	4.4E+03	-1.4E+01	2.2E+03	-4.7E+01	-3.2E+02	-4.6E+01
			10000	Entry	1.2E+01	6.9E+05	2.4E+02	8.5E+03	9.8E+03	7.9E+04	1.5E+06
				pptr/dsln	-8.7E+02	7.8E+03	-2.7E+01	4.4E+03	-9.3E+01	-3.2E+02	-8.8E+01
	12	with Mg	1000	Entry	1.2E+00	6.9E+04	2.4E+01	8.5E+02	9.8E+02	7.9E+03	1.5E+05
				pptr/dsln	-5.8E+02	1.2E+03	-2.0E+00	5.7E+02	-8.6E+00	7.9E+03	2.0E+00
			5000	Entry	5.8E+00	3.5E+05	1.2E+02	4.3E+03	4.9E+03	3.9E+04	7.7E+05
				pptr/dsln	-7.0E+02	4.4E+03	-1.0E+01	2.7E+03	-4.3E+01	3.9E+04	-4.2E+01
			10000	Entry	1.2E+01	6.9E+05	2.4E+02	8.5E+03	9.8E+03	7.9E+04	1.5E+06
				pptr/dsln	-8.0E+02	8.2E+03	-2.1E+01	5.4E+03	-8.4E+01	7.9E+04	-8.3E+01

Table 12 (continued) - Total number of moles of primary species that has entered the domain (entry) or reacted (precipitation(+) / dissolution(-)) for the different cases and for different times.

Q [l/a]	pH	with / without Mg	time (a)	Number of moles	Al	Ca	CO3	Si	K	Mg	Na
631 vble. T	10.5	without Mg	1000	Entry	4.9E-03	2.9E+02	1.0E-01	3.6E+00	4.1E+00	3.3E+01	6.5E+02
			5000	pptr/dsln	-3.5E+01	4.8E+01	-2.6E+01	-5.7E+00	-2.2E+00	-1.3E+02	7.4E+01
				Entry	2.5E-02	1.5E+03	5.0E-01	1.8E+01	2.1E+01	1.7E+02	3.2E+03
		with Mg	10000	pptr/dsln	-3.6E+01	-5.8E+00	-8.9E+01	-8.5E+01	-1.1E+01	-1.3E+02	7.2E+01
			1000	Entry	4.9E-02	2.9E+03	1.0E+00	3.6E+01	4.1E+01	3.3E+02	6.5E+03
				pptr/dsln	-3.8E+01	-7.3E+01	-1.7E+02	-1.8E+02	-2.2E+01	-1.3E+02	7.0E+01
	11	without Mg	1000	Entry	4.9E-03	2.9E+02	1.0E-01	3.6E+00	4.1E+00	3.3E+01	6.5E+02
			5000	pptr/dsln	-8.7E+01	4.2E+00	-3.8E+01	3.4E+00	-1.4E+00	-5.6E+00	3.6E+01
				Entry	2.5E-02	1.5E+03	5.0E-01	1.8E+01	2.1E+01	1.7E+02	3.2E+03
		with Mg	10000	pptr/dsln	-1.2E+02	-5.0E+01	-1.1E+02	2.6E+00	-9.4E+00	1.2E+02	3.5E+01
			1000	Entry	4.9E-02	2.9E+03	1.0E+00	3.6E+01	4.1E+01	3.3E+02	6.5E+03
				pptr/dsln	-1.4E+02	-1.2E+02	-1.9E+02	-1.1E+00	-1.9E+01	2.8E+02	2.3E+01
			10000	Entry	1.6E-02	9.7E+02	3.3E-01	1.2E+01	1.4E+01	1.1E+02	2.2E+03
				pptr/dsln	-3.8E+01	6.5E+01	-9.0E+00	-2.3E+01	-3.4E+00	-1.3E+02	7.3E+01
				Entry	8.2E-02	4.9E+03	1.7E+00	6.0E+01	6.8E+01	5.5E+02	1.1E+04
	12	without Mg	1000	pptr/dsln	-4.0E+01	4.7E+01	-4.0E+01	-1.6E+02	-1.7E+01	-1.3E+02	7.1E+01
			5000	Entry	1.6E-01	9.7E+03	3.3E+00	1.2E+02	1.4E+02	1.1E+03	2.2E+04
				pptr/dsln	-4.3E+01	2.5E+01	-7.8E+01	-3.2E+02	-3.4E+01	-1.3E+02	6.8E+01
		with Mg	1000	Entry	1.6E-02	9.7E+02	3.3E-01	1.2E+01	1.4E+01	1.1E+02	2.2E+03
			5000	pptr/dsln	-1.1E+02	4.4E+01	-8.8E+00	2.2E+00	-2.5E+00	8.5E+01	4.4E+01
				Entry	8.2E-02	4.9E+03	1.7E+00	6.0E+01	6.8E+01	5.5E+02	1.1E+04
			10000	pptr/dsln	-1.1E+02	2.5E+01	-3.9E+01	-9.2E+01	-1.5E+01	5.2E+02	4.2E+01
		without Mg	1000	Entry	1.6E-01	9.7E+03	3.3E+00	1.2E+02	1.4E+02	1.1E+03	2.2E+04
			5000	pptr/dsln	-1.1E+02	2.1E+00	-7.7E+01	-2.0E+02	-3.0E+01	1.1E+03	3.8E+01
				Entry	2.3E-01	1.4E+04	4.7E+00	1.7E+02	2.0E+02	1.6E+03	3.1E+04
		with Mg	1000	pptr/dsln	-1.6E+02	4.6E+02	-7.9E-01	7.3E+01	-8.8E+00	-1.3E+02	3.0E+01
			5000	Entry	1.2E+00	6.9E+04	2.4E+01	8.5E+02	9.8E+02	7.9E+03	1.5E+05
				pptr/dsln	-3.7E+02	1.6E+03	-3.1E+00	4.1E+02	-4.4E+01	-1.3E+02	-4.3E+01
			10000	Entry	2.3E+00	1.4E+05	4.7E+01	1.7E+03	2.0E+03	1.6E+04	3.1E+05
			10000	pptr/dsln	-4.6E+02	2.7E+03	-4.1E+00	8.3E+02	-7.7E+01	-1.3E+02	-7.4E+01
			1000	Entry	2.3E-01	1.4E+04	4.7E+00	1.7E+02	2.0E+02	1.6E+03	3.1E+04
			5000	pptr/dsln	-1.7E+02	3.3E+02	-3.2E-01	1.1E+02	-7.7E+00	1.5E+03	2.1E+01
				Entry	1.2E+00	6.9E+04	2.4E+01	8.5E+02	9.8E+02	7.9E+03	1.5E+05
			10000	pptr/dsln	-3.4E+02	1.5E+03	-2.0E+00	5.3E+02	-4.0E+01	7.8E+03	-3.9E+01
			10000	Entry	2.3E+00	1.4E+05	4.7E+01	1.7E+03	2.0E+03	1.6E+04	3.1E+05
			10000	pptr/dsln	-4.4E+02	2.7E+03	-4.1E+00	1.0E+03	-7.7E+01	1.5E+04	-7.5E+01

Table 12 (continued) - Total number of moles of primary species that has entered the domain (entry) or reacted (precipitation(+) / dissolution(-)) for the different cases and for different times.

Q [l/a]	pH	with / without Mg	time (a)	Number of moles	Al	Ca	CO3	Si	K	Mg	Na
631 exp.	9,7	without Mg	1000	Entry	6.3E-01	6.3E+04	6.3E-01	4.4E+01	5.0E+02	1.3E+03	1.3E+06
				pptr/dsln	-8.4E-01	2.7E+01	-2.4E+00	1.8E+01	-6.0E-01	-4.4E+01	3.0E+01
			5000	Entry	3.2E+00	3.2E+05	3.2E+00	2.2E+02	2.5E+03	6.3E+03	6.5E+06
				pptr/dsln	-1.4E+00	6.5E+01	-2.4E+01	2.5E+01	-5.7E+00	-1.3E+02	8.7E+01
			10000	Entry	6.3E+00	6.3E+05	6.3E+00	4.4E+02	5.0E+03	1.3E+04	1.3E+07
				pptr/dsln	-2.9E+00	4.6E+01	-4.8E+01	1.6E+01	-4.0E+01	-1.3E+02	9.7E+01
	with Mg	1000	Entry	6.3E-01	6.3E+04	6.3E-01	4.4E+01	5.0E+02	1.3E+03	1.3E+06	
				pptr/dsln	-6.6E+01	3.6E+01	-2.3E+01	2.1E+00	-2.5E+00	-5.3E+01	5.3E+01
		5000	Entry	3.2E+00	3.2E+05	3.2E+00	2.2E+02	2.5E+03	6.3E+03	6.5E+06	
				pptr/dsln	-7.1E+01	2.2E+01	-6.0E+01	-7.0E+01	-1.8E+01	1.1E+01	5.5E+01
	11,6	without Mg	1000	Entry	-	-	-	-	-	-	-
				pptr/dsln	-	-	-	-	-	-	-
			5000	Entry	3.2E+00	3.2E+05	3.2E+00	6.3E+01	1.9E+03	1.3E+01	6.6E+05
				pptr/dsln	-1.6E+02	3.2E+02	-2.0E+01	-2.6E+02	-3.1E+01	-1.3E+02	2.9E+01
		10000	Entry	6.3E+00	6.3E+05	6.3E+00	1.3E+02	3.8E+03	2.5E+01	1.3E+06	
				pptr/dsln	-2.8E+02	5.4E+02	-4.0E+01	-3.3E+02	-2.5E+02	-1.3E+02	5.0E+01
	12,17	with Mg	1000	Entry	6.3E-01	6.3E+04	6.3E-01	1.3E+01	3.8E+02	2.5E+00	1.3E+05
				pptr/dsln	-1.4E+02	9.3E+01	-3.8E+00	-3.8E+01	-6.4E+00	2.3E+00	3.4E+01
			5000	Entry	3.2E+00	3.2E+05	3.2E+00	6.3E+01	1.9E+03	1.3E+01	6.6E+05
				pptr/dsln	-2.3E+02	2.9E+02	-2.0E+01	-2.6E+02	-3.2E+01	1.1E+01	-1.8E+00
		10000	Entry	6.3E+00	6.3E+05	6.3E+00	1.3E+02	3.8E+03	2.5E+01	1.3E+06	
				pptr/dsln	-3.6E+02	5.1E+02	-4.0E+01	-5.3E+02	-6.1E+01	2.1E+01	-4.6E+01
	631 largeA	without Mg	1000	Entry	6.3E-01	7.6E+04	6.3E-01	3.2E+00	3.8E+02	6.3E-01	1.3E+05
				pptr/dsln	-2.8E+02	3.1E+03	-3.9E+00	-2.8E+01	-1.0E+01	-1.3E+02	-9.5E+00
			5000	Entry	6.3E-01	7.6E+04	6.3E-01	3.2E+00	3.8E+02	6.3E-01	1.3E+05
				pptr/dsln	-3.8E+02	1.4E+04	-2.0E+01	-9.0E+01	-4.9E+01	-1.3E+02	-4.6E+01
		with Mg	1000	Entry	6.3E-01	7.6E+04	6.3E-01	3.2E+00	3.8E+02	6.3E-01	1.3E+05
				pptr/dsln	-5.0E+02	2.7E+04	-4.0E+01	-1.7E+02	-9.3E+01	-1.4E+02	-8.7E+01
			5000	Entry	3.2E+00	3.8E+05	3.2E+00	1.6E+01	1.9E+03	3.2E+00	6.6E+05
				pptr/dsln	-3.8E+02	1.4E+04	-2.0E+01	-8.7E+01	-4.9E+01	3.2E+00	-4.6E+01
		10,5	1000	Entry	6.3E+00	7.6E+05	6.3E+00	3.2E+01	3.8E+03	6.3E+00	1.3E+06
				pptr/dsln	-5.0E+02	2.7E+04	-4.0E+01	-1.7E+02	-9.3E+01	6.0E+00	-8.7E+01
			5000	Entry	2.5E-02	1.5E+03	5.0E-01	1.8E+01	2.1E+01	1.7E+02	3.2E+03
				pptr/dsln	-3.3E+01	4.5E+02	-1.7E+02	-5.4E+02	-4.2E+02	-2.1E+02	2.2E+02
		10000	1000	Entry	4.9E-02	2.9E+03	1.0E+00	3.6E+01	4.1E+01	3.3E+02	6.5E+03
				pptr/dsln	-3.4E+01	4.4E+02	-2.6E+02	-1.2E+03	-4.9E+02	-2.3E+02	3.1E+02
			5000	Entry	2.5E-02	1.5E+03	5.0E-01	1.8E+01	2.1E+01	1.7E+02	3.2E+03
				pptr/dsln	-4.2E+01	4.1E+02	-1.5E+02	-3.6E+02	-4.0E+02	7.9E+01	2.4E+01
		with Mg	10000	Entry	4.9E-02	2.9E+03	1.0E+00	3.6E+01	4.1E+01	3.3E+02	6.5E+03
				pptr/dsln	-4.3E+01	4.3E+02	-2.5E+02	-8.3E+02	-4.9E+02	2.4E+02	1.3E+02

ACKNOWLEDGEMENTS

I thank my tutors, Josep M. Soler and Maarten W. Saaltink, for their patience, support and dedication in all this time. I also appreciate their helpful with writing in English. Financial support from Posiva (Finland) is also gratefully acknowledged.

REFERENCES

- Adler M. (2001) Interaction of Claystone and Hyperalkaline Solutions at 30°C: A Combined Experimental and Modeling Study. Ph.D. Dissertation, University of Bern.
- Andersson J., Ahokas H., Hudson J. A., Koskinen L., Luukkonen A., Löfman J., Keto V., Pitkänen P., Mattila J., Ikonen A. T. K. and Ylä-Mella M. (2007) Olkiluoto Site Description 2006. Posiva Report 2007-03.
- Astudillo J. (2001) El Almacenamiento Geológico Profundo de los residuos radioactivos de alta actividad. Principios Básicos y Tecnología. Enresa.
- Badillo-Almaraz V. and Vargas G. A. (2007) Concepto de diseño de la disposición definitiva para Desechos Radioactivos de Alto Nivel. International Joint Meeting Cancun 2007.
- Blum A. E. and Stillings L. L. (1995) Feldspar dissolution kinetics. In: White A. F., Brantley S. L. (Eds.), Chemical Weathering Rates of Silicate Minerals. Reviews in Mineralogy, Vol. 31., pp. 291-351. Mineralogical Society of America
- Brantley S. L. (2005) Reaction kinetics of primary rock-forming minerals under ambient conditions. In: Drever J. I. (Ed.), Surface and Ground Water, Weathering, and Soils. Treatise on Geochemistry, Vol. 5, pp. 73-117. Elsevier.
- Burch T. E., Nagy K. L. and Lasaga A. C. (1993) Free energy dependence of albite dissolution kinetics at 80°C and pH 8.8. Chemical Geology 105, 137-162.
- Chou L. and Wollast R. (1985) Steady-state kinetics and dissolution mechanisms of albite. American Journal of Science 285, 963-993.
- Ganor J., Mogollón J. L. and Lasaga A. C. (1995) The effect of pH on kaolinite dissolution rates and on activation energy. Geochimica et Cosmochimica Acta 59, 1037-1052.
- Gaucher E. C., Blanc Ph., Matray J.-M. and Michau N. (2004) Modeling diffusion of an alkaline plume in a clay barrier. Applied Geochemistry 19, 1505-1515.
- Helgeson H. C. and Kirkham D. H. (1974) Theoretical prediction of the thermodynamic behavior of aqueous electrolytes at high pressures and temperatures: II Debye-Hückel parameters for activity coefficients and relative partial molal properties. American Journal of Science 274, 1199-1261.
- Kärki A. and Paulamäki S. (2006) Petrology of Olkiluoto. Working Report 2006-02. Posiva Oy.
- Kirkner D. J. and Reeves H. (1988) Multicomponent mass transport with homogeneous and heterogeneous chemical reactions: Effect of the chemistry on the choice of numerical algorithm. 1. Theory. Water Resour. Res. 24, 1719-1729.
- Kulik D. A. and Kersten M. (2001) Aqueous solubility diagrams for cementitious waste stabilization systems: II, end-member stoichiometries of ideal calcium silicate hydrate solid solutions. Journal of the American Ceramic Society 84, 3017-3026.
- Lasaga A. C. (1998) Kinetic Theory in the Earth Sciences. Princeton University Press, Princeton.
- Lehikoinen J., Nordman H. and Luukkonen A. (2007) Cement Bentonite Study for the KBS-3H Drift. Saanio & Riekkola Oy Report.
- Lichtner P. C. (1985) Continuum model for simultaneous chemical reactions and mass transport in hydrothermal systems. Geochim. Cosmochim. Acta 49, 779-800.

- Lichtner P. C. and Eikenberg J. (1995) Propagation of a Hyperalkaline Plume into the Geological Barrier Surrounding a Radioactive Waste Repository. Paul Scherrer Institut Bericht Nr. 95-1.
- Mäder U. K., Fierz Th., Frieg B., Eikenberg J., Rüthi M., Albinsson Y., Möri A., Ekberg S. and Stille P. (2006) Interaction of hyperalkaline fluid with fractured rock: Field and laboratory experiments of the HPF project (Grimsel Test Site, Switzerland). Journal of Geochemical Exploration 90, 68-94.
- Mattila J., Aaltonen I., Kemppainen K., Wikström L., Paananen M., Paulamäki S., Front K., Gehör S., Kärki, A. and Ahokas T. (2008) Geological Model of the Olkiluoto Site Version 1.0. Working Report 2007-92. Posiva Oy
- Montori, J., Saaltink, M.W., Soler, J.M., (2008,) Reactive Transport Modeling of the Effect of Hyperalkaline Solutions Along a Fracture at the ONKALO Site, Working Report 2008-14, Posiva Oy.
- Morse J. W. and Arvidson R. S. (2002) The dissolution kinetics of major sedimentary carbonate minerals. Earth-Science Reviews 58, 51-84.
- Nagy K. L., Blum A. E. and Lasaga A. C.(1991) Dissolution and precipitation kinetics of kaolinite at 80°C and pH 3: The dependence on solution saturation state. American Journal of Science 291, 649-686.
- Paulamäki S., Paananen M., Gehör S., Kärki, A., Front K., Aaltonen I., Ahokas T., Kemppainen K., Mattila J. and Wikström L.(2006) Geological Model of the Olkiluoto Site Version 0. Working Report 2006-37. Posiva Oy
- Pfingsten W. (2002) Experimental and modeling indications for self-sealing of a cementitious low- and intermediate-level waste repository by calcite precipitation. Nuclear Technology 140, 63-82.
- Pfingsten W., Paris B., Soler J. M. and Mäder U. K. (2006) Tracer and reactive transport modelling of the interaction between high-pH fluid and fractured rock: Field and laboratory experiments. Journal of Geochemical Exploration 90, 95-113.
- Posiva (2009). *Onkalo*. Obtained on October 12 2009, from <http://www.posiva.fi/en>.
- Read D., Glasser F. P., Ayora C., Guardiola M. T. and Sneyers A. (2001) Mineralogical and microstructural changes accompanying the interaction of Boom Clay with Ordinary Portland Cement. Advances in Cement Research 13, 175-183.
- Reed M. H. (1982) Calculation of multicomponent chemical equilibria and reaction process in systems involving minerals, gases and aqueous phases. Geochim. Cosmochim. Acta 46, 513-528.
- Saaltink M. W., Batlle F., Ayora C., Carrera J. and Olivella S. (2004) RETRASO, a code for modeling reactive transport in saturated and unsaturated porous media. Geologica Acta 2, 235-251.
- Salamanca's University (2008). *Almacenamiento Geológico Profundo. Conceptos básicos, barreras de ingeniería, barreras geológicas*. Obtained on October 12 2009, from <http://ocw.usal.es/ciencias-experimentales/gestion-de-residuos-radiactivos/contenidos/AGP.pdf>
- Savage D., Noy D. and Mihara M. (2002) Modelling the interaction of bentonite with hyperalkaline fluids. Applied Geochemistry 17, 207-223.
- Schweda P.(1989) Kinetics of alkali feldspar dissolution at low temperature. In: Miles D. L. (Ed.) Proceedings of the 6th International Symposium on Water-Rock Interaction, pp. 609-612. Balkema.

- Schweda P. (1990) Kinetics and Mechanisms of Alkali Feldspar Dissolution at Low Temperatures. Ph.D. Thesis, Stockholm University.
- Soler J. M. (2003) Reactive transport modeling of the interaction between a high-pH plume and a fractured marl: the case of Wellenberg. *Applied Geochemistry* 18, 1555-1571.
- Soler J. M. and Lasaga A. C. (1998) An advection-dispersion-reaction model of bauxite formation. *Journal of Hydrology* 209, 311-330.
- Soler J. M. and Mäder U. K. (2005) Interaction between hyperalkaline fluids and rocks hosting repositories for radioactive waste: Reactive transport simulations. *Nuclear Science and Engineering* 151, 128-133.
- Soler J. M. and Mäder U. K. (2007) Mineralogical alteration and associated permeability changes induced by a high-pH plume: Modeling of a granite core infiltration experiment. *Applied Geochemistry* 22, 17-29.
- Soler J. M., Pfingsten W., Paris B., Mäder U. K., Frieg B., Neall F., Källvenius G., Yui M., Yoshida P., Shi P., Rochelle Ch. A. and Noy D. J. (2006) Grimsel Test Site – Investigation Phase V. HPF-Experiment: Modelling Report. Nagra Technical Report NTB 05-01.
- Steefel C. I. and Lichtner P. C. (1994) Diffusion and reaction in rock matrix bordering a hyperalkaline fluid-filled fracture. *Geochimica et Cosmochimica Acta* 58, 3595-3612.
- Wikipedia (2009). *KBS-3*. Obtained on October 12 2009, from <http://en.wikipedia.org/wiki/KBS-3>.
- Wolery T. J., Jackson K. J., Bourcier W. L., Bruton C. J., Viani B. E., Knauss K. G. and Delany J. M. (1990) Current status of the EQ3/6 software package for geochemical modeling. In: Melchior, C., Bassett, R.L. (Eds.), *Chemical Modeling of Aqueous Systems II*. ACS Symposium Series No 416, pp. 104-116.